Graphene based Electrode Materials for Printable, High Power and Photo-Switchable Micro-Supercapacitors

Dissertation
zur Erlangung des Grades
„Doktor der Naturwissenschaften“

im Fachbereich Chemie, Pharmazie, und Geowissenschaften der Johannes Gutenberg-Universität Mainz und in Kooperation mit dem Max-Planck-Institut für Polymerforschung Mainz

vorgelegt von

Zhaoyang Liu

geboren in Jilin/China

Mainz, 2017

Dekan: Prof. Dr.
1. Berichterstatter: Prof. Dr.
2. Berichterstatter: Prof. Dr.
Tag der mündlichen Prüfung:

Die vorliegende Arbeit wurde in der Zeit von August 2012 bis June 2017 im Max-Planck-Institut für Polymerforschung in Mainz unter der Betreuung von Prof. Dr. [redacted] durchgeführt.

Ich danke Prof. Dr. [redacted] für seine wissenschaftliche und persönliche Unterstützung sowie für seine ständige Diskussionsbereitschaft.

To my family

Table of Contents

Index of Abbreviations

2D two dimensional

AFM atomic force microscopy

CMOS complementary metal-oxide semiconductor

CNT carbon nanotube

CV cyclic voltammetry

CVD chemical vapour deposition

DAE 1,2-Bis(2,4-dimethyl-5-phenyl-3-thienyl)-3,3,4,4,5,5-hexafluoro-1-cyclopentene

DFT density functional theory

DMF N,N'-dimethylformamide

D* detectivity

EDL electric double layer

EDLC electrical double layer capacitance

ESDs energy storage devices

EG electrochemically Exfoliated Graphene

EQE external quantum efficiency

FET field-effect transistor

GO graphene oxide

HOPG highly oriented pyrolytic graphite

HOMO highest occupied molecular orbital

IPA 2-propanol

ITO indium tin oxide

LB Langmuir-Blodgett

LED light-emitting diode

LPE liquid-phase exfoliation

LUMO lowest unoccupied molecular orbital

mPANi mesoporous polyaniline

MSC micro-supercapacitor

NG nanographene

NMP N-methyl-2-pyrrolidone

OPD organic photodetectors

PAHs polycyclic aromatic hydrocarbons

PDMS polydimethylsiloxane

PEDOT: PSS poly(3, 4-ethylenedioxythiophene): poly(styrenesulphonate)

PET polyethylene terephthalate

PMMA poly(methyl methacrylate)

PS-*b*-PEO polystyrene-*b*-poly(ethylene oxide)

PVA poly(vinyl alcohol)

QHE quantum Hall effect

R2R roll-to-roll

R_λ responsivity

RGO reduced graphene oxide

RMS root mean square

R_s sheet resistance

SAED selected area electron diffraction

SC supercapacitor

SEM scanning electron microscopy

S/D Source/Drain

SLG single layer graphene

STM Scanning tunneling microscopy

SWCNTs single-walled carbon nanotubes

TCEs transparent conductive electrodes

TEM transmission electron microscopy

THz terahertz

UV-Vis ultraviolet-visible

UHV ultrahigh vacuum

XPS X-ray photoelectron spectroscopy

Chapter 1. Introduction

Carbon, one of the few elements known since ancient times, is the 4th most abundant element in the universe and 15th most abundant in the Earth's crust. In addition to the great abundance, carbon's huge presence in diverse organic compounds and the ability to form polymers rendering it to serve as a common element for our daily life.

In recent years, carbon-based structures are performing a major role in emerging modern field of renewable energy conversion technologies and environmental science: electrodes in energy storage devices, electro-catalysis, photocatalysis, heterogeneous catalysis, biofuels, as well as in water purification, gas separation/storage, and as a soil additive.[1] Among them, graphene is a rapidly rising star for both material science and condense-mater physics, due to its numerous unique properties.

1.1 **Graphene**

Graphene is a flat monolayer of sp^2-hybridized carbon atoms packed into a two-dimensional (2D) honeycomb lattice, and it can be considered as a basic building block for all graphitic materials in different dimensionalities (Figure 1-1). It can be wrapped up into 0D fullerenes, rolled into 1D nanotubes or stacked into 3D graphite.[2] The importance and huge potential applications of these carbon-based materials have already been recognized in recent decades by some of the highest scientific awards including the 1996 Nobel Prize in Chemistry (fullerenes), the 2008 Kavli Prize in Nanoscience (carbon nanotubes).

The word "Graphene" came from the combination of graphite and the suffix -ene, was first used by [redacted] to describe single-layer carbon foils in the history.[3] The theoretical study of graphene (or 2D graphite) began seventy years ago.[4] Although known as an integral part of 3D materials, graphene was presumed not to exist in the *free state* at the beginning, and being labelled as an "academic" material for several decades. According to the physicists [redacted], strictly 2D crystals were thermodynamically unstable, because the melting temperature of thin films rapidly decreases with decreasing thickness, and the films will segregate into islands or decompose at a thickness of several atomic layers. [5]

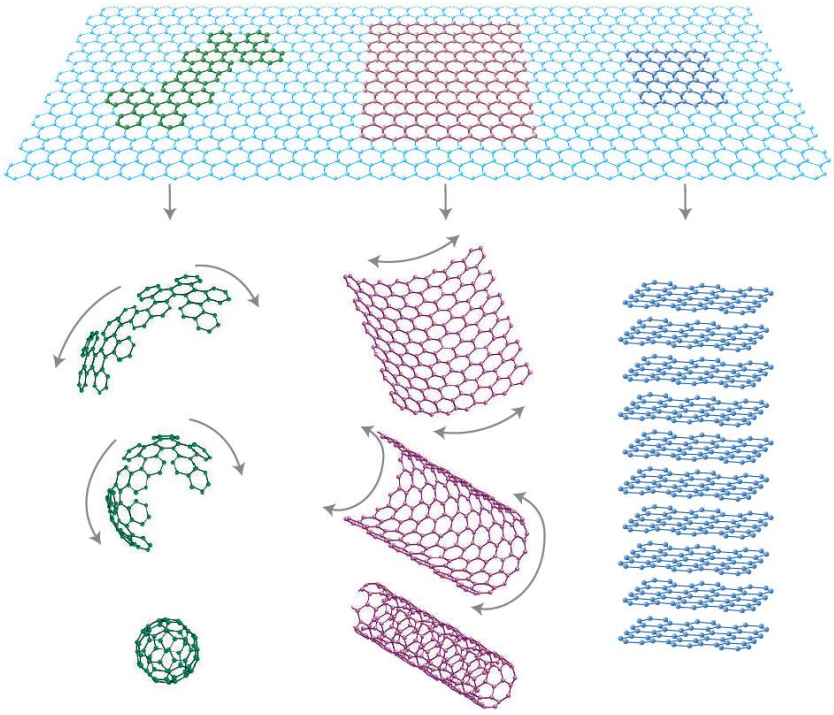

Figure 1-1. Mother of all graphitic forms. Graphene is a 2D building material for carbon materials of all other dimensionalities. Reprinted with permission from Ref. [2]; copy right: 2007, Nature publishing group.

Until 2004, the vintage model finally turned into reality, when [redacted] and [redacted] at the University of Manchester isolated single-atom-thick graphene crystallites for the first time, via "micromechanical cleavage" method. The idea was conceived from their "Friday evening experiment", its simplicity allowed a great number of researchers throughout the world to follow up their experiments. These discoveries led to the beginning of "graphene gold rush" till today, and also the Nobel Prize in Physics in 2010 for the two pioneers.

Soon, it is confirmed that the charge carriers of graphene were massless Dirac fermions.[6] Graphene's ambipolar electric field effect and high mobility exceeding 15000 $cm^2\ V^{-1}s^{-1}$ under ambient conditions were also demonstrated.[7] Transistors based on graphene with an intrinsic cut-off frequency of as high as ca. 300 GHz can be achieved with a channel length of 140 nm, suggesting a promising future for ultrahigh-speed radio-frequency logic devices.[8] Many characteristics of graphene measured in experiments have already exceeded those obtained in any other materials, some of them are reaching the theoretically predicted limits: thermal conductivity of 5,000 W/mK,[9] Young's modulus of ~1 TPa and intrinsic

tensile strength of ~130 GPa,[10] as well as transparency of 97.7% to incident light for a wide wavelength range,[11] complete impermeability to any gases,[12] ability to sustain extremely high densities of electric currents (a million times higher than copper)[13]. Moreover, the quantum Hall effect (QHE) can be observed in graphene even at room temperature, extending the previous temperature range for the QHE by a factor of 10.[14]

1.2 **Production of graphene**

The superior and unique properties justify graphene's nickname as the "miracle material". However, most of these characteristics are achieved only from the highest-quality graphene samples (by micromechanical cleavage[7a]) or from graphene deposited on special substrates like hexagonal boron nitride (atomically flat)[15]. So far, equivalent characteristics have never been achieved from graphene prepared using other techniques, although these methods are rapidly improving.

Obviously, when mass-produced graphene has the same outstanding performance as the high-quality samples obtained from research laboratories, graphene would be of more significant interest for practical industrial applications, with the real possibility of changing our lifes. Thus, reliably producing high quality graphene samples in any scalable fashion, with properties appropriate for the specific applications, became a major issue for all chemists.[16] This 2-fold challenge is depending on both the number of graphene layers present and the overall quality of the obtained graphene crystal lattice.[17]

In order to exfoliate a single graphene sheet from graphite, van der Waals attraction between the first and second layers must be overcome without disturbing any subsequent sheets. Generally, there are two main strategies for graphene production: top-down and bottom-up. The former occurs via exfoliation of bulk graphite into individual graphene sheets. The latter relies on the use of covalent chemistry approaches on properly designed molecular building blocks undergoing chemical reaction to form 2D covalent networks. These approaches are categorized in the following aspects. Each has its own advantages and drawbacks.

1.2.1 **Exfoliation approaches**

Micromechanical cleavage

Micromechanical cleavage, also known as "Scotch tape method", was initiated by [redacted] and [redacted], from repeatedly peeling highly oriented pyrolytic graphite (HOPG) with a scotch tape and pressing it onto a SiO_2 substrate. Attempts prior to this approach were unable to isolate single graphene layers. The size of obtained individual crystals can reach the millimetre range. Till today, this method is still widely used to prepare high-quality graphene samples, for the study of fundamental physics properties such as carrier mobility, ballistic transport, thermal conductivity, etc. However, although this original top-down approach of mechanical exfoliation has produced the highest quality samples, this method gives neither a high throughput nor a high yield, thereby hampering any practical applications.

Liquid-phase exfoliation

Before the first report of graphene, scientists have been focusing on single-walled carbon nanotubes (SWCNTs) for a long time due to their amazing electrical, mechanical and thermal properties.[18] Many applications of carbon nanotubes require the exfoliation of the nanotubes to give individual tubes in the liquid phase.[19] Therefore, after the success of micromechanical exfoliation of graphene, it soon became apparent that these previous strategies used to exfoliate SWCNTs in the liquid phase could be successfully transferred to graphene exfoliation.

In this regard, the [redacted] group pioneered the production of high quality graphene in high volumes by means of liquid-phase exfoliation (LPE) via ultrasonication in 2008.[20] This approach is possible because the energy required to exfoliate graphene is balanced by the solvent–graphene interaction for solvents whose surface energies match that of graphene, and the solvent–graphene interaction is indeed of the van der Waals type. By simply sonicating graphite powder in N-methylpyrroidone (surface tension close to 40 mJ m^{-2}) followed by mild centrifugation, a homogeneous colloidal suspension of graphene sheets with concentrations up to 0.01 mg mL^{-1} can be achieved. The exfoliation procedure is non-destructive, as evidenced by the absence of defects or oxides from XPS, infrared and Raman spectroscopy studies.

In order to increase the concentration of the graphene dispersion, low power sonication for prolonged period (460 hours) was performed in 2010, and yielded a high concentration of monolayer graphene (2 mg mL^{-1}).[21] They also sonicated graphite powder in aqueous solutions of some surfactants, i.e. sodium dodecylbenzene sulphonate (SDBS), and obtained few layer graphene (3-5 layers, flake size ranging from 100 nm to 3 μm) dispersion with a concentration of 0.1 mg mL^{-1}.[22] However, the scalability of this exfoliation approach is limited since ultrasonication is used as energy source.

In 2014, "Scalable production of large quantities of defect-free few-layer graphene by shear exfoliation in liquids" was demonstrated by the same group (Figure 1-2).[23] They employed high-shear mixing process, which is a commonly used technology in industry, as alternative to ultrasonication for the exfoliation of graphite. Large-scale exfoliation of graphene nanosheets in suitable stabilizing liquids would be achieved (as high as hundreds of litres), once the shear rate exceeds 10^4 s^{-1}. This simple and yet efficient method can be further extended to the exfoliation of BN, MoS_2 and a wide range of other 2D layered crystals.

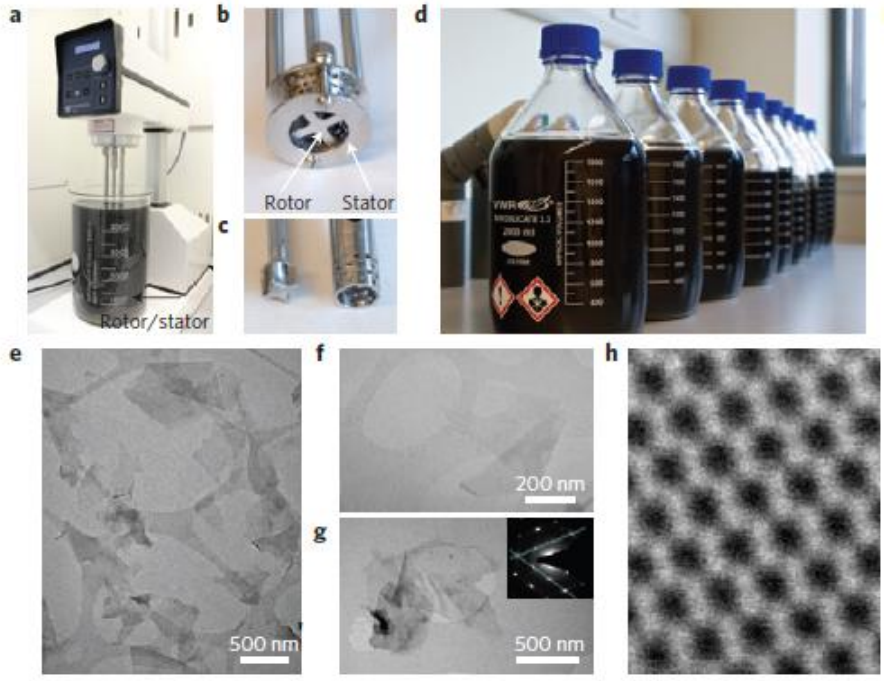

Figure 1-2. Production of graphene by shear mixing. **a**, A Silverson model L5M high-shear mixer with mixing head in a 5 l beaker of graphene dispersion. **b,c**, Close-up view of a D=32mm mixing head (b) and a D=16mm mixing head with rotor (left) separated from stator (c). **d**, Graphene–NMP dispersions produced by shear exfoliation. **e**,Wide-field TEM image of SEG nanosheets (after centrifugation). **f–h** TEM images of individual nanosheets (f), a

multilayer (g, bottom left) and monolayer (g, right) as evidenced by its electron diffraction pattern (g, inset) and a monolayer (h; imaged by high-resolution scanning TEM). Reprinted with permission from Ref. [23]; copy right: 2014, Nature publishing group.

Chemical exfoliation

Chemical exfoliation of graphite represents another important approach to produce graphene in low cost and high scalability. Compared with the direct physical cleavage or liquid phase exfoliation, reactants are employed to intercalate between graphite layers, which significantly weaken the cohesive van der Waals force.[24]

In 2006, [redacted] group reported a method for producing single-layer graphene via a solution process.[25] First, the chemical modification of graphite resulted in a water dispersible intermediary, graphite oxide (GO), via Hummers' method. After that, the interlayer spacing in graphite increased from 0.34 nm to above 0.6 nm, thus the van der Waals force between layers was weakened. The obtained GO is a pile of puckered graphene sheets with AB stacking type, which would completely exfoliate upon mild sonication. Abundant oxygen-containing (epoxide and hydroxyl) groups were introduced into the graphene basal plane during oxidation, and resulted in a hydrophilic surface of GO, which prompts water to readily intercalate between graphene sheets and disperse them as individuals. Although GO is an insulator, the conductive graphitic network can be restored by reduction with chemical reducing agents (hydrazine hydrate,[26] Vitamin C,[27] etc.). This method can easily be scaled-up to produce graphene in gram quantities. One problem with the reduction of GO solution is the quick aggregation of RGO due to its low hydrophilicity. Dan Li and co-workers solved this colloid stability issue by tuning the pH during reduction.[28] Another problem is that chemical reduction usually cannot completely remove all the oxygen-containing groups on GO, leading to relatively poor electronic properties compared with pristine graphene. Thus, post treatments of GO utilizing thermal annealing,[29] laser-scribing,[30] or microwave reduction[31] were explored.

With the aim of producing stable suspensions of graphene in organic solvents for easy processing, [redacted]'s group reported an exfoliation-reintercalation-expansion method and achieved high quality single-layer graphene sheets.[32] They first prepared expandable graphite by chemical intercalation of sulfuric acid and nitric acid. Due to volatile gaseous species released from the intercalant upon heating, the graphite exfoliated violently into

multilayer graphene form, followed by a reintercalation process with oleum and later inserted by tetra-butyl alcohol to expand the distance between graphene layers. This process facilitates the separation of graphene sheets upon sonication in a surfactant solution, which is a key step for achieving high-quality single-layer graphene. As evidenced by AFM measurements, about 90% of the obtained graphene sheets are single layer.

Electrochemical exfoliation

Compared with the above mentioned exfoliation methods, recent progress in electrochemical exfoliation of graphite has drawn increasing attention as an efficient method to produce high quality graphene (by the [redacted] group and the [redacted] group),[33] in a large amount and with larger lateral size. As shown in Figure 1-3a, the electrochemical exfoliation process mainly involves the use of an electrolyte (aqueous or organic solution), a working electrode (graphite material for exfoliation) and a counter electrode (i.e. Platinum). A voltage will be applied between the two electrodes to drive structural expansion and subsequent exfoliation at the graphite side. This method is not equipment-intensive and is typically performed under ambient conditions.[34] Most importantly, the whole exfoliation process is generally very fast, in some cases only several minutes are enough, and thus producing gram quantities of graphene sheets can be easily achieved.

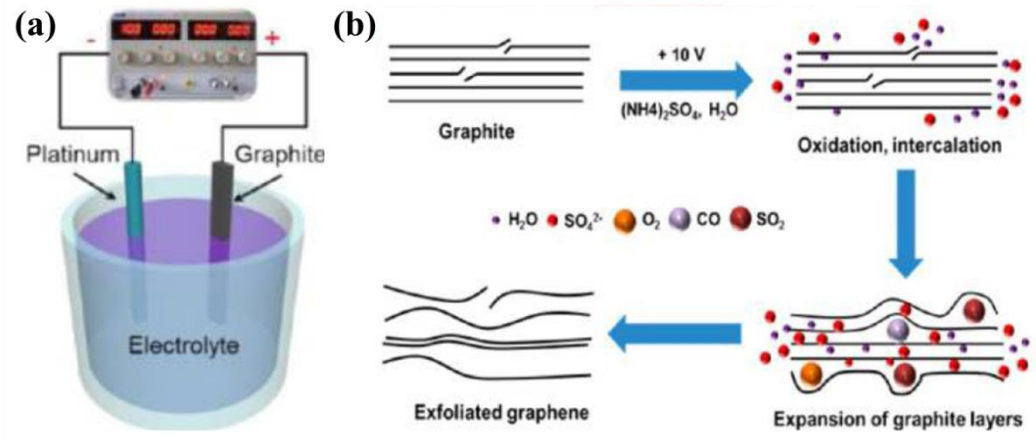

Figure 1-3. a, Setup for electrochemical exfoliation. **b,** Schematic illustration of the mechanism of electrochemical exfoliation of graphite. Reprinted with permission from Ref. [35]; copy right: 2014, American Chemical Society.

In 2013, the [redacted] group reported a high yield (≈60 wt%) production of electrochemically exfoliated graphene (EG), with concentrations up to 1 mg mL^{-1} in DMF dispersion.[33b] By precise control of electrolyte (H_2SO_4) concentration for electrochemical exfoliation, an optimized condition based on 0.1 M H_2SO_4 was found. After exfoliation, over 80% of the obtained graphene sheets are of one to three layers, with a C/O ratio of 12.3. Bilayer EG sheet, based on a field-effect transistor (FET) device geometry, showed a mobility of up to 233 $cm^2\ V^{-1}\ s^{-1}$, demonstrating its excellent intrinsic electronic properties.

In 2014, in order to avoid the over-oxidation of graphene sheets caused by acid electrolytes, aqueous solution of 0.1 M $(NH_4)_2SO_4$ was selected as electrolyte.[35] After exfoliation, over 85% graphene sheets consisting of 1-3 layers were obtained, with an average lateral size of 5 μm and high C/O ratio of 17.2, forming a fine dispersion with concentrations of up to 2.5 mg mL^{-1} in DMF. A low defect density of the obtained EG sheets was confirmed by Raman spectra, with an extremely low I_D/I_G ratio of 0.25. A high mobility of 310 $cm^2\ V^{-1}\ s^{-1}$ was also demonstrated based on single layer EG sheet in a FET device. Most importantly, this electrochemical exfoliation process can be easily scaled up; over 16 g of high-quality EG can be produced within one hour. The proposed mechanism of electrochemical exfoliation process is depicted in Figure 1-3b:

(i) The applied bias voltage causes the reduction of water at the cathode side, and creates abundant free hydroxyl radicals (•OH) in the electrolyte.

(ii) The attack by •OH leads to oxidation at the edge and grain boundary sites of graphite, and further depolarization and expansion of the graphite layers, therefore facilitating the intercalation of sulfate anions (SO_4^{2-}) between the graphite layers. Water molecules would also co-intercalate with the SO_4^{2-} anions in this step.

(iii) Accompanied by the vigorous gas evolution during the electrochemical exfoliation process, large forces on the graphite layers are introduced, which are sufficient to separate the weakly bonded graphite layers from one to another.

While the above mentioned “top-down” exfoliation approaches aim to avoid the need of supporting substrates, some techniques can take advantage of specially chosen platforms to encourage the “bottom-up” growth of high quality graphene. The major advantage of these substrate-based methods is the high compatibility with current CMOS technology. In

principle, they are able to produce single sheets of graphene on an entire wafer, which facilitates the processing of device fabrication.

1.2.2 **Epitaxy on Silicon Carbide**

In 2006, [redacted] and co-workers at Georgia Institute of Technology pioneered the epitaxial growth of graphene by heating 6H-SiC in ultrahigh vacuum (UHV, $<10^{-10}$ Torr) in the temperature range of 1200-1600 °C.[36] After the silicon atoms sublime from the surface at around 1000 °C, the underlying substrate, having the space group P63mc with a hexagonal lattice, provides excellent symmetry matching for the reconstruction of exposed carbon atoms, thus forming "epitaxial graphene".[37] The obtained graphene shows small islands of hexagonal crystallites under SEM, and a long-range order as well as a low density of defects from STM study. The UHV condition keeps graphene away from being oxidized. The approach is quite straightforward, and has been already demonstrated for the wafer scale production of graphene for carbon-based electronics.[38]

Some physical properties of epitaxial graphene still differ from those of mechanically exfoliated graphene, due to the influence of interfacial effects. For epitaxial approach, though graphene can grow on both the C-terminated and Si-terminated surfaces, the growth on a carbon surface is much faster,[39] and the coupling effect between the substrate and graphene layer is weaker.[40] Selective growth of graphene has been realized on templated substrates by patterning techniques.[41] Other polytypes of SiC, such as cubic 3C-SiC, are also proven to be capable of epitaxial growth of graphene.[42] Besides UHV conditions, epitaxial growth of several-micrometer graphene domains has also been demonstrated in an argon atmosphere.[43] In regards to practical applications, dry transfer of epitaxial graphene to arbitrary substrates has been accomplished, using thermal release tape, without a significant drop in carrier mobility.[44]

So far, industrial scale epitaxial growth of graphene is still limited by the high cost of single-crystal SiC wafers. That leads to the development of other substrate-based methods, with much lower cost.

1.2.3 **Chemical Vapour Deposition**

Another substrate-based method for graphene production is by chemical vapour deposition (CVD) approach. Compared with exfoliated graphene, CVD graphene has much better morphological and optical/electric properties, and considerably lower cost than epitaxial graphene. Nowadays, the CVD method has already emerged as one of the most promising techniques for the bottom-up growth of large-area graphene films, by the pyrolysis of hydrocarbon precursors (i.e. methane) at high temperatures on various substrates.

In the history, the CVD method has been extensively employed for CNT growth in the presence of catalytic nanoparticles,[45] and later extended to graphene growth. So far, it has proven to be efficient for producing large area graphene films on different transition metal surfaces, i.e. ruthenium,[46] platinum,[47] nickel[48], iridium[49], palladium[50] and copper[51]. The carbon solubility of these substrates determines the number of obtained graphene layers. Since nickel has relatively high carbon solubility, the *"surface segregation/precipitation"* growth mechanism is applied. Carbon atoms will first dissolve in at high temperatures then precipitate onto the metal surface upon cooling, to form single or multilayer graphene films. This always led to non-uniform films with thickness ranging from monolayer to 10 layers.

By contrast, copper has a relatively low carbon solubility, whereas the *"surface adsorption"* growth mechanism is applied, and always results in complete monolayer coverage. In addition, taking the cost into consideration, copper is always preferred and widely used for CVD growth of graphene over large areas. Pioneering work of uniformly deposited high-quality monolayer graphene on copper was accomplished by [redacted] group in 2009.[51] They loaded a piece of copper foil into a quartz-tube chamber, and evacuated by a vacuum pump, followed by back filling with hydrogen gas. After heating to the growth temperature, they introduced methane gas into the chamber as carbon source. During growth, the temperature was kept in millitorr range, thus this process was referred as low-pressure CVD (LPCVD). The dominated uniform monolayer coverage of graphene by LPCVD method is proposed to be a "*self-limited*" process, i.e. once the copper surface is fully covered, its catalytic activity for methane decomposition to provide carbon source will be hindered, thus the graphene growth process terminates.[52]

The detailed nucleation and growth process of a graphene single-crystal during CVD can be summarized into three steps as illustrated in Figure 1-4 a.[53]

(1) The copper oxide layer on the Cu foil is reduced by annealing in H_2 atmosphere. This step is very important for increasing the Cu grain size and rearranging the surface morphology to facilitate graphene growth.

(2) Due to the catalytic activity of the Cu surface, methane is decomposed to provide CH_x radicals or C. The uniform nucleation of graphene islands occurs on the surface of Cu foil.

(3) As the growth time increases, the size of each individual graphene domains is still increasing, and finally they merged into a continuous graphene film.

Based on the detailed understanding of the above mechanisms for nucleation and growth, a compromise must be made between lower nucleation rates and faster growth and fuller coverage. A two-step approach during CVD was thus developed by controlling different parameters for nucleation and growth process, i.e. different combinations of temperature and pressure will yield graphene domains in hundreds of squared micrometres large[54] or even millimetre size[55].

Etching of the underlying copper substrates allows the graphene film to be transferred onto other dielectric substrates for further electronics device applications. Poly(methyl methacrylate) (PMMA) is widely as “carrier layer” to maintain the integrity of the graphene film during the “lift-off” wet transfer method, and will be removed by organic solvents after transfer. To date, the largest continuous graphene film by CVD is 30-inch in diagonal length, grown on copper foil in a quartz tube (8-inch diameter) at low pressure, and can be further transferred onto a PET substrate by a roll-to-roll (R2R) setup (Figure 1-4 b-e).[11b] After doping by HNO_3, the sheet resistance (R_s) can reach a resistance as low as 30 Ohm/□ with 90% transmittance, this breakthrough suggests the huge potential of graphene as alternative to Indium Tin Oxide (ITO) in transparent conductors.

In order to lower the growth temperature for further practical applications, other carbon sources in the form of liquids and solids have also been employed for the CVD process.[56]

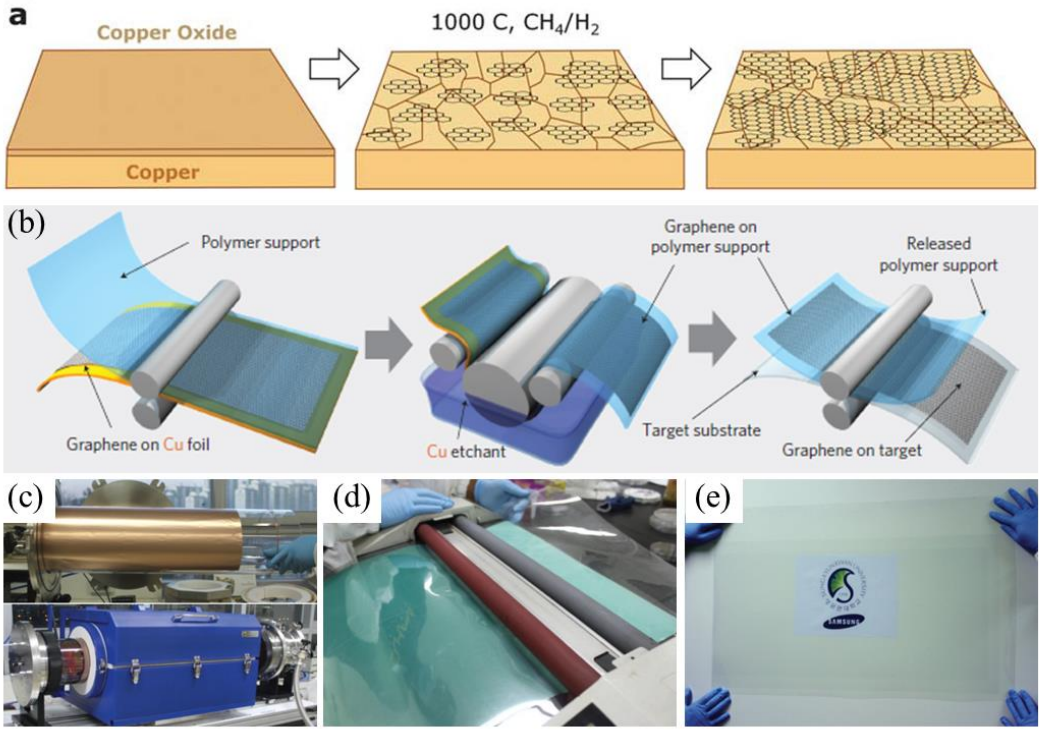

Figure 1-4. a, Schematic illustration of the three main steps of nucleation and growth process relevant for graphene growth on copper by CVD. Reprinted with permission from Ref. [53]; copy right: 2011, The Royal Society of Chemistry. **b,** Schematic description of the roll-based production of graphene films grown on a copper foil. **c,** Copper foil wrapping around a 7.5-inch quartz tube to be inserted into an 8-inch quartz reactor. The lower image shows the stage in which the copper foil reacts with CH_4 and H_2 gases at high temperatures. **d,** Roll-to-roll transfer of graphene films from a thermal release tape to a PET film at 120 °C. **e,** A transparent ultra large-area graphene film transferred on a 35-inch PET sheet. Reprinted with permission from Ref. [11b]; copy right: 2010, Nature publishing group.

There are still several challenges for CVD produced graphene: (1) Limited single crystals size due to low grow rate; (2) Presence of defects, such as vacancies and wrinkles in the crystal structure, or holes, cracks, and impurities which are introduced during the film transfer process. (3) Fine control of the graphene layer number and stacking order during growth. (4) Optimized growth conditions based on low temperature and ambient pressure are still preferred to lower the cost. (5) Multiple film-transfer process degrades the graphene quality and increases the overall cost. Thus direct growth of graphene on target substrates is preferred.

1.2.4 **Organic synthesis from PAH**

The synthesis of large interconnected polycyclic aromatic hydrocarbons (PAHs), which can be regarded as small graphene segments from the "molecular" to "macromolecular" level, is attracting great interest as possible alternative route towards graphene production. As mentioned above, "top-down" approaches for graphene production suffer from uncontrollable size and edge structures, using the "tool box" of organic synthesis is a controllable "bottom-up" approach to tailor the shape and edge of graphene within atomic precision. The advantage of this approach is the high versatility and modified solubility, based on PAHs substituted with different side chains.

The typical synthesis procedure for large PAH molecules is based on the intramolecular cyclodehydrogenanion, and hexa-*peri*-hexabenzocoronene (HBC) is one of the most extensively studied PAH molecules. The [redacted] group pioneered this field, in 2008 they reported the synthesis of nanoribbons like PAHs with lengths up to 12 nm.[57] In 2014, they descripted a solution synthesis of ultralong (>200 nm) graphene nanoribbons (GNR) with well-defined structure and excellent charge-carrier mobilities (from THz measurement).[58] They also introduced the on-surface synthesis of GNRs with length up to 30 nm (under STM), based molecular precursors coupling and cyclodehydrogenation in UHV conditions.[59] And till today, the largest graphene-type molecule based on organic synthesis is C_{222}, a disk-shape nanographene (NG) composed of 222 sp^2 carbon atoms.[60]

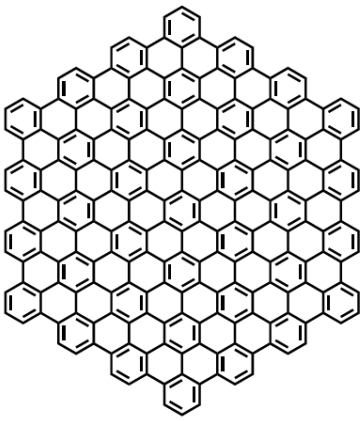

Figure 1-5. Molecular structure of the disk-shape nanographene molecule, C_{222}.

Besides the cyclodehydrogenation and planarization of dendritic precursors to obtain NGs, the direct pyrolysis of PAHs is also an efficient approach towards graphene-based

conductive films. The pyrolysis of hexadodecyl-substituted superphenalene C_{96}-C_{12} film has been successfully employed as a route to transparent electrode for organic solar cells.[61]

So far, the major drawback of this approach is the limited size of PAHs based NG-type molecules and the scale-up. This is because the only way to extend the size of NG is by increasing the molecular weight, which will generally decrease the solubility of the PAH and increase the chance of side reactions. Under such conditions, keeping a planar morphology with certain dispersibility for large PAHs is always very challenging. Moreover, for the surface-assisted synthesis of GNRs, the H passivation at the termini during the polymerization step is a challenging issue, which may result in the limited GNR growth.[62]

1.3 **Transfer and Processing of graphene**

After the production of graphene flakes or films, suitable transfer and processing procedures are required before further practical applications. The ideal case would be to grow graphene films directly on surfaces where they are needed. However, till today, this goal is far-fetched, especially on non-metallic substrates.

1.3.1 **Transfer of mechanically exfoliated graphene flakes**

So far, different transfer processes of mechanically exfoliated graphene flakes can be classified as “wet” or “dry”. For the wet transfer process, first a PMMA sacrificial layer is spin-coated on top of graphene. After solidification, the sample is immersed in an alkaline solution, which will partially etch the SiO_2 interface to release the polymer-coated graphene flake. Thus the sample can be transferred onto any substrates. At last, PMMA is dissolved by an organic solvent like acetone, releasing graphene. During this process, the graphene flake is in contact with a liquid at some stage, which may introduce contaminations.

In order to obtain a clean interface of graphene for the fabrication of heterostructures with other 2D crystals, dry transfer methods are developed. The main difference from wet transfer is: the upper face of graphene flake is prohibited from any liquid contacts, and directly pressed onto target substrates, thus minimizing contamination; while the other side is still in contact with PMMA and a releasing layer, which will be dissolved in steps.

1.3.2 **Transfer of CVD graphene films**

The transfer of CVD graphene films is similar to the above mentioned wet transfer process. In 2009, the transfer of graphene films grown by CVD on Ni was first reported. A layer of PMMA was used to support graphene, and the Ni substrate underneath was etched away by HCl aqueous solution. The floating PMMA/graphene was transferred onto a target substrate, and then the PMMA layer was removed by solvent rinsing.[63] In the same year, the [redacted] group reported the transfer of graphene films grown by CVD on Cu. A PMMA sacrificial layer was also used and the Cu was etched by iron nitrite aqueous solution.[64] This is the basis for the later thermal release tape assisted roll-to-roll transfer of graphene films as large as 30-inch (diagonal length).[11b] In order to avoid the Fe contamination caused by the $FeCl_3$ etchant, ammonium persulfate [$(NH_4)_2S_2O_8$] was also used to etch the Cu foil.[65]

To transfer CVD graphene without degrading the quality is a basic requirement for its large-scale applications. Till today, the PMMA sacrificial layer based method is still widely used for CVD graphene film transfer. However, the major drawback of this method is the insulating PMMA residues on graphene surface after the wet transfer process, and the solvent rinsing process may also introduce structural damages such as cracks to the film.[66]

In order to tackle this problem, [redacted] developed a “clean-lifting transfer” (CLT, Figure 1-6), which does not involve any polymeric support or adhesives, thus avoid unnecessary residues and rinsing process.[67] First, they used an electrostatic generator to form efficient accumulated charges on the surface of target substrates. Due to the electrostatic force between the Cu foil and the accumulated charges, the graphene/Cu sample was attracted onto the target substrate. After pressing to enable uniform attachment between graphene and the substrate, the Cu foil was etched by immersing the whole substrate into iron nitrate aqueous solution. This novel approach realised an ideally clean transfer of CVD graphene, and paved the way for a cost- and time-effective production of graphene in wafer scale for electronic devices.

PDMS stamps are also found to be efficient for graphene transfer. The stamps are first directly/tightly attached to the graphene surface, followed by the chemical etching of metallic substrates leaving only graphene on the stamps. The transfer process is then finished by pressing and peeling off the PDMS stamps onto other target substrates.

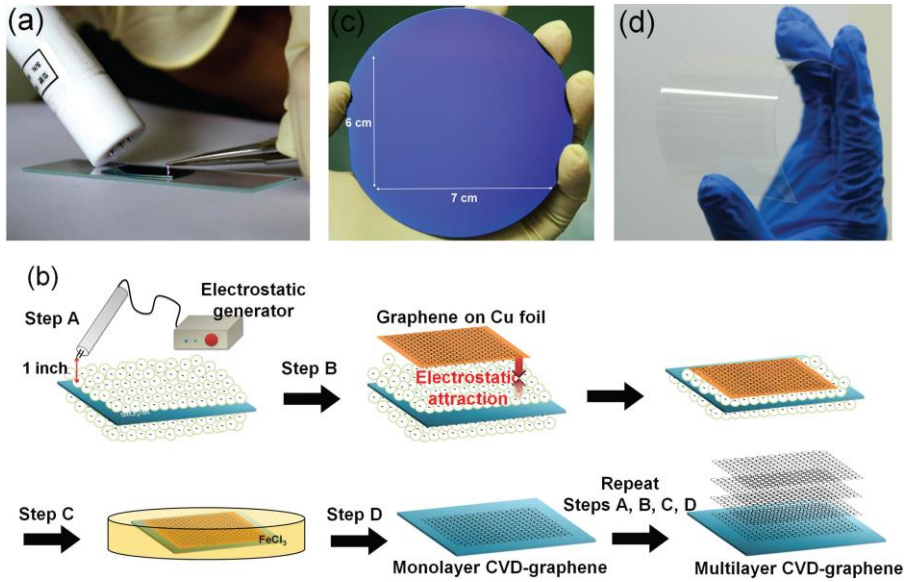

Figure 1-6. a, Photograph of electrostatic discharging on the substrate using an electrostatic generator. **b**, Schematic illustrations of the CLT processes of as-grown graphene on Cu foil onto a substrate. Large-area graphene films transferred onto **c**, a SiO_2/Si wafer and **d**, a flexible PET substrate using the CLT technique. Reprinted with permission from Ref. [67]; copy right: 2013, "John Wiley and Sons" publishing group.

1.3.3 **Processing of graphene dispersions**

Graphene dispersions obtained from exfoliation methods can be handled by various processing methods, including Langmuir-Blodgett (LB) assembly, vacuum filtration, spin-coating, spray-coating, rod-coating, ink-jet printing etc., some of which are compatible with large-scale R2R processes.

In 2008, after producing stable graphene suspensions in organic solvents, the [redacted] group assembled graphene sheets in a layer-by-layer packing manner by the **LB method** for the fabrication of transparent conductive films.[32] This was accomplished by first adding graphene suspensions onto the water surface (floating due to hydrophobicity), then vaporizing the organic solvent, followed by compressing the floating graphene sheets, and consequently transferring the graphene LB film onto target substrates by dip-coating. The whole process was repeated to achieve multilayer graphene films. The obtained three-layer LB film showed Rs of 8000 Ohm/□, with transmittance over 80% at 1000 nm wavelength.

In 2008, the [redacted] group demonstrated a **vacuum filtration** method to deposit RGO thin films on various substrates, in a uniform and controllable manner across large areas.[68] During the filtration of GO dispersion through a membrane, water was able to freely pass through the pores while GO sheets became lodged upon the filter. The whole process is self-regulating, which allows fine control over the graphene film thickness ranging from monolayer to several layers by varying the concentration or volume of GO dispersion. This method can be applied to both rigid and flexible substrates.

In 2009, the [redacted] group fabricated graphene films by **spin-coating** of GO water dispersion and subsequent thermal annealing in vacuum (1100 °C, 3h), which can be successfully applied as transparent conductive electrode in OLEDs.[69] The optimised thickness of the film is 7 nm, with R_s and transmission of 800 Ohm/□ and 82% transmittance (at 550 nm). The above mentioned methods are facile for lab use, however cannot be easily scaled up for large area film production in industry, thus hinders their future practical applications.

Continuous **R2R** approaches are ideal for high throughput productions, and become more and more attractive due to their manufacturing characteristics, i.e. programmable control, fast speed, low cost, and over large area flexible substrates. Based on different purposes, R2R techniques can process functional inks into uniform coating over the whole substrate area or with specific patterns. Although still in development, R2R techniques can already achieve similar resolutions comparing with conventional vacuum deposition or lithography technologies.[70] In a standard R2R process, some well-established solution processing methods, e.g., spray-coating, rod-coating, screen-printing, Gravure-printing, and ink-jet printing, are usually applied.

Spray coating usually employs an airbrush system, which is widely used in painting arts. During each spray process, ink aerosols are formed under certain pressure and further dried on a substrate, which result in uniform nanometre or micrometre thick thin film coatings. In 2010, [redacted] reported the facile fabrication and reduction of RGO films by spray coating of GO-hydrazine dispersions on preheated substrates.[71] The excess amount of hydrazine would guarantee the reduction from GO to RGO upon film formation process. The obtained RGO films showed R_s of 2200 Ohm/□, with a transmittance of 84% at 550 nm wavelength.

Rod-coating, also known as Mayer bar coating (invented by Charles W. Mayer), employs a stainless steel rod wound with a tight wire spiral, which creates a thin layer of ink (~tens μms) on target substrates during coating. In 2012, the [redacted] group reported large-scale fabrication of RGO films directly on flexible substrates (**Figure 1-7**a), by combining a rod-coating technique for GO dispersion and subsequent room-temperature reduction of the film.[26] The obtained graphene films displayed excellent uniformity, good transparency and conductivity, and great flexibility in a touch screen, which demonstrated huge potential for the R2R production of RGO films in various flexible electronic devices.

Spray-coating and rod-coating can both form uniform films over the whole substrate areas, without specific patterns. Thus various printing techniques are employed for the controllable selective deposition of inks to create desired patterns on the substrates, especially with high resolutions of tens of microns.

Screen-printing uses a pre-patterned stencil, which is placed closely (several millimetres) above the surface of the target substrate. During deposition, the ink is loaded onto the stencil, followed by a rubber blade sweeping slowly across the whole surface. Thus the ink flows from the stencil to the surface of the substrate. The pattern transfer is accomplished upon drying. In 2015, [redacted] and co-workers utilized screen-printing to achieve high-resolution (40 μm) patterns based on pristine graphene (Figure 1-7b).[72]

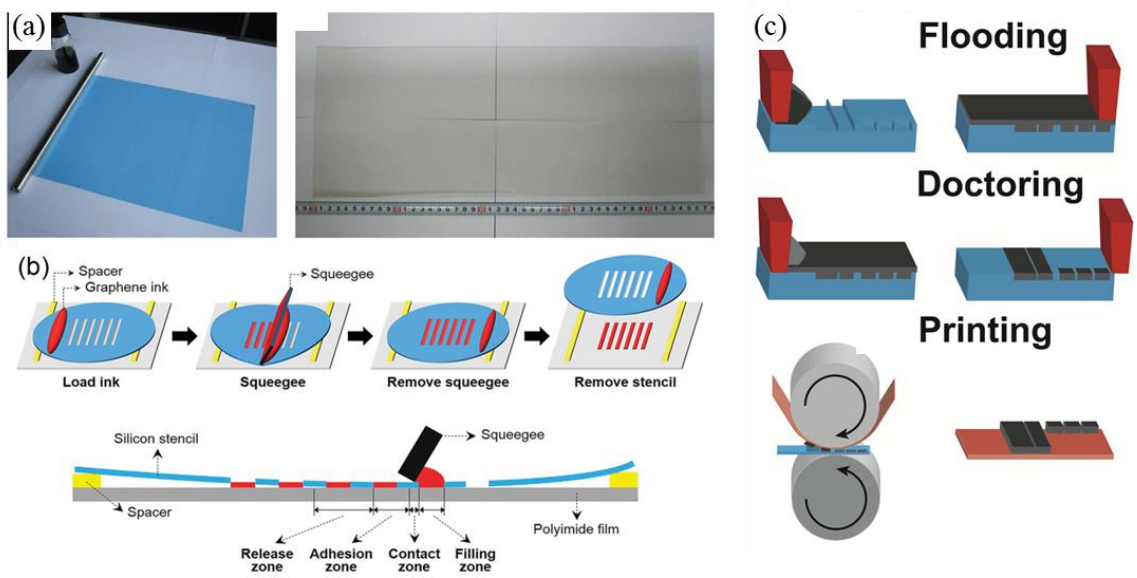

Figure 1-7. a, Rod-coating setup and picture of a large-scale GO film deposited by rod-coating on PET substrate. **b**, Schematic process of screen-printing using a thin silicon stencil

based on pristine graphene ink. **c**, Schematic process of gravure-printing of pristine graphene ink. Reprinted with permission from Ref. [26], [72] and [74]; copy right: 2012, 2015, and 2014, "John Wiley and Sons" publishing group.

Flexographic printing uses a flexible relief plate to transfer specific patterns onto target substrates. The raised sections (pattern) on the relief plate are coated with ink, followed by transferring onto target substrates by contact printing. Flexographic printing of a graphene ink on plastic substrates was demonstrated in 2014.[73]

Gravure-printing, derived from the Italian word for carving, employs an opposite type of patterning plate from flexographic printing. The carved metallic plate for gravure-printing is composed of individual empty areas which represent pixels, and the volume of the empty areas defines the amount of stored ink. In 2014, the [redacted] group demonstrated the rapid production of conductive graphene patterns on flexible substrates by gravure printing, which was consisting of flooding-doctoring-printing process (Figure 1-7c).[74] The ink was based on pristine graphene sheets from liquid phase exfoliation. Through careful tailoring of the ink viscosity and printing parameters, uniformly patterned lines with resolution of 30 μm are printed over large areas. Electrical conductivity as high as 10,000 S m^{-1} was achieved for the printed graphene lines.

All of the above mentioned printing techniques require a stencil or specially designed and carved hard plate with high resolutions, whereas the **ink-jet printing** technique offers a mask-less process with the great ease of designable patterns, which can be automatically controlled by a computer with less human involvement. The selective deposition during ink-jet printing also reduces the ink consumption significantly, rendering itself a cost-effective process. Based on these advantages, ink-jet printing of high-mobility graphene films is expected to play an important role for future generation electronics, such as all-carbon post-CMOS electronics. In 2012, the [redacted] group reported the ink-jet printing of pristine graphene dispersions obtained from liquid phase exfoliation.[75] The printed graphene thin-film transistors showed a high mobility of 95 cm^2 V^{-1} s^{-1}, as well as transparent conductive patterns with transmittance of 80 % and R_s of 30,000 Ohm/□. They also demonstrated in order to minimize the clustering of the nozzle, that the graphene flake size should be smaller

than 1/50 of the nozzle diameter, i.e., for a nozzle diameter of 50 μm, the graphene flake size should be less than 1 μm.

Moreover, recent developed **3D printing** techniques and **laser writing** techniques have also been applied for graphene electrodes fabrications.[76]

1.4 **Applications of graphene-based electrodes**

Motivated by many appealing and unique properties of graphene, it is believed that this material could revolutionize many aspects of our daily lifes, in terms of various practical applications. Among these, employing graphene as electrode materials is the core constituent for the realization of flexible electronics and optoelectronics. To achieve equal device performance on flexible substrates, compared with those from well-established technologies on rigid substrates, but in light weight, bendable, stretchable and even wearable formats, would encourage many novel applications. This could also lead to reduced costs of current electronic devices by the integration of various R2R manufacturing approaches as discussed in section **1.3**.

Graphene-based electrodes, fabricated via suitable transfer and processing methods, can be available over a large scale complying with various R_s and transmittance requirements, according to different device applications. E.g. regarding graphene based transparent conductive electrodes (TCEs), for touch panels, R_s over few hundred Ohm/□ would still be acceptable, whereas less than 50 Ohm/□ are usually needed for electrodes in organic solar cells and OLEDs.[77] High transparency is certainly required for these optoelectronic devices, however not mandatory for most energy storage devices, which preferentially demand both high conductivity and surface area. Thus, suitable graphene production and processing methods should be chosen according to different proposes.

1.4.1 **Transparent conductive electrodes for optoelectronic devices**

The current dominant material in the market of TCEs is ITO, which is composed of ~90% In_2O_3 and ~10% SnO_2. The commercial available ITO normally shows 80% transmittance at 550 nm with R_s around 10 Ohm/□ on glass, and 60-300 Ohm/□ on PET.

However, ITO suffers from several fatal limitations: (1) the optical and electrical properties of ITO can be significantly affected by impurities; (2) the scarcity of indium on earth leads to the high costs of ITO; (3) corrosion issues, ITO is very sensitive to both acidic and base conditions; (4) processing difficulties, it is not easy to pattern ITO electrodes according to different device requirements. (5) Most importantly, the inflexible nature: ITO is very brittle and cannot afford bending or stretching conditions, which is highly demanded for future generation flexible devices or even electronic skins. Thus, the search for ITO replacement materials becomes a hot topic in the past decade.

Single layer graphene only absorbs 2.3% of the incoming light, and few layer graphene films have higher transmittance over a wider wavelength range compared with ITO films, CNT films, and thin metallic films. Such high transmittance combined with its high conductivity, in addition to the mechanical stability under extreme bending and stretching conditions, makes graphene-based TCEs ideal for integration in to flexible substrates. This also brings a new level of "operational flexibility", which is unlikely for current TCEs on rigid glass substrates, and could potentially lower the manufacturing cost.

Moreover, the work function of graphene electrodes can be readily tuned via doping or chemical functionalisation, to achieve proper ohmic contacts and low contact resistance at the interface in organic electronic devices. The contact between inorganic metals and organic semiconductors is generally bad. However, graphene, which is composed of sp^2-hybridized carbon atoms packed into a 2D honeycomb lattice, possesses a similar molecular structure to that of conjugated molecules, such as anthracene and pentacene. The strong interactions between graphene and these conjugated molecules could form excellent interface contacts. Furthermore, the low work function of metallic electrodes like Cu or Ag usually leads to a large hole injection barrier, while graphene has a higher work function of 4.5-4.9 eV, which is more matching with the highest occupied molecular orbital (HOMO) level of conjugated molecules to realize ohmic contacts at the interface.

Therefore, graphene based Source/Drain (S/D) electrodes are favourable choice in OFETs. In 2008, the [redacted] and [redacted] group reported a facile approach to obtain patterned graphene S/D electrodes on SiO_2/Si substrates.[78] The graphene electrodes exhibited outstanding interface contact with pentacene and excellent hole-injection characteristics. The OFET device showed a high mobility of 0.53 $cm^2\ V^{-1}\ s^{-1}$, which is one order of magnitude

higher than devices based on Cu or Ag S/D electrodes. This work successfully demonstrated the major advantages of graphene over metals when employed as electrode materials.

Besides the CVD graphene films, RGO and liquid-phase exfoliated graphene films discussed before, some hybrid structures were also employed to fabricate TCEs. Among them, graphene/metal grids showed R_s of 20 Ohm/□ with 90% transmittance,[79] solution processed graphene/CNTs hybrid film showed R_s of 100 Ohm/□ with 80% transmittance.[80]

Graphene can provide TCEs or counter-electrodes for different optoelectronic devices (Figure 1-8), including inorganic or organic solar cells, DSSCs, OLEDs, capacitive touch screens, and smart windows.[81] Here we only discuss graphene based TCEs for organic solar cells and OLEDs.

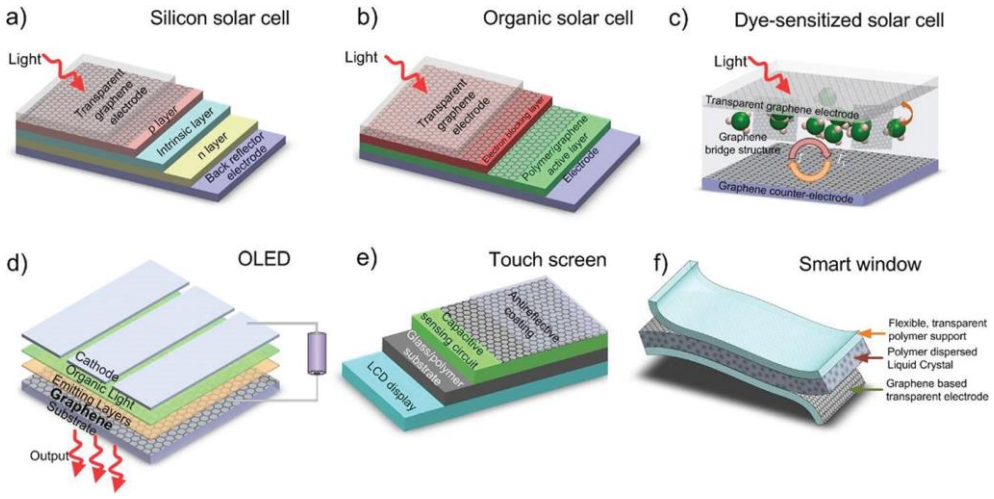

Figure 1-8. Device architectures of graphene-based optoelectronics. **a**, inorganic solar cell, **b**, organic solar cell, **c**, DSSC, **d**, organic LED, **e**, capacitive touch screen, **f**, smart windows. Reprinted with permission from Ref. [81]; copy right: 2010, Nature publishing group.

The requirements of TCE layers in all thin-film solar cells are quite strict since this has a major impact on the overall power conversion efficiency. Theoretical calculations suggested that an ideal TCE should have a transparency over 90% and a R_s less than 10 Ohm/□.[82] In 2008, the [redacted] group reported graphene films as TCE in organic solar cell, by spin-coating a GO dispersion and subsequent thermal annealing in vacuum (1100 ^{0}C, 3h).[83] For film thicknesses less than 20 nm, the optical transmittance is around 80%, the

corresponding R_s varies from 5 k to 1 M Ohm/□. Such high R_s resulted in the lower short circuit current and fill factor of the bilayer solar cell, leading to a low efficiency.

A breakthrough in this field was achieved in 2014. A group at MIT employed CVD graphene films (R_s of 300 Ohm/□, 92% transmittance) as anode or cathode for flexible polymer solar cells with record-high power conversion efficiencies of 6.1% and 7.1%, respectively.[84] This result is comparable to those of ITO based reference cells. Such a high performance was achieved based on blends of low bandgap polymer PTB7 and $PC_{71}BM$, through interface modification via thermal treatment of a MoO_3 electron blocking layer and direct deposition of a ZnO electron transporting layer on graphene. They also demonstrated flexible solar cells based on graphene electrodes on polyethylene naphthalate substrates, and showed the device stability under different bending conditions, which opened up a promising future of graphene-based TCEs for flexible optoelectronic devices.

Generally, the requirement of TCEs for OLED is quite similar to that of organic solar cells, since they have the same laminated sandwiched structures. The only difference is the electron-photon conversion process, whereas electron-hole pairs are generated by incident photons in organic solar cells, while photons are formed via injected electron-hole pairs in OLEDs. In an OLED, the electroluminescent layer is sandwiched between two charge-injecting electrodes, one of which should be transparent for light output. Holes are injected into the HOMO of the light-emitting molecule/polymer from the anode, with electrons injected into the LUMO from the cathode simultaneously. For efficient injection, the work function of both anode and cathode should match the HOMO and LUMO of various light-emitting molecules/polymers, which makes graphene promising in this field.

After the [redacted] group reported the first case of RGO film based TCE for OLED in 2009, the [redacted] group demonstrated flexible and highly efficient OLED based on graphene TCE in 2012.[85] They transferred four-layers of CVD graphene film on PET substrates as anode, which were subsequently p-doped by HNO_3 or $AuCl_3$ to reduce the R_s to 30 Ohm/□. A conducting polymer composition was used to modify the surface of graphene anode, creating a gradient work function from graphene to the overlying NPB layer. The surface work function of graphene film was increased to 5.95 eV, which is close to the HOMO level of NPB (5.4 eV), thus facilitating the hole injections in the overall device. Extremely high maximum current efficiencies (30.2 cd A^{-1} and 98.1 cd A^{-1}) and luminous efficiencies (37.2 lm W^{-1} and 102.7 lm W^{-1}) were achieved in the fabricated flexible fluorescent and

phosphorescent OLEDs, which are significantly higher than those of optimized reference devices based on ITO. Flexible white OLED lighting devices were also fabricated using such graphene TCE. These results demonstrated the huge potential of graphene based TCEs in a wide variety of flexible organic optoelectronic devices, maintaining high-performance.

1.4.2 **Electrochemical active electrodes for energy storage devices**

Due to the limited availability of fossil fuels on earth and the following greenhouse effects generated from burning of fossil fuels, societies are facing an energy crisis all over the world in this century. Exploring renewable energy sources from solar, wind etc. requires efficient energy storage technologies. Moreover, with the fast-growing market for portable and wearable electronic devices, as well as electric vehicles, there is an urgent demand for highly efficient and environmentally friendly energy storage devices (ESDs).

Among all the developed ESDs, batteries and supercapacitors (SCs) are the two most promising technological systems that have found a broad range of applications on various scales, due to their outstanding electrochemical performances.[86] However, current state-of-the-art batteries suffer from various limitations, including: (1) low power density, which severely hinders their practical applications where a high power discharge rate is required, such as electric vehicles; (2) abrupt failure and poor low-temperature kinetics; (3) limited cycle life, which is due to the lack of fully reversible redox reactions during charging/discharging processes; (4) safety concerns associated with the use of lithium[87] and the risk of overheating from redox reactions, the recent fire hazard of some cellphones raised peoples' concerns again.

According to the above mentioned critical issues, batteries alone are unable to perform as compact, durable and reliable ESDs for power supply in consumer, industry, and military applications. SCs, also known as ultra-capacitors or electrochemical capacitors, have attracted much attention as promising candidate for ESDs because of the following **advantages**:[88]

(1) High power density. As illustrated in Figure 1-9, where various ESDs are listed and compared in the *Ragone plot*, SCs can fill the gap between batteries and electrolytic capacitors in terms of specific power densities as well as specific energy densities. SCs

display much higher power densities than lithium ion batteries. Since SCs store charges at/near the surfaces of the electrode materials, rather than within the entire bulky electrodes (as in batteries), the charging-discharging process will not be limited by ionic conduction, thus results in fast charging-discharging rates. Also shown in Figure 1-9, SCs can be fully charged or discharged in several seconds, while for batteries the charging time is normally on the scale of hours. These fast charging-discharging rates lead to the high power densities of SCs.

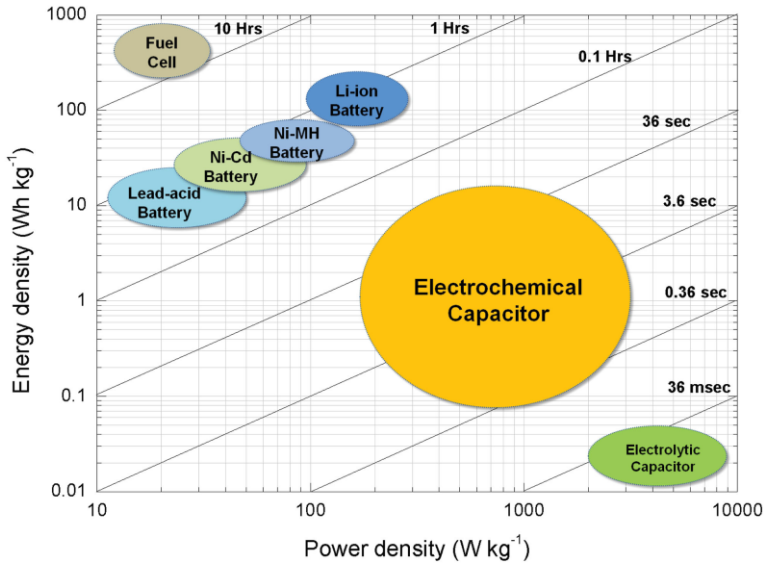

Figure 1-9. An illustration of the power and energy densities for several electrical energy storage devices via Ragone plot. Reprinted with permission from Ref. [90]; copy right: 2015, "John Wiley and Sons" publishing group.

(2) Long cycle life and shelf life. Due to the non-Faradic nature of SCs based on electrical double layer capacitance, no charge transfer redox reactions are involved during charging-discharging. Thus SCs have almost unlimited cycle life in theory. SCs can be operated at high rates over 100,000 cycles with only small changes in their characteristics. Moreover, SCs can maintain their capacitance and are capable of being recharged to their original condition upon being left on the shelf unused for months.

(3) Safety and high efficiency. In general, SCs are much safer than batteries, especially lithium-ion batteries. Besides, due to the simpler charge storage mechanisms, SCs generate less thermochemical heat during each cycle, which avoid the risks of overheating. This also suggests the high cycle efficiency of SCs (around 95%).

(4) Wide range of operating temperatures. SCs can function well at both high and low temperatures. Their typical operating temperature ranges from -40 to 70 °C, which is quite enough for our daily life situations.

(5) Environmentally friendly. Generally, SCs do not employ hazardous or toxic materials, and their waste materials can be easily disposed.

Based on the above mentioned advantages, SCs are currently widely used in consumer electronics, industrial power managements, as well as emergency doors on airplanes, which highlight their safe and reliable performance. Another promising application of SCs is their use in hybrid electric vehicles, where SCs are integrated with batteries to temporarily restore kinetic energies during braking with a high-power capability.

SC Charge Storage Mechanisms

Generally, there are two different charge storage mechanisms for the operation of SCs, including (a) electrostatically storing the charges via electrochemical adsorption/desorption of cations and anions at the electrode/electrolyte interface (i.e., electrical double layer capacitance (EDLC), Figure 1-10a), and (b) storing the charges at the electrode surface via fast and reversible Faradic redox reactions (i.e., pseudo-capacitance, Figure 1-10b).[89]

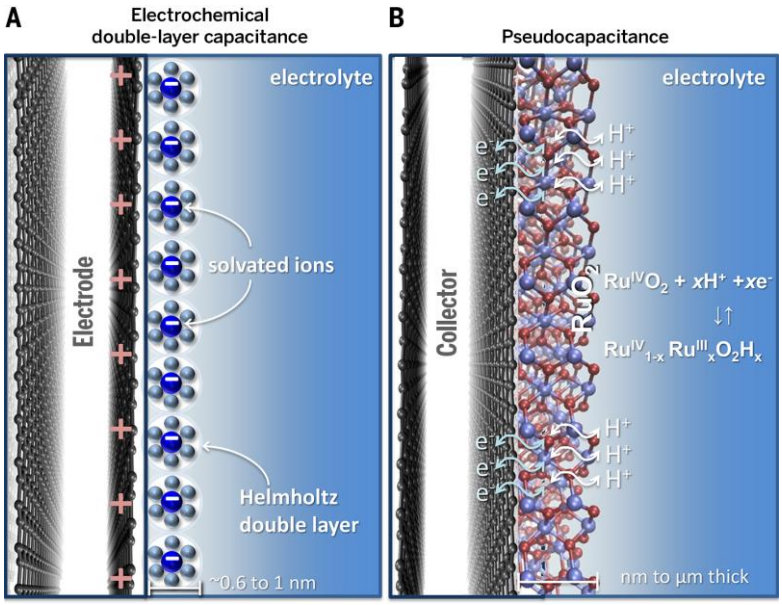

Figure 1-10. Scheme of charge storage in supercapacitors. **a**, Ion adsorption at the electrode surface (EDLC). **b**, Charge transfer near the surface of the electrode (pseudo-capacitance). Reprinted with permission from Ref. [89]; copy right: 2015, Science publishing group.

(a) The charge storage mechanism of EDLC.

Electric double layer (EDL) is defined as the two electrically charged layers formed at the electrode/electrolyte interfaces, and the resulting potential-dependent charge storage ability is ascribed to EDLC.[90]

[redacted] first proposed and modeled the concept of EDL in the 19th century, when he was investigating the charge distribution at the interface of colloidal particles, thus EDL is also referred to as Helmholtz double-layer. The EDL model suggests that two layers of opposite charges are formed at the electrode/electrolyte interfaces and are separated in an atomic scale distance. This model is similar to that of conventional two-plate capacitors. Thus, the capacitance of EDL-type SCs can be generally assumed based on the simple model of two-plate capacitors:

$$C = \frac{\varepsilon_r \varepsilon_0}{d} A$$

where ε_r is the electrolyte dielectric constant, ε_0 is the vacuum permittivity, A is the accessible specific surface area of the electrode, and d is the effective thickness of the EDL (the Debye length).

Based on this equation, it is easy to understand that conventional two-plate capacitors are only capable of storing little energy, because of the limited charge storage areas and geometric constrains of the separation distance between the two charged plates; whereas SCs based on EDLC, which normally has porous structured electrodes, can store much more energy due to the presence of large electrode/electrolyte interfacial areas and the atomic scale charge separation distances. Later, the combined [redacted] model was established to more accurately describe the charge distribution of EDLs, by recognizing the inner [redacted] plane (IHP, also referred to as compact layer or Stern layer) and outer [redacted] plane (OHP, also referred to as diffuse layer).

In 1957, [redacted] first proposed the storage and delivery of electricity via EDL (U.S. Patent 2 800 616), i.e., SCs based on EDLC. During the past decades, high-surface-area carbon materials were widely employed as working electrodes of SCs. Because of their large surface areas, such SCs can store much more electricity for which the capacitance is usually evaluated in Farad (F), whereas the capacitance of conventional electrolytic and dielectric capacitors is evaluated in microfarads (μF) and picofarads (pF), respectively.

(b) The charge storage mechanism of Pseudo-capacitance.

Compared with EDLC, pseudo-capacitance originates from thermodynamic reasons. Upon an applied potential, fast and highly reversible redox reactions between the electrolyte and electro-active species take place at/near the surfaces of electrode materials. The involved passages of charges across the EDLs result in a Faradaic current through the SC electrode. Such a Faradaic charge transfer process results in an additional potential-dependent charge accumulation (charging) or release (discharging) behavior, the corresponding dQ/dV is equivalent to a capacitance, which is defined as the pseudo-capacitance.

There are mainly three types of Faradaic processes for pseudo-capacitive electrodes: (1) reversible adsorption (such as adsorption-desorption of hydrogen on the surface of platinum or gold); (2) redox reactions of transition metal oxides (e.g. ruthenium oxide,[91] manganese oxide,[92] and vanadium nitride[93]), and (3) reversible electrochemical doping-dedoping in electrically conductive polymers (e.g. polyaniline and polypyrrole)[94].

Hydrous ruthenium oxide is a good example of pseudo-capacitive materials, due to its intrinsic reversibility for various redox transitions (i.e., Ru(IV)/Ru(III) and Ru(III)/Ru(II)). During charging, the surface regions of RuO_2 are reduced to lower oxidation states, coupled with hydrogen cations adsorption/insertion from the electrolyte. Upon discharging, the process can be almost fully reversed. The whole charging/discharging process can be expressed as:

$$RuO_x(OH)_y + \delta H^+ + \delta e^- \Leftrightarrow RuO_{x-\delta}(OH)_{y+\delta}$$

One major advantage of such Faradaic electrochemical processes is that they can readily occur both on the surface and in the bulk near the surface of the electrode materials. Thus SCs based on pseudo-capacitance exhibits capacitance and energy density values 10-100 times larger than SCs based on EDLC, as reported by Conway et al.[95] However, SCs based on pseudo-capacitance suffers from lower power densities, since Faradaic processes are normally slower than non-Faradaic processes. Moreover, the limited stability issue during cycling is also challenging.

Above all, for both charge storage mechanisms of EDLC and pseudo-capacitance, large surface area, appropriate pore-size distribution, and high conductivity are essential requirements for the electrode materials to achieve better electrochemical performance.

Figure of merit for SC performance evaluation

Cyclic voltammetry (CV), galvanostatic charge/discharge (GCD), and electrochemical impedance spectroscopy (EIS) measurements are commonly used to evaluate the performance of a supercapacitor. In principle, there are three fundamental parameters: voltage (V), current (I), and time (t). Other figure of merits, including the capacitance (C), energy (E) and power (P) densities, operating voltage (V_O) and equivalent series resistance (R_{ES}) of the SC can be calculated from them.

When addressing the total charge storage ability of a SC device, the total capacitance C_T of a SC is a calculated by the stored electrical charge ΔQ under a given voltage change ΔV:

$$C_T = \Delta Q / \Delta V$$

Generally, a more intrinsic specific capacitance C_S is employed to demonstrate the charge storage ability of SC materials:

$$C_S = \Delta Q / \Delta V \Pi$$

where Π can be the mass, surface area and volume of the SC electrode material, and the result in specific capacitance C_S is often named correspondingly as the gravimetric capacitance (F g^{-1}), areal capacitance (F cm^{-2}), and volumetric capacitance (F cm^{-3}).

The MSC device capacitance values can be calculated from the CV curves according to the following equation:

$$C_{device} = \frac{1}{\nu(V_f - V_i)} \int_{V_i}^{V_f} I(V) dV$$

Where ν is the scan rate, V_f and V_i is are the integration potential limits of the CV curve. I (V) is the voltammetric discharge current. Specific areal and volumetric capacitance was calculated according to:

$$C_{areal} = C_{device} / A$$

where A is the total area of the device.

$$C_{volumetric} = C_{device} / V$$

where V is the total volume of the device.

As for GCD tests, a constant current is used, thus C_T calculation can be expressed as:

$$C_T = I * \Delta t / \Delta V$$

where I is the constant discharge current, Δt is the discharge time, ΔV is the voltage change.

The energy density of a MSC device can be calculated as:

$$E = \frac{1}{2} \times C_{volumetric} \times \frac{(\Delta V)^2}{3600}$$

where E is the energy density (in Wh cm^{-3}), ΔV is the discharge voltage range.

The power density of the MSC device can be calculated as:

$$P = \frac{E}{\Delta t} \times 3600$$

where P is the power density (in W cm^{-3}), Δt is the discharge time (in seconds).

The operating voltage V_O is defined as the potential applied to the electrochemical system or the suitable potential window within which a SC device is normally operated. Both the solvent of electrolytes and cell configuration determines the V_O. In an aqueous system, V_O is normally 1 V due to the decomposition potential of water. While based on organic electrolyte, the V_O varies between 2.3 to 2.7 V. In an aqueous system based on an asymmetric configuration, V_O can be increased to 2.0-2.3 V by employing different SC electrode materials.

A SC has its own internal resistance, which can be regarded as an equal RC circuit: a capacitor (C) connected in series with a resistor (R_{ES}). That is how the equivalent series resistance (R_{ES}) is defined. R_{ES} is normally evaluated through the analysis of the IR drop or voltage variation at the initial stage of the discharging curve from GCD tests. By applying Ohm's law to the IR drop, R_{ES} can be obtained readily:

$$R_{ES} = \Delta V / \Delta I$$

where ΔV and ΔI are the voltage and current of the IR drop, respectively.

Graphene based materials for SCs and micro-supercapacitors

Besides being employed as the charge conductors for optoelectronic devices, graphene based materials can also store massive amounts of electrical charges for ESDs. Particularly, the unique 2D nature of graphene leads to an extraordinarily high specific surface area of up to 2600 m^2 g^{-1}, which is much larger than that of other carbon based materials, e.g., carbon black (<900 m^2 g^{-1}) and CNTs (100 to 1000 m^2 g^{-1})[96], and is similar to that of activated porous carbon[97]. For a single-layer graphene, the intrinsic capacitance was reported to be ~21 μF cm^{-2}, which sets the upper limit for EDLC for all carbon-based materials. The large specific surface area combined with its excellent electrical conductivity, high mechanical strength, ease of surface-functionalization, and great potential for mass production, makes graphene an ideal platform for SC electrode applications.

RGO was first employed as SC electrode, a specific capacitance as high as 190 F g^{-1} was obtained in an aqueous electrolyte. In real device applications, a large packing density is always preferred to avoid empty space in the electrode and to achieve a better performance. Through capillary compression of RGO, a specific capacitance of 206 F cm^{-3} was obtained in ionic liquids, with an electrode density of 1.25 g cm^{-3}.[98]

In 2011, the [redacted] group reported the chemical activation of RGO, which can create 3D hierarchically distributed meso- and microporous carbon network, with a specific surface area of up to 3,100 m^2 g^{-1}, a high electrical conductivity, and low oxygen/hydrogen content. The highly curved graphene walls can also prevent re-stacking during cycling. Such activated graphene delivered high gravimetric capacitance of 200 F g^{-1} in ionic liquid electrolytes.

In 2012, the [redacted] group developed a facile laser scribing approach to reduce GO films into graphene, which can be directly used as SC electrodes without the need for binders or current collectors. Based on a typical sandwiched structure, the device showed an areal capacitance of up to 4.82 mF cm^{-2} in organic electrolyte, and exhibited an energy density of 1.36 mWh cm^{-3}, as well as a power density of 20 W cm^{-3}.

Compared with the conventional sandwiched structured SCs, the recently developed in-plane structured micro-supercapacitors (MSCs) can significantly improve the device performance, due to the short ion diffusion length (Figure 1-11).[30a, 87c, 99]

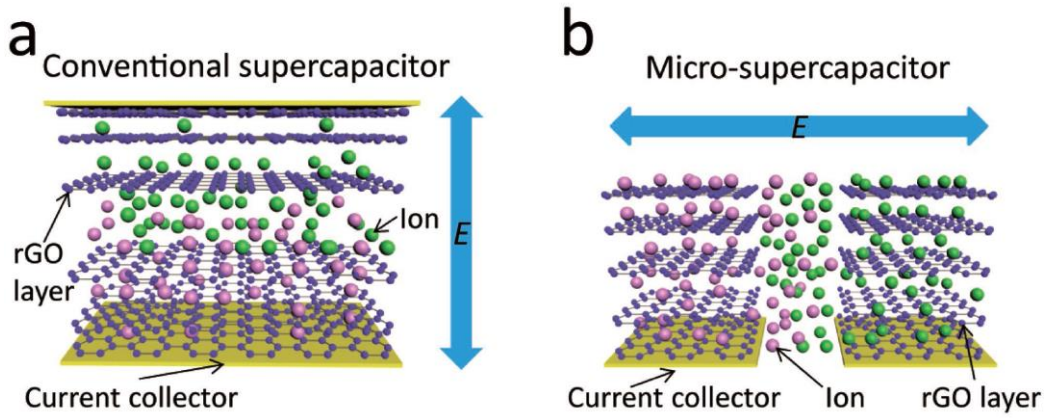

Figure 1-11. Schematic depiction of the operating principle of: a) the stacked-geometry conventional supercapacitors, and b) in-plane micro-supercapacitors. Reprinted with permission from Ref. [99b]; copy right: 2016, "John Wiley and Sons" publishing group.

In 2011, the [redacted] group demonstrated a scalable fabrication of MSCs by direct laser reduction and patterning of hydrated GO films.[30a] The trapped water made GO serve as both good ionic conductor and electrical insulator. Thus, the in-plane structured MSC delivered an areal capacitance of 0.51 mF cm^{-2}, which is nearly twice that of the SC based on conventional sandwiched structure. However, the fabricated MSCs showed poor frequency response, large internal resistance and low rate capability, which could be attributed to the long gap between the micro-electrodes of the designed geometry.

Smaller gaps between the micro-electrodes were achieved in 2013. Continued from their previous laser scribing approach, the [redacted] group reported the scalable fabrication of graphene-based planar MSCs by direct laser writing of GO films.[100] As shown in Figure 1-12, the disc with GO films on top is inserted into a standard LightScribe DVD burner, where a computer-designed MSC geometry is written directly on the GO film to produce graphene electrode patterns by laser reduction. This process is readily scalable for the efficient fabrication of all solid-state MSCs with certain flexibility. For instance, an array composed of more than 100 MSCs can be produced on a flexible substrate within 30 min. The MSCs could be operated at voltage window of 1 V or 2.5 V depending on different electrolytes. The MSCs showed excellent charge-storage capacity and rate capability, offering a significantly high power density of 200 W cm^{-3}.

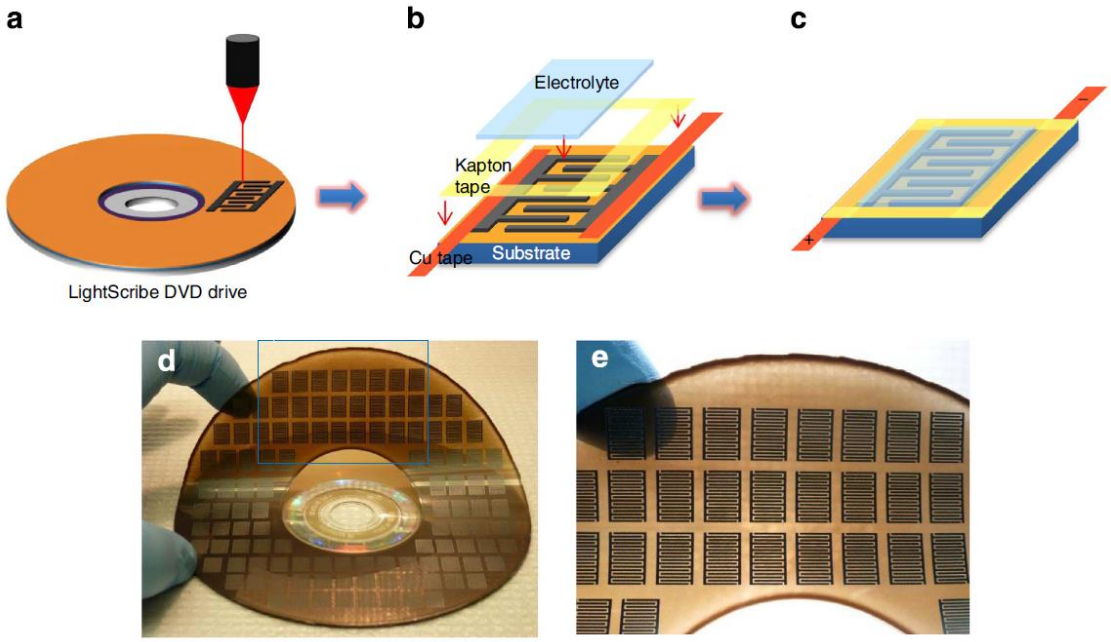

Figure 1-12. (a-c) Schematic of the fabrication process for LSG-MSCs. (d, e) Direct writing of LSG-MSCs with more than 100 micro-devices on a single disc. Reprinted with permission from Ref. [100]; copy right: 2013, Macmillan publishing group.

Recently, the [redacted] group demonstrated a highly efficient graphene-based in-plane MSCs via methane plasma treatment of GO films.[101] The obtained films displayed a high electrical conductivity of 345 S cm^{-1}, combined with the planar geometry of the device, the resulting all solid-state MSCs delivered a significantly high power density of 495 W cm^{-3} (higher than that of electrolytic capacitors) and an energy density of 2.5 mWh cm^{-3} (comparable to that of lithium thin-film batteries). These MSCs even allow operation at 1000 V s^{-1}, which is three orders of magnitude higher than conventional sandwich-structured supercapacitors, demonstrating the advantage of in-plane device geometry. Furthermore, the extremely small time constant of 0.28 ms suggested that the MSCs are capable of working in an ultrafast charging/discharging process. This work may pave the way for future miniaturized and flexible electronic applications.

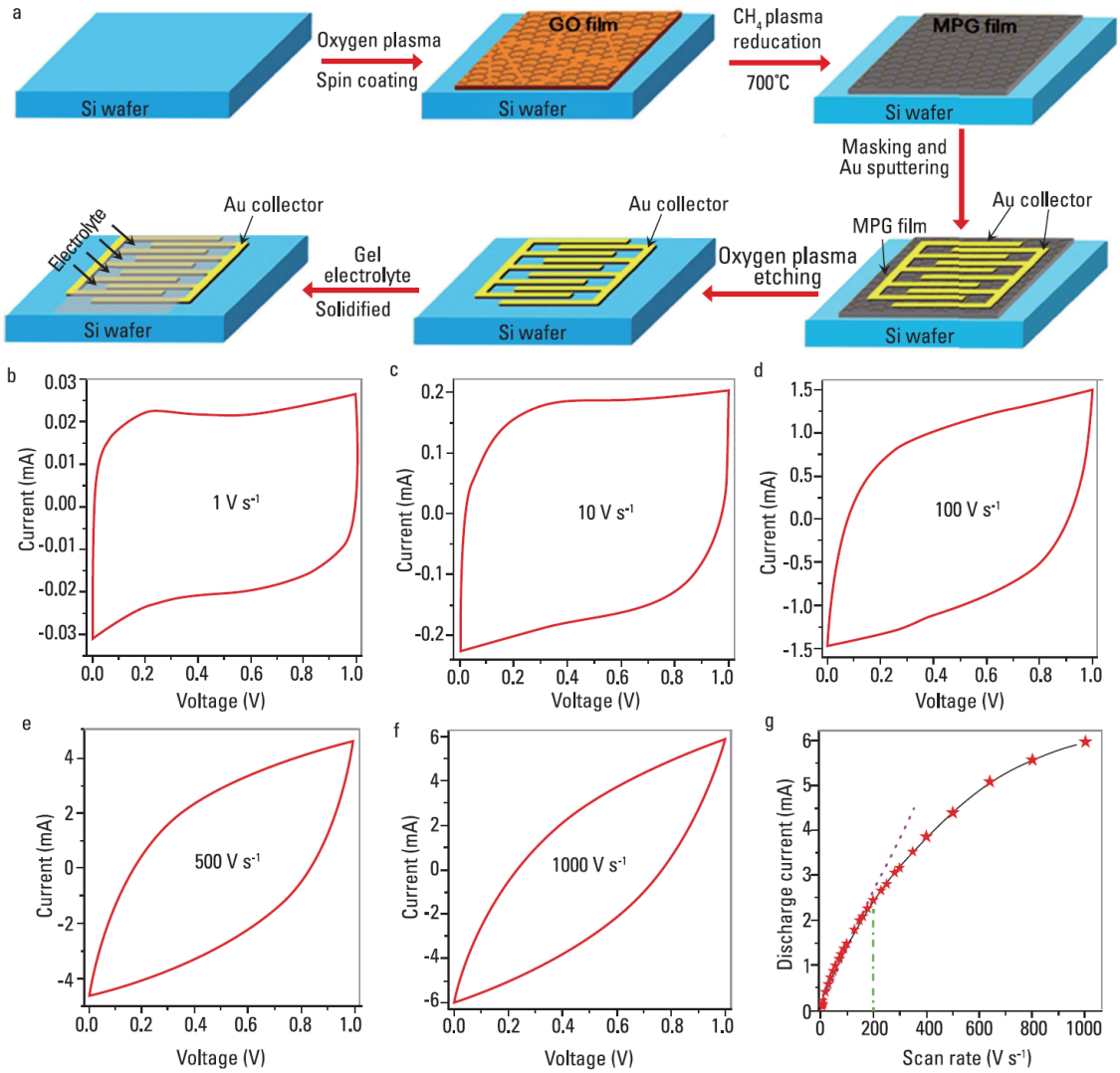

Figure 1-13. (a) Illustration of the fabrication of all-solid-state interdigital graphene-based MSCs integrated onto a silicon wafer. (b-f) CV curves of the graphene-based MSCs at different scan rates from 1 to 1000 V s^{-1}. (g) A plot of the discharge current as a function of the scan rate. Reprinted with permission from Ref. [101]; copy right: 2013, Macmillan publishing group.

1.5 **Motivation and Objectives**

The discovery of graphene provided a natural choice for flexible and transparent electronic systems. Due to its unique electrical, mechanical and optical properties, graphene will be widely employed in novel applications regarding optoelectronics and energy storage devices, with enhanced performance compared with current dominating materials. Taking advantage of its intrinsic flexibility, graphene is also ideal for sensors (detectors) that shall adhere and interact with the human body, or wearable on-chip power supplies, enabling new consumer, medical and even military applications which cannot be realized by present materials and technologies.

As discussed in section 1.2.1, different production methods of graphene have their own advantages and drawbacks. For current CVD approaches, although a low R_s has been achieved, the requirements of high temperature, sacrificial metal etching, and multistep transfer processes onto the desired substrates are still critical. Chemical exfoliation based on Hummers method is capable of producing solution processed GO in bulk-scale, however post thermal/chemical reduction is still necessary to restore certain electronic properties of graphene. Further development based on solvent-assisted liquid-phase exfoliation can produce graphene flakes with better quality than GO, but the low yield and extensive sonication processes are the major limitations of this method. Recently, the electrochemical exfoliation method demonstrates itself as a promising alternative approach for high quality graphene production at room temperature, in particular, via a solution process, which is of significant importance for practical applications of graphene based electrode materials.

In this thesis, we will mainly focus on applications of electrochemically exfoliated graphene, in regards of transparent electrodes in organic photo-detectors as well as electrochemical active electrodes for MSCs, which is specifically demonstrated according to the important requirements of the future generation devices. Figure 1-14 illustrates the outline of this thesis.

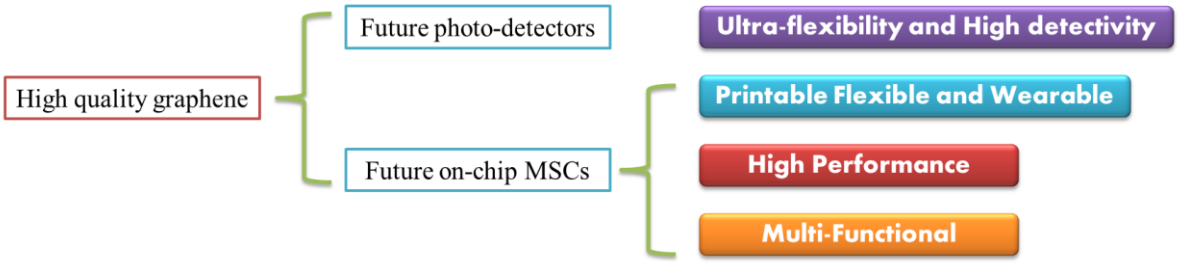

Figure 1-14. Outline of this thesis.

With the ever-increasing demand for miniaturized, portable, wearable and highly efficient electronic devices become pervasive in our daily lifes, flexible electronics is definitely the next ubiquitous platform for future electronics industry. The realization of electronics with performances equal to those of well-established technologies based on rigid platforms, only in lightweight, foldable, and flexible formats, would broaden their functions and enable many new applications. This will bring truly conformal, reliable or even transparent electronics. It is also essential for on-chip circuits with tightly assembled units. Large industrial scale produced flexible electronics with reduced cost also become possible by employing novel mass manufacturing approaches, such as R2R printing technologies, which is hitherto unavailable from traditional brittle materials and device platforms.

As discussed in section 1.4.1, graphene acting as ITO replacement material is very promising for flexible electronics. The major challenge for current high quality graphene is still the high R_s level compared to ITO. The chemical modification of graphene is thus needed in order to significantly decrease R_s while maintaining the high transparency. Increasing the carrier density by various foreign atomic/molecular doping is an effective way to reduce R_s. However, the stability of the doping is the major issue in most cases. Innovative doping routes in regards of non-covalent functionalization of graphene need to be investigated, in order to achieve stable doping.

Thus in Chapter 2, we demonstrated a novel solution fabrication of large area, highly conductive graphene films by spray coating of EG/PH1000 hybrid ink. The fabricated graphene films exhibit excellent mechanical properties, enabling their application as bottom electrodes in ultrathin organic photodetector devices with performance comparable to that of the state-of-art Si based inorganic photodetectors.

Flexible power supply unit is the very core of flexible electronics, which is demonstrated by energy storage systems, such as supercapacitors. As suggested in Chapter 3 and Chapter 4, graphene-based electrodes could display both high capacitance and power densities in MSCs, if the excellent electronic property of electrochemically exfoliated graphene and a porous structure are realized. In this thesis, we are trying to address the important requirements for future on-chip MSCs including (1) Printable, flexible and wearable (2) High performance (3) Expansion of the fabrication techniques to spray-coating and even ink-jet printing, with a potentially rapid and high volume R2R manufacturability.

In Chapter 3, we demonstrated a novel direct printing approach for in-plane micro-supercapacitor (MSC) fabrication. Solution processed graphene/conductive polymer hybrid inks were utilized. The fabricated MSCs on paper substrate offered significant areal capacitance and excellent rate capabilities. An ultra-thin MSC on PET (2.5-μm-thick) substrate exhibited "ultraflexiblity", making it suitable for next-generation flexible micro-electrochemical energy storage devices. Graphene-based printable, flexible and wearable energy storage devices are highly promising and should be further developed.

A high device performance is always required for MSCs, especially the power densities. In Chapter 4, MSCs based on mesoporous polyaniline patterned graphene is demonstrated. The synergic effect from both electron-double-layer-capacitive graphene and pseudocapacitive mesoporous-PANi leads to excellent MSC device performances, in regards to excellent volumetric capacitance and rate capabilities, which further resulted in a high power density of 600 W cm^{-3}, suggesting opportunities for future portable and wearable power supplies in diverse applications.

As for another important aspect for future perspective, developing novel 'smart' responsive MSCs is highly appealing for more practical functions. Efficient photo-switchable MSCs based on graphene/diarylethene molecules, with the ability to tune the capacitance of MSCs by remote light stimuli at certain wavelength, is demonstrated in Chapter 5. The in-plane structured MSCs are based on DAE/graphene composite film, the micro-device delivers an outstanding and reversible capacitance modulation up to 20%, demonstrating a prototype photo-switchable MSC.

References

[1] a) N. Linares, A. M. Silvestre-Albero, E. Serrano, J. Silvestre-Albero, J. Garcia-Martinez, *Chem. Soc. Rev.* **2014**, *43*, 7681; b) M.-M. Titirici, R. J. White, N. Brun, V. L. Budarin, D. S. Su, F. del Monte, J. H. Clark, M. J. MacLachlan, *Chem. Soc. Rev.* **2015**, *44*, 250.

[2] A. K. Geim, K. S. Novoselov, *Nat Mater* **2007**, *6*, 183.

[3] H. P. Boehm, R. Setton, E. Stumpp, in *Pure Appl. Chem.*, Vol. 66, 1994, 1893.

[4] a) J. W. McClure, *Physical Review* **1956**, *104*, 666; b) J. C. Slonczewski, P. R. Weiss, *Physical Review* **1958**, *109*, 272; c) P. R. Wallace, *Physical Review* **1947**, *71*, 622; d) E. Fradkin, *Physical Review B* **1986**, *33*, 3263.

[5] a) J. W. Evans, P. A. Thiel, M. C. Bartelt, *Surf. Sci. Rep.* **2006**, *61*, 1; b) J. A. Venables, G. D. T. Spiller, M. Hanbucken, *Rep. Prog. Phys.* **1984**, *47*, 399.

[6] a) K. S. Novoselov, A. K. Geim, S. V. Morozov, D. Jiang, M. I. Katsnelson, I. V. Grigorieva, S. V. Dubonos, A. A. Firsov, *Nature* **2005**, *438*, 197; b) Y. Zhang, Y.-W. Tan, H. L. Stormer, P. Kim, *Nature* **2005**, *438*, 201.

[7] a) K. S. Novoselov, A. K. Geim, S. V. Morozov, D. Jiang, Y. Zhang, S. V. Dubonos, I. V. Grigorieva, A. A. Firsov, *Science* **2004**, *306*, 666; b) K. S. Novoselov, D. Jiang, F. Schedin, T. J. Booth, V. V. Khotkevich, S. V. Morozov, A. K. Geim, *Proceedings of the National Academy of Sciences of the United States of America* **2005**, *102*, 10451.

[8] L. Liao, Y.-C. Lin, M. Bao, R. Cheng, J. Bai, Y. Liu, Y. Qu, K. L. Wang, Y. Huang, X. Duan, *Nature* **2010**, *467*, 305.

[9] a) A. A. Balandin, S. Ghosh, W. Bao, I. Calizo, D. Teweldebrhan, F. Miao, C. N. Lau, *Nano Lett.* **2008**, *8*, 902; b) S. Ghosh, I. Calizo, D. Teweldebrhan, E. P. Pokatilov, D. L. Nika, A. A. Balandin, W. Bao, F. Miao, C. N. Lau, *Appl. Phys. Lett.* **2008**, *92*, 151911.

[10] C. Lee, X. Wei, J. W. Kysar, J. Hone, *Science* **2008**, *321*, 385.

[11] a) R. R. Nair, P. Blake, A. N. Grigorenko, K. S. Novoselov, T. J. Booth, T. Stauber, N. M. R. Peres, A. K. Geim, *Science* **2008**, *320*, 1308; b) S. Bae, H. Kim, Y. Lee, X. Xu, J.-S. Park, Y. Zheng, J. Balakrishnan, T. Lei, H. Ri Kim, Y. I. Song, Y.-J. Kim, K. S. Kim, B. Ozyilmaz, J.-H. Ahn, B. H. Hong, S. Iijima, *Nat Nano* **2010**, *5*, 574.

[12] J. S. Bunch, S. S. Verbridge, J. S. Alden, A. M. van der Zande, J. M. Parpia, H. G. Craighead, P. L. McEuen, *Nano Lett.* **2008**, *8*, 2458.

[13] J. Moser, A. Barreiro, A. Bachtold, *Appl. Phys. Lett.* **2007**, *91*, 163513.

[14] K. S. Novoselov, Z. Jiang, Y. Zhang, S. V. Morozov, H. L. Stormer, U. Zeitler, J. C. Maan, G. S. Boebinger, P. Kim, A. K. Geim, *Science* **2007**, *315*, 1379.

[15] a) C. R. Dean, A. F. Young, MericI, LeeC, WangL, SorgenfreiS, WatanabeK, TaniguchiT, KimP, K. L. Shepard, HoneJ, *Nat Nano* **2010**, *5*, 722; b) A. S. Mayorov, R. V. Gorbachev, S. V. Morozov, L. Britnell, R. Jalil, L. A. Ponomarenko, P. Blake, K. S. Novoselov, K. Watanabe, T. Taniguchi, A. K. Geim, *Nano Lett.* **2011**, *11*, 2396.

[16] R. Ruoff, *Nat Nano* **2008**, *3*, 10.

[17] a) S. V. Morozov, K. S. Novoselov, M. I. Katsnelson, F. Schedin, D. C. Elias, J. A. Jaszczak, A. K. Geim, *Phys. Rev. Lett.* **2008**, *100*, 016602; b) E. V. Castro, K. S. Novoselov, S. V. Morozov, N. M. R. Peres, J. M. B. L. dos Santos, J. Nilsson, F. Guinea, A. K. Geim, A. H. C. Neto, *Phys. Rev. Lett.* **2007**, *99*, 216802.

[18] a) M.-F. Yu, O. Lourie, M. J. Dyer, K. Moloni, T. F. Kelly, R. S. Ruoff, *Science* **2000**, *287*, 637; b) J. N. Coleman, U. Khan, Y. K. Gun'ko, *Adv. Mater.* **2006**, *18*, 689; c) B. Q. Wei, R. Vajtai, P. M. Ajayan, *Appl. Phys. Lett.* **2001**, *79*, 1172; d) P. Kim, L. Shi, A. Majumdar, P. L. McEuen, *Phys. Rev. Lett.* **2001**, *87*, 215502.

[19] J. N. Coleman, *Adv. Funct. Mater.* **2009**, *19*, 3680.

[20] Y. Hernandez, V. Nicolosi, M. Lotya, F. M. Blighe, Z. Sun, S. De, I. T. McGovern, B. Holland, M. Byrne, Y. K. Gun'Ko, J. J. Boland, P. Niraj, G. Duesberg, S. Krishnamurthy, R. Goodhue, J. Hutchison, V. Scardaci, A. C. Ferrari, J. N. Coleman, *Nat Nano* **2008**, *3*, 563.

[21] U. Khan, A. O'Neill, M. Lotya, S. De, J. N. Coleman, *Small* **2010**, *6*, 864.

[22] M. Lotya, Y. Hernandez, P. J. King, R. J. Smith, V. Nicolosi, L. S. Karlsson, F. M. Blighe, S. De, Z. Wang, I. T. McGovern, G. S. Duesberg, J. N. Coleman, *J. Am. Chem. Soc.* **2009**, *131*, 3611.

[23] K. R. Paton, E. Varrla, C. Backes, R. J. Smith, U. Khan, A. O'Neill, C. Boland, M. Lotya, O. M. Istrate, P. King, T. Higgins, S. Barwich, P. May, P. Puczkarski, I. Ahmed, M. Moebius, H. Pettersson, E. Long, J. Coelho, S. E. O'Brien, E. K. McGuire, B. M. Sanchez, G. S. Duesberg, N. McEvoy, T. J. Pennycook, C. Downing, A. Crossley, V. Nicolosi, J. N. Coleman, *Nat Mater* **2014**, *13*, 624.

[24] C. Soldano, A. Mahmood, E. Dujardin, *Carbon* **2010**, *48*, 2127.

[25] S. Stankovich, D. A. Dikin, G. H. B. Dommett, K. M. Kohlhaas, E. J. Zimney, E. A. Stach, R. D. Piner, S. T. Nguyen, R. S. Ruoff, *Nature* **2006**, *442*, 282.

[26] J. Wang, M. Liang, Y. Fang, T. Qiu, J. Zhang, L. Zhi, *Adv. Mater.* **2012**, *24*, 2874.

[27] J. Gao, F. Liu, Y. Liu, N. Ma, Z. Wang, X. Zhang, *Chem. Mater.* **2010**, *22*, 2213.

[28] D. Li, M. B. Muller, S. Gilje, R. B. Kaner, G. G. Wallace, *Nat Nano* **2008**, *3*, 101.

[29] Q. Su, S. Pang, V. Alijani, C. Li, X. Feng, K. Müllen, *Adv. Mater.* **2009**, *21*, 3191.

[30] a) W. Gao, N. Singh, L. Song, Z. Liu, A. L. M. Reddy, L. Ci, R. Vajtai, Q. Zhang, B. Wei, P. M. Ajayan, *Nat Nano* **2011**, *6*, 496; b) M. F. El-Kady, R. B. Kaner, *Nat Commun* **2013**, *4*, 1475.

[31] D. Voiry, J. Yang, J. Kupferberg, R. Fullon, C. Lee, H. Y. Jeong, H. S. Shin, M. Chhowalla, *Science* **2016**.

[32] X. Li, G. Zhang, X. Bai, X. Sun, X. Wang, E. Wang, H. Dai, *Nat Nano* **2008**, *3*, 538.

[33] a) C. Y. Su, A. Y. Lu, Y. P. Xu, F. R. Chen, A. N. Khlobystov, L. J. Li, *Acs Nano* **2011**, *5*, 2332; b) K. Parvez, R. Li, S. R. Puniredd, Y. Hernandez, F. Hinkel, S. Wang, X. Feng, K. Müllen, *ACS Nano* **2013**, *7*, 3598.

[34] S. Yang, M. R. Lohe, K. Müllen, X. Feng, *Adv. Mater.* **2016**, *28*, 6213.

[35] K. Parvez, Z.-S. Wu, R. Li, X. Liu, R. Graf, X. Feng, K. Müllen, *J. Am. Chem. Soc.* **2014**, *136*, 6083.

[36] a) C. Berger, Z. Song, X. Li, X. Wu, N. Brown, C. Naud, D. Mayou, T. Li, J. Hass, A. N. Marchenkov, E. H. Conrad, P. N. First, W. A. de Heer, *Science* **2006**, *312*, 1191; b) W. A. de Heer, C. Berger, X. Wu, P. N. First, E. H. Conrad, X. Li, T. Li, M. Sprinkle, J. Hass, M. L. Sadowski, M. Potemski, G. Martinez, *Solid State Commun.* **2007**, *143*, 92.

[37] G. Yazdi, T. Iakimov, R. Yakimova, *Crystals* **2016**, *6*, 53.

[38] a) S. Guo, S. Dong, *Chem. Soc. Rev.* **2011**, *40*, 2644; b) A. d. H. Walt, B. Claire, W. Xiaosong, S. Mike, H. Yike, R. Ming, A. S. Joseph, N. F. Phillip, H. Robert, P. Benjamin, F. Clément, P. Marek, M. Jeong-Sun, *J. Phys. D: Appl. Phys.* **2010**, *43*, 374007.

[39] S. Shivaraman, R. A. Barton, X. Yu, J. Alden, L. Herman, M. V. S. Chandrashekhar, J. Park, P. L. McEuen, J. M. Parpia, H. G. Craighead, M. G. Spencer, *Nano Lett.* **2009**, *9*, 3100.

[40] J. Hass, W. A. d. Heer, E. H. Conrad, *J. Phys.: Condens. Matter* **2008**, *20*, 323202.

[41] N. Camara, G. Rius, J.-R. Huntzinger, A. Tiberj, N. Mestres, P. Godignon, J. Camassel, *Appl. Phys. Lett.* **2008**, *93*, 123503.

[42] V. Y. Aristov, G. Urbanik, K. Kummer, D. V. Vyalikh, O. V. Molodtsova, A. B. Preobrajenski, A. A. Zakharov, C. Hess, T. Hänke, B. Büchner, I. Vobornik, J. Fujii, G. Panaccione, Y. A. Ossipyan, M. Knupfer, *Nano Lett.* **2010**, *10*, 992.

[43] K. V. Emtsev, A. Bostwick, K. Horn, J. Jobst, G. L. Kellogg, L. Ley, J. L. McChesney, T. Ohta, S. A. Reshanov, J. Rohrl, E. Rotenberg, A. K. Schmid, D. Waldmann, H. B. Weber, T. Seyller, *Nat Mater* **2009**, *8*, 203.

[44] J. D. Caldwell, T. J. Anderson, J. C. Culbertson, G. G. Jernigan, K. D. Hobart, F. J. Kub, M. J. Tadjer, J. L. Tedesco, J. K. Hite, M. A. Mastro, R. L. Myers-Ward, C. R. Eddy, P. M. Campbell, D. K. Gaskill, *ACS Nano* **2010**, *4*, 1108.

[45] a) Z. F. Ren, Z. P. Huang, J. W. Xu, J. H. Wang, P. Bush, M. P. Siegal, P. N. Provencio, *Science* **1998**, *282*, 1105; b) G. Che, B. B. Lakshmi, E. R. Fisher, C. R. Martin, *Nature* **1998**, *393*, 346.

[46] S. Marchini, S. Günther, J. Wintterlin, *Physical Review B* **2007**, *76*, 075429.

[47] V. Roumen, M. Alexander, H. P. Roumen, K. Raymond, M. Myrjam, V. Annick, H. Chris Van, *Nanotechnology* **2010**, *21*, 095602.

[48] K. S. Kim, Y. Zhao, H. Jang, S. Y. Lee, J. M. Kim, K. S. Kim, J.-H. Ahn, P. Kim, J.-Y. Choi, B. H. Hong, *Nature* **2009**, *457*, 706.

[49] J. Coraux, A. T. N'Diaye, C. Busse, T. Michely, *Nano Lett.* **2008**, *8*, 565.

[50] S.-Y. Kwon, C. V. Ciobanu, V. Petrova, V. B. Shenoy, J. Bareño, V. Gambin, I. Petrov, S. Kodambaka, *Nano Lett.* **2009**, *9*, 3985.

[51] X. Li, W. Cai, J. An, S. Kim, J. Nah, D. Yang, R. Piner, A. Velamakanni, I. Jung, E. Tutuc, S. K. Banerjee, L. Colombo, R. S. Ruoff, *Science* **2009**, *324*, 1312.

[52] X. Li, W. Cai, L. Colombo, R. S. Ruoff, *Nano Lett.* **2009**, *9*, 4268.

[53] C. Mattevi, H. Kim, M. Chhowalla, *J. Mater. Chem.* **2011**, *21*, 3324.

[54] X. Li, C. W. Magnuson, A. Venugopal, J. An, J. W. Suk, B. Han, M. Borysiak, W. Cai, A. Velamakanni, Y. Zhu, L. Fu, E. M. Vogel, E. Voelkl, L. Colombo, R. S. Ruoff, *Nano Lett.* **2010**, *10*, 4328.

[55] X. Li, C. W. Magnuson, A. Venugopal, R. M. Tromp, J. B. Hannon, E. M. Vogel, L. Colombo, R. S. Ruoff, *J. Am. Chem. Soc.* **2011**, *133*, 2816.

[56] a) Z. Sun, Z. Yan, J. Yao, E. Beitler, Y. Zhu, J. M. Tour, *Nature* **2010**, *468*, 549; b) Z. Li, P. Wu, C. Wang, X. Fan, W. Zhang, X. Zhai, C. Zeng, Z. Li, J. Yang, J. Hou, *ACS Nano* **2011**, *5*, 3385.

[57] X. Yang, X. Dou, A. Rouhanipour, L. Zhi, H. J. Räder, K. Müllen, *J. Am. Chem. Soc.* **2008**, *130*, 4216.

[58] A. Narita, X. Feng, Y. Hernandez, S. A. Jensen, M. Bonn, H. Yang, I. A. Verzhbitskiy, C. Casiraghi, M. R. Hansen, A. H. R. Koch, G. Fytas, O. Ivasenko, B. Li, K. S. Mali, T. Balandina, S. Mahesh, S. De Feyter, K. Müllen, *Nat Chem* **2014**, *6*, 126.

[59] J. Cai, P. Ruffieux, R. Jaafar, M. Bieri, T. Braun, S. Blankenburg, M. Muoth, A. P. Seitsonen, M. Saleh, X. Feng, K. Mullen, R. Fasel, *Nature* **2010**, *466*, 470.

[60] C. D. Simpson, J. D. Brand, A. J. Berresheim, L. Przybilla, H. J. Räder, K. Müllen, *Chemistry – A European Journal* **2002**, *8*, 1424.

[61] X. Wang, L. Zhi, N. Tsao, Ž. Tomović, J. Li, K. Müllen, *Angew. Chem. Int. Ed.* **2008**, *47*, 2990.

[62] L. Talirz, H. Söde, J. Cai, P. Ruffieux, S. Blankenburg, R. Jafaar, R. Berger, X. Feng, K. Müllen, D. Passerone, R. Fasel, C. A. Pignedoli, *J. Am. Chem. Soc.* **2013**, *135*, 2060.

[63] A. Reina, X. Jia, J. Ho, D. Nezich, H. Son, V. Bulovic, M. S. Dresselhaus, J. Kong, *Nano Lett.* **2009**, *9*, 30.

[64] X. Li, Y. Zhu, W. Cai, M. Borysiak, B. Han, D. Chen, R. D. Piner, L. Colombo, R. S. Ruoff, *Nano Lett.* **2009**, *9*, 4359.

[65] B. Alemán, W. Regan, S. Aloni, V. Altoe, N. Alem, C. Girit, B. Geng, L. Maserati, M. Crommie, F. Wang, A. Zettl, *ACS Nano* **2010**, *4*, 4762.

[66] J. W. Suk, A. Kitt, C. W. Magnuson, Y. Hao, S. Ahmed, J. An, A. K. Swan, B. B. Goldberg, R. S. Ruoff, *ACS Nano* **2011**, *5*, 6916.

[67] D.-Y. Wang, I. S. Huang, P.-H. Ho, S.-S. Li, Y.-C. Yeh, D.-W. Wang, W.-L. Chen, Y.-Y. Lee, Y.-M. Chang, C.-C. Chen, C.-T. Liang, C.-W. Chen, *Adv. Mater.* **2013**, *25*, 4521.

[68] G. Eda, G. Fanchini, M. Chhowalla, *Nat Nano* **2008**, *3*, 270.

[69] J. Wu, M. Agrawal, H. A. Becerril, Z. Bao, Z. Liu, Y. Chen, P. Peumans, *ACS Nano* **2010**, *4*, 43.

[70] M.-C. Choi, Y. Kim, C.-S. Ha, *Prog. Polym. Sci.* **2008**, *33*, 581.

[71] V. H. Pham, T. V. Cuong, S. H. Hur, E. W. Shin, J. S. Kim, J. S. Chung, E. J. Kim, *Carbon* **2010**, *48*, 1945.

[72] W. J. Hyun, E. B. Secor, M. C. Hersam, C. D. Frisbie, L. F. Francis, *Adv. Mater.* **2015**, *27*, 109.

[73] J. Baker, D. Deganello, D. T. Gethin, T. M. Watson, *Mater. Res. Innovations* **2014**, *18*, 86.

[74] E. B. Secor, S. Lim, H. Zhang, C. D. Frisbie, L. F. Francis, M. C. Hersam, *Adv. Mater.* **2014**, *26*, 4533.

[75] F. Torrisi, T. Hasan, W. P. Wu, Z. P. Sun, A. Lombardo, T. S. Kulmala, G. W. Hsieh, S. J. Jung, F. Bonaccorso, P. J. Paul, D. P. Chu, A. C. Ferrari, *Acs Nano* **2012**, *6*, 2992.

[76] K. Fu, Y. Wang, C. Yan, Y. Yao, Y. Chen, J. Dai, S. Lacey, Y. Wang, J. Wan, T. Li, Z. Wang, Y. Xu, L. Hu, *Adv. Mater.* **2016**, *28*, 2587.

[77] B. Sukang, K. Sang Jin, S. Dolly, A. Jong-Hyun, H. Byung Hee, *Phys. Scr.* **2012**, *2012*, 014024.

[78] C. a. Di, D. Wei, G. Yu, Y. Liu, Y. Guo, D. Zhu, *Adv. Mater.* **2008**, *20*, 3289.

[79] Y. Zhu, Z. Z. Sun, Z. Yan, Z. Jin, J. M. Tour, *Acs Nano* **2011**, *5*, 6472.

[80] P. J. King, U. Khan, M. Lotya, S. De, J. N. Coleman, *ACS Nano* **2010**, *4*, 4238.

[81] F. Bonaccorso, Z. Sun, T. Hasan, A. C. Ferrari, *Nat Photon* **2010**, *4*, 611.

[82] M. W. Rowell, M. D. McGehee, *Energy & Environmental Science* **2011**, *4*, 131.

[83] J. Wu, H. A. Becerril, Z. Bao, Z. Liu, Y. Chen, P. Peumans, *Appl. Phys. Lett.* **2008**, *92*, 263302.

[84] H. Park, S. Chang, X. Zhou, J. Kong, T. Palacios, S. Gradečak, *Nano Lett.* **2014**, *14*, 5148.

[85] T.-H. Han, Y. Lee, M.-R. Choi, S.-H. Woo, S.-H. Bae, B. H. Hong, J.-H. Ahn, T.-W. Lee, *Nat Photon* **2012**, *6*, 105.

[86] a) J. F. M. Oudenhoven, L. Baggetto, P. H. L. Notten, *Advanced Energy Materials* **2011**, *1*, 10; b) Y. Shao, M. F. El-Kady, L. J. Wang, Q. Zhang, Y. Li, H. Wang, M. F. Mousavi, R. B. Kaner, *Chem. Soc. Rev.* **2015**, *44*, 3639.

[87] a) J. W. Long, B. Dunn, D. R. Rolison, H. S. White, *Chem. Rev.* **2004**, *104*, 4463; b) M. Armand, J. M. Tarascon, *Nature* **2008**, *451*, 652; c) J. Chmiola, C. Largeot, P.-L. Taberna, P. Simon, Y. Gogotsi, *Science* **2010**, *328*, 480.

[88] G. Wang, L. Zhang, J. Zhang, *Chem. Soc. Rev.* **2012**, *41*, 797.

[89] F. Bonaccorso, L. Colombo, G. Yu, M. Stoller, V. Tozzini, A. C. Ferrari, R. S. Ruoff, V. Pellegrini, *Science* **2015**, *347*, 1246501.

[90] S. Zhang, N. Pan, *Advanced Energy Materials* **2015**, *5*, 1401401.

[91] C.-C. Hu, K.-H. Chang, M.-C. Lin, Y.-T. Wu, *Nano Lett.* **2006**, *6*, 2690.

[92] H. Zhang, G. Cao, Z. Wang, Y. Yang, Z. Shi, Z. Gu, *Nano Lett.* **2008**, *8*, 2664.

[93] D. Choi, G. E. Blomgren, P. N. Kumta, *Adv. Mater.* **2006**, *18*, 1178.

[94] T. Liu, L. Finn, M. Yu, H. Wang, T. Zhai, X. Lu, Y. Tong, Y. Li, *Nano Lett.* **2014**, *14*, 2522.

[95] B. E. Conway, V. Birss, J. Wojtowicz, *J. Power Sources* **1997**, *66*, 1.

[96] A. Peigney, C. Laurent, E. Flahaut, R. R. Bacsa, A. Rousset, *Carbon* **2001**, *39*, 507.

[97] Y. Zhu, S. Murali, M. D. Stoller, K. J. Ganesh, W. Cai, P. J. Ferreira, A. Pirkle, R. M. Wallace, K. A. Cychosz, M. Thommes, D. Su, E. A. Stach, R. S. Ruoff, *Science* **2011**, *332*, 1537.

[98] X. Yang, C. Cheng, Y. Wang, L. Qiu, D. Li, *Science* **2013**, *341*, 534.

[99] a) D. Pech, M. Brunet, H. Durou, P. Huang, V. Mochalin, Y. Gogotsi, P.-L. Taberna, P. Simon, *Nat Nano* **2010**, *5*, 651; b) D. Qi, Y. Liu, Z. Liu, L. Zhang, X. Chen, *Adv. Mater.* **2017**, *29*, 1602802.

[100] M. F. El-Kady, R. B. Kaner, *Nat. Commun.* **2013**, *4*, 1475.

[101] Z. S. Wu, K. Parvez, X. Feng, K. Müllen, *Nat Commun* **2013**, *4*, 2487.

Chapter 2. Transparent Conductive Electrodes from Graphene/PEDOT: PSS Hybrid Inks for Ultrathin Organic Photodetectors

Keywords: electrochemically exfoliated graphene, transparent conductive electrode, organic photodetector, spray-coating

ToC Figure

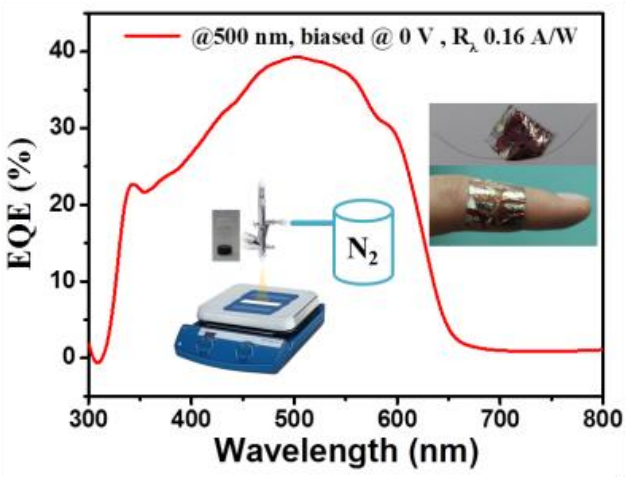

A novel solution fabrication of large area, highly conductive graphene films by spray coating of EG/PH1000 hybrid ink is demonstrated. The fabricated graphene films exhibit excellent mechanical properties, thus enabling their application as bottom electrodes in ultrathin organic photodetector devices with performance comparable to that of the state-of-art Si based inorganic photodetectors.

Published in:

Advanced Materials

Reprinted with permission from (*Adv. Mater.* **2015**, *27*, 669-675.) Copyright : 2015, “John Wiley and Sons” publishing group.

Transparent conductive electrodes (TCEs) are essential elements of numerous flexible optoelectronic devices such as organic solar cells, organic light emitting diodes, organic photodetectors (OPDs), liquid crystal displays, and touch screens.[1] The most common TCEs today are based on indium tin oxide (ITO) owing to its low sheet resistance (R_s=10 Ω/□) coupled with high transmittance (T=80% @ 550 nm) and favorable work function (~ 4.8 eV).[2] However, ITO suffers from several limitations: an ever increasing cost due to indium scarcity, the ceramic nature, and sensitivity to both acidic and alkaline environments. Therefore, the search for alternative TCEs to replace ITO has been an essential issue in recent years.[3] For the future generation of organic optoelectronic devices, novel electrode materials with lightweight, high electrical conductivity, stability, flexibility and transparency are essential.[4] Metallic nanowires,[5] carbon nanotubes (CNTs)[6] and conductive polymers[7] have been explored as potential TCEs, as they all exhibit high transparency across the visible light spectrum. However, TCEs composed of metallic nanowires suffer from large surface roughness, while CNTs films have limitations due to high contact resistances between nanotube bundles; finally, for conductive polymers, the stability upon exposure to high temperature, humidity, or UV light is a major obstacle.[8]

Graphene, which combines high transparency and conductivity, chemical and thermal stability, stretchability, and low contact resistance with organic materials, offers tremendous advantages as TCEs in optoelectronic devices.[9] Currently, the preparation of transparent graphene film mainly relies on chemical vapour deposition (CVD) using catalytic metal substrates such as Ni or Cu.[10] Although a sheet resistance as low as 125 Ω/□ (at T=90%) has been achieved,[11] the major hurdles to realize cost-effective industrial-scale production of CVD grown graphene, are the requirements of high temperature, a sacrificial metal etching, and multistep transfer processes onto the desired substrates. Moreover, the graphene transfer process involves the use of poly(methylmethacrylate) and/or polydimethylsiloxane, which

cannot be completely removed and may even damage the graphene film.[10, 12] Therefore, searching for alternative approaches to construct highly conductive graphene films, in particular, via a solution process is of significant importance. Chemical exfoliation of graphite based on the [redacted] method is an appealing route to produce solution processable graphene oxide (GO) in bulk-scale, but thermal or chemical reduction is required to partially restore the electronic properties of graphene.[1a, 13] Solvent- and/or surfactant-assisted liquid-phase exfoliation,[14] electrochemical expansion,[15] and formation of graphite intercalated compounds,[16] can overcome the limitations of GO, but still do not yield graphene films with satisfying electronic properties, not to mention that extensive sonication processes are indispensable for these methods.

Recently, electrochemical exfoliation of graphite has attracted much attention due to its easy, fast, and environmentally friendly nature to produce high-quality graphene in bulk scale.[17] However, due to the lack of abundant functional groups on the surface, electrochemically exfoliated graphene (EG) can only be dispersed in high boiling point solvents like N-methyl-2-pyrrolidone (NMP) or N,N'-dimethylformamide (DMF). This makes it difficult to employ conventional solution processing techniques for thin film preparation, such as spin-coating, inkjet-printing, rod-coating and/or layer-by-layer deposition.[18] In this work, we demonstrate a novel solution fabrication of large area graphene films by spray coating of a hybrid ink of EG and commercially available poly(3, 4-ethylenedioxythiophene): poly(styrenesulphonate) (PEDOT:PSS) formulation (Clevios PH1000, **Figure 1**a) in DMF. The PH1000 is utilized to non-covalently functionalize EG due to its superior electronic properties and solution compatibility with EG, thus forming EG/PH1000 hybrid inks. Conductive graphene films with tailored thickness from 10 to 20 nm can be readily obtained by a spray coating method, yielding a conductivity of about 1000 S/cm with a transmittance of 80% at 500 nm. An ultrathin organic photodetector device based

on P3HT: PCBM blend as photoactive layer is fabricated by employing EG/PH1000 hybrid film as transparent electrode, with a total device thickness of about 3 μm including the substrate. This device exhibits a remarkable performance with detectivity of 1.33×10^{12} Jones at 500 nm irradiation, which is well comparable to the state-of-art Si based inorganic photodetectors.

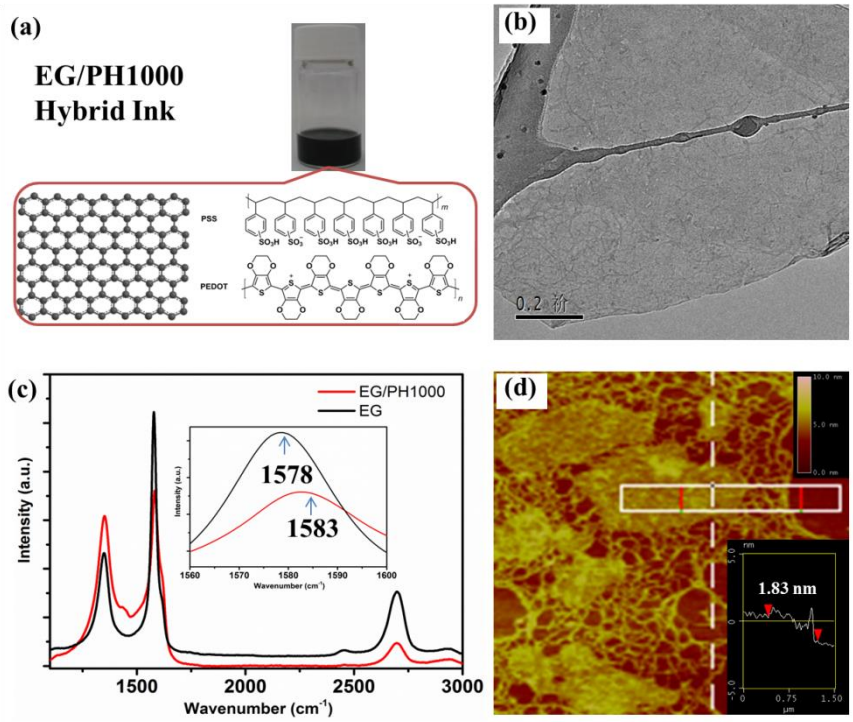

Figure 1. (a) Digital image of EG/PH1000 hybrid ink; molecular structures of EG and PH1000. (b) TEM image of a single graphene sheet from EG/PH1000 hybrid ink. (c) Raman spectra of graphene flakes from EG and EG/PH1000 hybrid ink. Inset shows the shift of the G peak. (d) AFM image of graphene sheets from EG/PH1000 hybrid ink.

The EG was prepared as previously reported.[17a] The EG dispersion is stable with a concentration of 0.3 mg/ml in DMF for two weeks. To overcome the dispersibility of EG at a higher concentration which is essential for the preparation of graphene-based inks, PH1000 was selected as surfactant due to its conjugated aromatic chains which can strongly anchor

onto the graphene surface via π-π interactions without disrupting the electronic structure of graphene. In a typical experiment procedure, 5 ml of the EG dispersion in DMF (1 mg/ml) was mixed with 0.1 ml PH1000 aqueous solution (1-1.3 wt %) followed by a mild sonication and gentle stirring, thus forming a homogenous EG/PH1000 dispersion. The resulting hybrid ink was stable for at least one month without apparent precipitation (Figure 1a). Figure 1b presents the transmission electron microscopy (TEM) image of a single graphene sheet obtained from the EG/PH1000 dispersion. The wavy morphology of PH1000 chains can be clearly identified on top of the graphene surface, indicating the strong interactions between EG and PH1000 in the hybrid ink. The significant π-π interactions between the EG basal plane and PH1000 are supposed to produce charge-transfer effects, which can be confirmed by Raman spectroscopy (Figure 1c). The peak at 1433 cm^{-1} clearly demonstrates the presence of PH1000, and the G-band of EG in Raman spectra is shifted to higher frequency from 1578 cm^{-1} to 1583 cm^{-1}, suggesting the p-type doping of EG.[19]

An atomic force microscopy (AFM) image reveals the morphology of graphene sheets from EG/PH1000 hybrid inks when deposited on a SiO_2 substrate by spin coating (Figure 1d). A typical cross-section picture of a single graphene sheet shows an average thickness of 1.83 nm, where the wavy morphology of PH1000 chains on EG surface can be also observed in accordance with TEM study (Figure 1b). Taking into account that the thickness of the monolayer EG is 0.86 ± 0.1 nm, [17a] the increased thickness of the graphene sheet further demonstrates the strong binding of PH1000 chains on the EG surface by non-covalent functionalization. Moreover, the PH1000 chains are acting as glue coupling the EG sheets together; and such an interpenetrating-network structure should be beneficial for the electron transport across the graphene-graphene junctions.

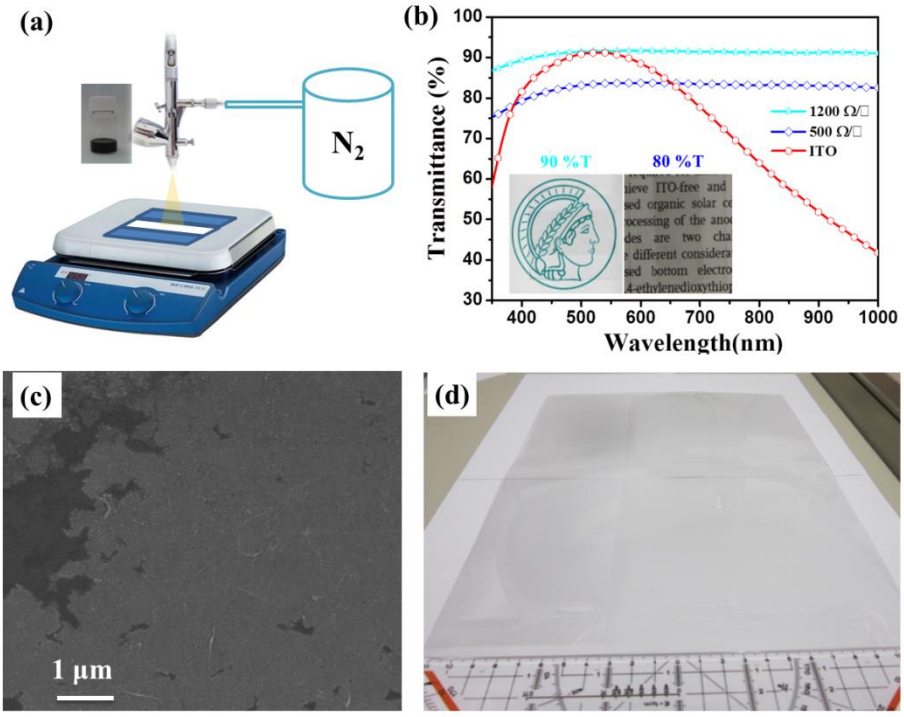

Figure 2. (a) Schematic illustration of spray coating an EG/PH1000 hybrid ink onto desired substrates. (b) Transmittance spectrum of both EG/PH1000 hybrid films and ITO on PET substrates. Inset shows the optical images of the EG/PH1000 hybrid films on PET substrates with 90 % and 80 % transmittance, respectively. (c) SEM image of spray-coated EG/PH1000 hybrid film. (d) A4 paper sized hybrid transparent conductive film obtained by spray coating.

Next, the hybrid ink of EG and PH1000 was used for the preparation of TCE film, as illustrated in **Figure 2**a. The hybrid ink was first loaded into the chamber of an airbrush gun, and then spray coated onto pre-patterned substrates (PET or SiO_2, size: 2.4 cm×2.4 cm) which was kept at 90 ºC by a hot plate to assist solvent evaporation. The diameter of the airbrush nozzle was 0.15 mm and the spray coating pressure was fixed at 3 bar supported by nitrogen gas. The distance between the substrate and airbrush nozzle was 15 cm. In order to achieve a homogeneous film, each spray process was carried out in a gentle manner, so that the output ink was thin enough and could avoid severe aggregation on substrates. Thus, by

adjusting the spray coating cycles, EG/PH1000 hybrid films with thicknesses of 11 and 20 nm (Figure 2b, with 90% and 80% transmittance at 550 nm, respectively) were fabricated applying 60 and 100 cycles of spray coating, respectively. The corresponding R_s were measured to be 500 and 1200 Ω/□, respectively, which are well comparable with the most reported CVD graphene from a PMMA assisted transfer method.[10a, 11] Moreover, the calculated conductivity is about 1000 S/cm for the 20 nm thick film, which is superior to the reported solution-processed graphene films without ultrahigh temperature post treatment (over 1000 ºC).[1a, 20]

To examine the morphology of the fabricated EG/PH1000 hybrid film, scanning electron microscopy (SEM) was conducted on the sample deposited on SiO_2/Si substrate (Figure 2c). A "face on" and densely packed orientation of graphene nanosheets were clearly identified. Such film morphology rather than "wrinkled graphene sheets" is beneficial for electron conduction. An AFM image (Figure S1) of a 20 nm thick hybrid film shows a low surface roughness (RMS) of 3.4 nm over an area of 2 × 2 μm^2 on SiO_2/Si substrate. Moreover, since the hybrid graphene film was manufactured at a relatively low temperature (90 ºC), the spray coating process offers a compatibility of TCE production on large area flexible substrates. Thereby, the A4 paper sized (21 cm × 30 cm) hybrid transparent conductive film was readily produced by spray coating on PET substrate (Figure 2d). The averaged R_s value of such large area films was 600 Ω/□ (with 80 % transmittance at 550 nm), which was slightly higher than those of the small area films mentioned above (PET, 2.4 cm×2.4 cm), probably due to the inhomogeneity of spray coating and limited size of our nozzle over such large area.

To investigate the mechanical stretchability of the hybrid films, we spray coated EG/PH1000 hybrid ink onto a polydimethylsiloxane (PDMS) substrate with 70% transmittance at 550 nm. As shown in **Figure 3**a, the R_s increased almost linearly when the

film was stretched from 0 to 20%. Remarkably, the resistance nearly resumed to the original value (R_0, on flat unstretched PDMS) after recovering the film to the flat state. Furthermore, the stretching to 20% was examined over 50 cycles without any noticeable change of the resistance in the unstretched state (Figure 3b). In contrast, the CVD-graphene (monolayer or bilayer) film transferred onto a PDMS substrate only showed stretchability up to about 6%.[10a] We further performed the bending test of the spray coated EG/PH1000 film on PET substrate as shown in Figure 3c. Compared with ITO on PET substrate (thickness of ITO is 75 nm, commercially obtained from Sigma-Aldrich), R_s of the spray coated EG/PH1000 hybrid film perfectly maintained the original value after 1000 times of bending with a radius of 5 mm, while the R_s of ITO increased dramatically after 300 cycles of bending. Moreover, foldable circuits can be manufactured by printing EG/PH1000 hybrid ink on paper, as shown in Figure 3d. Such circuits can be stable during folding and unfolding for over 100 cycles. Therefore, the pronounced stretching and bending stability of EG/PH1000 hybrid films qualify them as flexible transparent electrode for optoelectronic devices (see below).

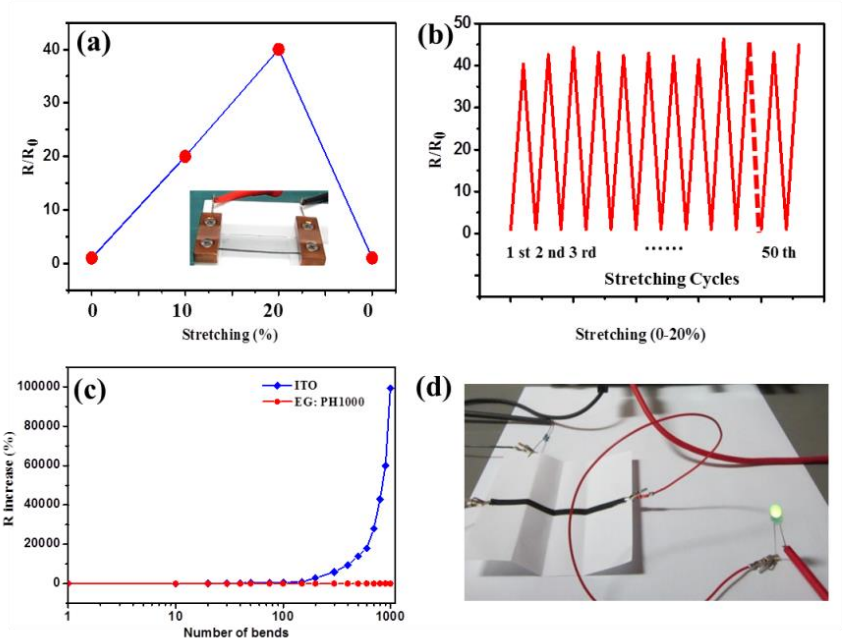

Figure 3. (a) First cycle of stretchablity test of EG/PH1000 hybrid film on PDMS. (b) 50 cycles of stretchablity test of EG/PH1000 hybrid film on PDMS. (c) Bending test of EG/PH1000 hybrid film. (d) Printed foldable graphene circuits on paper.

EG/PH1000 hybrid films on PET substrates were thus examined as bottom electrodes for flexible OPD devices. The digital image of the fabricated OPD device is displayed in **Figure 4**a inset with a device configuration of EG/PH1000/PEDOT: PSS/P3HT: PCBM/Al, in which EG/PH1000 hybrid films have been employed as bottom electrodes. Another formulation of PEDOT: PSS (Clevios P VP AI 4083) was used as hole transporting layer. Photosensitive polymer P3HT was blended with PCBM in a chlorobenzene solution (18 mg/ml in total concentration, weight ratio is 1:0.8), acting as photoactive layer. Current-voltage (I-V) characteristics of P3HT: PCBM photodetectors are shown in Figure 4a. Under weak illumination (20 mW cm^{-2}), the photodetector behaves as a typical photovoltaic device. The large difference of the currents in the dark and under illumination around the origin (0, 0) allows the device to be operated at very low bias voltage, offering the possibility of working at low energy consumption.[21] In contrast, photodetectors based on colloidal inorganic semiconductor quantum dots generally require a high driving voltage (over 40 V).[22] By switching the shielded light alternately on and off causes the current of the devices to exhibit two distinct steady states: the “low” current state in the dark and the “high” current state under illumination. Figure 4b reveals the typical on/off characteristics of the photodetector at 0 V bias, the photocurrent jumps sharply by more than four orders of magnitude upon irradiation. The high I_{on}/I_{off} ratio (8.4×10^4) indicates high photosensitivity of the device, which is close to the state-of-art organic photodetector performance.[21, 23] The mechanical durability of the fabricated OPD based on EG/PH1000 electrode was further investigated by measuring I_{on}/I_{off} ratio change before/after bending the device. As shown in Figure 4b, after

200 cycles of bending with a radius of 5 mm, the photocurrent only decreased by 1% and the I_{on}/I_{off} ratio remained at the same order of magnitude, suggesting the great potential of EG/PH1000 hybrid film as a flexible electrode. Further bending over 500 cycles resulted in the damage of Al electrode.

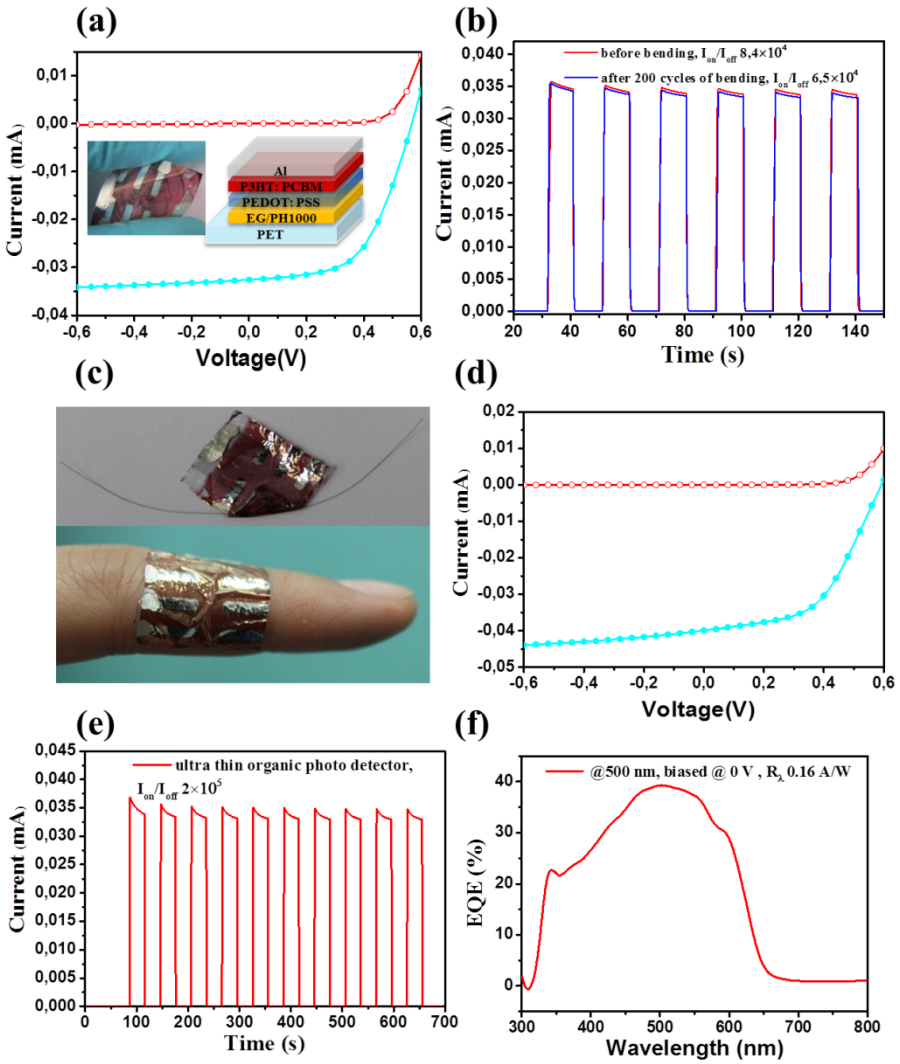

Figure 4. (a) I-V characteristics of the photodetectors fabricated on regular PET (Inset shows the fabricated device and schematic device structures of the OPDs). (b) The on/off characteristics of the photodetector at 0 V bias on regular PET before and after 200 cycles of bending test. (c) Ultrathin and flexibility demonstration of the fabricated photodetector, thinner than a human hair, could be attached to the human body. (d) I-V characteristics of the

ultrathin photodetectors. (e) The on/off characteristics of the ultrathin photodetectors. (f) EQE spectrum of the ultrathin photodetectors.

We further fabricated ultra-thin OPD devices based on EG/PH1000 hybrid films. To this end, ultrathin PET foils with a thickness of 2.5 μm were employed as substrates. For the convenience of device fabrication, ultrathin PET foils were attached to PDMS coated rigid glass slides. By adhering the ultrathin PET foils to the supports, all subsequent processing steps including spray coating, spin coating, thermal annealing and vacuum deposition, were exactly the same as processed on regular PET foils. Afterwards, the as-fabricated ultra-thin OPD device was carefully peeled off from the supporting PDMS without causing any damage to the device. As shown in Figure 4c, the total thickness of the fabricated photodetector device is below 3 μm including the substrate. Interestingly, the ultrathin OPD device can be attached to a human finger or other body parts, manifesting tremendous flexibility and compatibility with artificial intelligent devices. The I-V characteristics under illumination (Figure 4d) displayed a typical photodiode character with an open circuit voltage of 0.58 V and a short circuit current density of 0.61 mA cm^{-2}. Based on the on/off characteristics of the ultrathin OPD as shown in Figure 4e, a remarkably high I_{on}/I_{off} ratio of 2×10^5 could be obtained. In order to obtain the responsivity ($\mathbf{R}_\lambda$ in A/W) at certain wavelength irradiation, the external quantum efficiency (EQE) of the device under 0 V bias was measured and plotted in Figure 4f. $R_\lambda = J_{ph}/L_{light}$, where J_{ph} is the photocurrent and L_{light} is the incident light intensity.

The device was sensitive to a spectral response ranging from 300 to 650 nm due to the strong absorption of P3HT, and the maximum value reached 40% at 500 nm irradiation. We assume that the major contribution of the shot noise of the OPD is from the dark current of the device. The detectivity (D* in units of Jones) can be expressed as

$D^* = R/ (2qJ_d)^{1/2} = (J_{ph}/L_{light})/(2qJ_d)^{1/2}$,

where q is the absolute value of electron charge (1.6×10^{-19} Coulombs) and J_d is the dark current. The responsivity $\mathbf{R_\lambda}$ and detectivity **D*** of the ultra-thin OPD at 500 nm were thus calculated to be 0.16 A/W and 1.33×10^{12} Jones respectively.[24] The results clearly demonstrate that achieving high detectivity requires not only high photoresponsivity (high photocurrent) but also low noise (low dark current). The detectivity of 1.33×10^{12} Jones achieved in our work is of the same magnitude as that of reported inorganic photodetectors based on Si, GaAs, or other colloidal quantum dots.[22, 24-25]

In conclusion, we have developed a novel solution fabrication of large area, highly conductive graphene films by spray coating of EG/PH1000 hybrid ink. The fabricated graphene films exhibited excellent mechanical properties, thus enabling their application as bottom electrodes in ultrathin organic photodetector devices with performance comparable to that of the state-of-art Si based inorganic photodetectors. The hybrid ink of EG/PH1000 employing further optimized electrochemically exfoliated graphene may pave the way to the future development of transparent electrodes for optoelectronics, and other emerging flexible devices such as wearable supercapacitors and electronic skins.[26]

Experimental Section

Experimental Details including Materials, EG Production, EG/PH1000 hybrid thin film produced by spray coating, and Photodetector devices fabrication and characterization, are listed in supporting information.

Supporting Information

Supporting Information is available online from the Wiley Online Library or from the author.

Acknowledgements

This work was financially supported by the ERC Grant on NANOGRAPH and 2DMATER, EU Project GENIUS and MoQuas, EC under Graphene Flagship (No. CNECT-ICT-604391) and MaxNet Energy.

Reference

[1] a) H. A. Becerril, J. Mao, Z. Liu, R. M. Stoltenberg, Z. Bao, Y. Chen, *Acs Nano* **2008**, *2*, 463; b) E. Artukovic, M. Kaempgen, D. S. Hecht, S. Roth, G. Grüner, *Nano Lett.* **2005**, *5*, 757; c) S. Bae, H. Kim, Y. Lee, X. Xu, J.-S. Park, Y. Zheng, J. Balakrishnan, T. Lei, H. R. Kim, Y. I. Song, Y.-J. Kim, K. S. Kim, B. Ozyilmaz, J.-H. Ahn, B. H. Hong, S. Iijima, *Nature Nanotechnology* **2010**, *5*, 574; d) N. Behabtu, J. R. Lomeda, M. J. Green, A. L. Higginbotham, A. Sinitskii, D. V. Kosynkin, D. Tsentalovich, A. N. G. Parra-Vasquez, J. Schmidt, E. Kesselman, Y. Cohen, Y. Talmon, J. M. Tour, M. Pasquali, *Nature Nanotechnology* **2010**, *5*, 406.

[2] a) X. Wang, L. Zhi, N. Tsao, Ž. Tomović, J. Li, K. Müllen, *Angew. Chem. Int. Ed.* **2008**, *47*, 2990; b) J. Y. Kim, K. Lee, N. E. Coates, D. Moses, T.-Q. Nguyen, M. Dante, A. J. Heeger, *Science* **2007**, *317*, 222.

[3] a) A. Kumar, C. Zhou, *ACS Nano* **2010**, *4*, 11; b) T.-H. Han, Y. Lee, M.-R. Choi, S.-H. Woo, S.-H. Bae, B. H. Hong, J.-H. Ahn, T.-W. Lee, *Nat Photon* **2012**, *6*, 105; c) J. Zou, C.-Z. Li, C.-Y. Chang, H.-L. Yip, A. K. Y. Jen, *Adv. Mater.* **2014**, *26*, 3618.

[4] a) S. Bauer, S. Bauer-Gogonea, I. Graz, M. Kaltenbrunner, C. Keplinger, R. Schwödiauer, *Adv. Mater.* **2014**, *26*, 149; b) H. Wu, D. S. Kong, Z. C. Ruan, P. C. Hsu, S. Wang, Z. F. Yu, T. J. Carney, L. B. Hu, S. H. Fan, Y. Cui, *Nature Nanotechnology* **2013**, *8*, 421.

[5] a) J.-Y. Lee, S. T. Connor, Y. Cui, P. Peumans, *Nano Lett.* **2008**, *8*, 689; b) S. De, T. M. Higgins, P. E. Lyons, E. M. Doherty, P. N. Nirmalraj, W. J. Blau, J. J. Boland, J. N. Coleman, *ACS Nano* **2009**, *3*, 1767.

[6] a) Z. Wu, Z. Chen, X. Du, J. M. Logan, J. Sippel, M. Nikolou, K. Kamaras, J. R. Reynolds, D. B. Tanner, A. F. Hebard, A. G. Rinzler, *Science* **2004**, *305*, 1273; b) M. W. Rowell, M. A. Topinka, M. D. McGehee, H.-J. Prall, G. Dennler, N. S. Sariciftci, L. Hu, G.

Gruner, *Appl. Phys. Lett.* **2006**, *88*, 233506; c) J. Du, S. Pei, L. Ma, H.-M. Cheng, *Adv. Mater.* **2014**, *26*, 1958.

[7] a) W. F. Zhang, B. F. Zhao, Z. C. He, X. M. Zhao, H. T. Wang, S. F. Yang, H. B. Wu, Y. Cao, *Energy Environmental Science* **2013**, *6*, 1956; b) N. Kim, S. Kee, S. H. Lee, B. H. Lee, Y. H. Kahng, Y.-R. Jo, B.-J. Kim, K. Lee, *Adv. Mater.* **2014**, *26*, 2268.

[8] D. S. Hecht, L. Hu, G. Irvin, *Adv. Mater.* **2011**, *23*, 1482.

[9] a) K. S. Novoselov, V. I. Falko, L. Colombo, P. R. Gellert, M. G. Schwab, K. Kim, *Nature* **2012**, *490*, 192; b) F. Bonaccorso, Z. Sun, T. Hasan, A. C. Ferrari, *Nat Photon* **2010**, *4*, 611.

[10] a) K. S. Kim, Y. Zhao, H. Jang, S. Y. Lee, J. M. Kim, K. S. Kim, J.-H. Ahn, P. Kim, J.-Y. Choi, B. H. Hong, *Nature* **2009**, *457*, 706; b) Z. P. Chen, W. C. Ren, L. B. Gao, B. L. Liu, S. F. Pei, H.-M. Cheng, *Nature Materials* **2011**, *10*, 424; c) L. Gao, G.-X. Ni, Y. Liu, B. Liu, A. H. Castro Neto, K. P. Loh, *Nature* **2014**, *505*, 190; d) D. C. Wei, B. Wu, Y. L. Guo, G. Yu, Y. Q. Liu, *Acc. Chem. Res.* **2013**, *46*, 106; e) H. Zhou, W. J. Yu, L. Liu, R. Cheng, Y. Chen, X. Huang, Y. Liu, Y. Wang, Y. Huang, X. Duan, *Nat. Commun.* **2013**, *4*, 2096.

[11] S. Bae, H. Kim, Y. Lee, X. F. Xu, J. S. Park, Y. Zheng, J. Balakrishnan, T. Lei, H. R. Kim, Y. I. Song, Y. J. Kim, K. S. Kim, B. Ozyilmaz, J. H. Ahn, B. H. Hong, S. Iijima, *Nature Nanotechnology* **2010**, *5*, 574.

[12] A. Pirkle, J. Chan, A. Venugopal, D. Hinojos, C. W. Magnuson, S. McDonnell, L. Colombo, E. M. Vogel, R. S. Ruoff, R. M. Wallace, *Appl. Phys. Lett.* **2011**, *99*, 122108.

[13] a) G. Eda, G. Fanchini, M. Chhowalla, *Nat Nano* **2008**, *3*, 270; b) X. Cao, D. Qi, S. Yin, J. Bu, F. Li, C. F. Goh, S. Zhang, X. Chen, *Adv. Mater.* **2013**, *25*, 2957.

[14] a) K. R. Paton, E. Varrla, C. Backes, R. J. Smith, U. Khan, A. O'Neill, C. Boland, M. Lotya, O. M. Istrate, P. King, T. Higgins, S. Barwich, P. May, P. Puczkarski, I. Ahmed, M. Moebius, H. Pettersson, E. Long, J. Coelho, S. E. O'Brien, E. K. McGuire, B. M. Sanchez, G.

S. Duesberg, N. McEvoy, T. J. Pennycook, C. Downing, A. Crossley, V. Nicolosi, J. N. Coleman, *Nat. Mater.* **2014**, *13*, 624; b) Y. Hernandez, V. Nicolosi, M. Lotya, F. M. Blighe, Z. Sun, S. De, I. T. McGovern, B. Holland, M. Byrne, Y. K. Gun'Ko, J. J. Boland, P. Niraj, G. Duesberg, S. Krishnamurthy, R. Goodhue, J. Hutchison, V. Scardaci, A. C. Ferrari, J. N. Coleman, *Nat Nano* **2008**, *3*, 563.

[15] J. Wang, K. K. Manga, Q. Bao, K. P. Loh, *J. Am. Chem. Soc.* **2011**, *133*, 8888.

[16] C.-J. Shih, A. Vijayaraghavan, R. Krishnan, R. Sharma, J.-H. Han, M.-H. Ham, Z. Jin, S. Lin, G. L. C. Paulus, N. F. Reuel, Q. H. Wang, D. Blankschtein, M. S. Strano, *Nat Nano* **2011**, *6*, 439.

[17] a) K. Parvez, R. Li, S. R. Puniredd, Y. Hernandez, F. Hinkel, S. Wang, X. Feng, K. Müllen, *ACS Nano* **2013**, *7*, 3598; b) K. Parvez, Z.-S. Wu, R. Li, X. Liu, R. Graf, X. Feng, K. Müllen, *J. Am. Chem. Soc.* **2014**, *136*, 6083.

[18] J. Shim, J. M. Yun, T. Yun, P. Kim, K. E. Lee, W. J. Lee, R. Ryoo, D. J. Pine, G.-R. Yi, S. O. Kim, *Nano Lett.* **2014**, *14*, 1388.

[19] a) DasA, PisanaS, ChakrabortyB, PiscanecS, S. K. Saha, U. V. Waghmare, K. S. Novoselov, H. R. Krishnamurthy, A. K. Geim, A. C. Ferrari, A. K. Sood, *Nat Nano* **2008**, *3*, 210; b) V. Z. Poenitzsch, D. C. Winters, H. Xie, G. R. Dieckmann, A. B. Dalton, I. H. Musselman, *J. Am. Chem. Soc.* **2007**, *129*, 14724.

[20] X. Wang, L. Zhi, K. Müllen, *Nano Lett.* **2007**, *8*, 323.

[21] S. Pang, S. Yang, X. Feng, K. Müllen, *Adv. Mater.* **2012**, *24*, 1566.

[22] G. Konstantatos, I. Howard, A. Fischer, S. Hoogland, J. Clifford, E. Klem, L. Levina, E. H. Sargent, *Nature* **2006**, *442*, 180.

[23] a) X. Wang, W. Song, B. Liu, G. Chen, D. Chen, C. Zhou, G. Shen, *Adv. Funct. Mater.* **2013**, *23*, 1202; b) H. F. Zhu, T. Li, Y. J. Zhang, H. L. Dong, J. S. D. Song, H. P. Zhao, Z. M. Wei, W. Xu, W. P. Hu, Z. S. Bo, *Adv. Mater.* **2010**, *22*, 1645.

[24] X. Gong, M. Tong, Y. Xia, W. Cai, J. S. Moon, Y. Cao, G. Yu, C.-L. Shieh, B. Nilsson, A. J. Heeger, *Science* **2009**, *325*, 1665.

[25] F. Guo, B. Yang, Y. Yuan, Z. Xiao, Q. Dong, Y. Bi, J. Huang, *Nat Nano* **2012**, *7*, 798.

[26] a) M. L. Hammock, A. Chortos, B. C. K. Tee, J. B. H. Tok, Z. Bao, *Adv. Mater.* **2013**, *25*, 5997; b) T. Chen, Y. Xue, A. K. Roy, L. Dai, *ACS Nano* **2013**, *8*, 1039.

Supporting Information

Transparent Conductive Electrodes from Graphene/PEDOT: PSS Hybrid Inks for Ultrathin Organic Photodetectors

Experimental Section

Materials:

Graphite foil was purchased from Alfa Aesar. Clevios PH1000 (1.3 wt %) and P VP AI 4083 (used for hole transporting layer) were purchased from Heraeus Clevios GmbH. ITO on PET substrate and PCBM were obtained from Sigma-Aldrich. P3HT was purchased from Rieke Metals Inc. Airbrush (Infinity CRplus) was purchased from Harder & Steenbeck GmbH. Ultrathin PET foils were supported by Pütz GmbH + Co. Folien KG.

EG Production:

EG was produced as previously reported. Briefly, graphite foil, platinum wires, and 0.1 M H_2SO_4 solutions were used as working electrodes, counter electrodes, and electrolytes, respectively. When a positive voltage (i.e., +10 V) was applied to a graphite electrode, the graphite foil begins to expand, quickly dissociate, and spread into the solution. The bias voltage was kept constant for 2 min to complete the exfoliation process. Afterward, the exfoliated graphitic material was collected by vacuum filtration and washed repeatedly with water to remove the residual acid. Finally, the obtained powder was dispersed in DMF, resulting in EG sheets with a concentration of 1 mg/ml.

EG/PH1000 hybrid thin film produced by spray coating:

PH1000, 0.1 ml was drop wisely added into 5ml of graphene DMF suspension (1 mg/ml) with vigorously stirring for 1 h, to realize a weight content of 20% PH1000 in the graphene

composite. The mixed solution was spray coated with an airbrush on pre-heated PET substrates at 90 ºC under a pressure of 3 bar supported by nitrogen gas. The PET substrates were precut into 2.4 cm×2.4 cm, and scotch tape was used for the cover of certain areas for the desired electrode pattern, after which will be peeled off carefully. After each spray, a pause of 20 s should be taken for the film to be dried. The hybrid film will be heated 90 ºC in the oven overnight to remove residual solvent before use. R_s was measured by a standard four-point probe system with a Keithley 2700 Multimeter (probe spacing: 0.635 mm, R_s= 4.5324 V/I). Stretchability test was carried out on a home-made machine. The two point resistance was also measured by a Keithley 2700 Multimeter.

Photodetector devices fabrication and characterization:

Photodetector devices with a structure of EG: PH1000/PEDOT: PSS/P3HT: PCBM/Al was fabricated. PEDOT: PSS was spin coated on patterned EG: PH1000 electrode at 4000 rpm, 60s. The film was then heated at 120 ºC for 20 min to dry. P3HT: PCBM (weight ratio 1:0.8, total concentration 18 mg/ml in chlorobenzene) was spin coated on top of PEDOT: PSS layer, followed by aluminum deposition of 100 nm under vacuum (10^{-5} Pa). For the ultra-thin devices, rigid glass slides, coated with a 100 μm-thick PDMS layer, served as supporting substrates for the 2.5-μm-thick PET foils. By adhering the ultrathin PET foils to the supports, all subsequent processing steps including spray coating, spin coating, thermal annealing and vacuum deposition, were exactly the same as processed on regular PET foils. The devices could be peeled off from the supporting PDMS without causing any damage to the photodetectors.

The photodetectors were tested in a glove box under nitrogen atmosphere with a Keithley SCS 4200 semiconductor characterization system. The light of a Nikon microscope (SMZ1000, ca. 20 mW cm^{-2}) was directly used to switch on/off the photodiode with an interval of 10 s or 30s.

The external quantum efficiency (EQE) characterization of all devices was performed under the protection of an N_2 atmosphere. The light output from a Xe lamp was monochromatedby a Digichrom 240 monochromator and the short-circuit device photocurrent was monitored by a Kethley electrometer as the monochromator was scanned. A calibrated Si photodiode (818-UVNewport) was used as a reference in order to determine the intensity of the light incident on the device, allowing the EQE spectrum to be deduced.

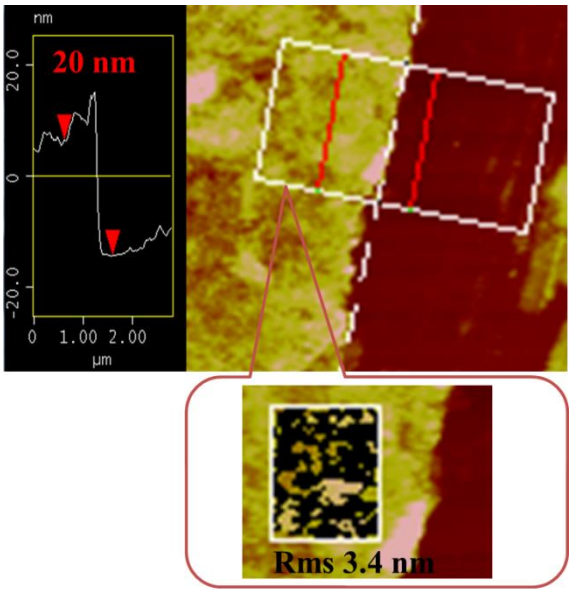

Figure S1. AFM image of spray-coated EG/PH1000 hybrid film with a thickness of 20 nm.

Chapter 3. Ultraflexible in-plane Micro-Supercapacitors by Direct Printing of Solution-Processable Electrochemically Exfoliated Graphene

Key words: printing, in-plane, micro-supercapacitors, electrochemically exfoliated graphene, energy storage

ToC Figure

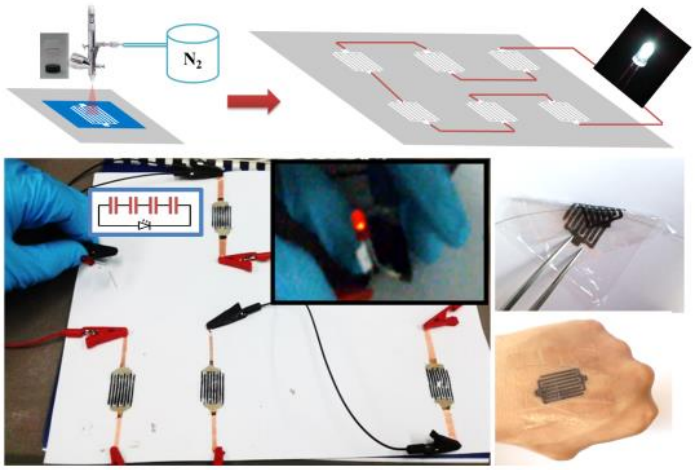

A novel direct printing approach for in-plane micro-supercapacitors (MSCs) fabrication was demonstrated. Solution processed graphene/conductive polymer hybrid inks were utilized. The fabricated MSC on paper substrate offered significant areal capacitance and excellent rate capability. An ultra-thin MSC on PET (2.5-μm-thick) substrate exhibited "ultraflexiblity," making it suitable for the next-generation flexible micro-electrochemical energy storage devices.

Published in:

Advanced Materials

Reprinted with permission from (*Adv. Mater.* **2016**, *28*, 2217-2222.)

With portable and miniaturized electronic devices becoming increasingly pervasive in our daily lives, there is a growing demand for lightweight, flexible, and highly efficient micro-scale energy storage devices.[1] Current commercially available thin-film batteries, which incorporate micro-scale power sources into electronics and micro-systems, suffer from various limitations, such as a short cycle life, abrupt failure, poor low-temperature kinetics, and safety concerns associated with using lithium.[2] Moreover, the integration of batteries with electronic circuits is challenging and often limits the miniaturization of the entire system.[3] This effect occurs because the necessary energy-storage components scale down in size poorly and are not well suited for the in-plane geometries of integrated micro-fabrication processes. Recently, in-plane micro-supercapacitors (MSCs) have emerged as potential candidates to complement or even replace micro-batteries in various applications because they can provide a high power density, a fast charge/discharge rate, and a long cycle life.[4] Advanced progress in micro-fabrication technology has enabled on-chip MSCs in an interdigitated planar form.[2c, 3, 5] All-solid-state MSCs that do not use a liquid electrolyte can be directly implemented as embedded energy-storage devices for portable and wearable microelectronics systems. However, the conventional fabrication techniques for MSC devices rely primarily on photolithography or on oxidative channel-etching methods to define patterns on substrates, which are difficult to apply to the construction of cost-effective and flexible devices for commercial applications. To overcome the obstacles surrounding scalability, high-cost and flexibility, new strategies to manufacture MSCs efficiently on flexible substrates are highly appealing.

Direct printing techniques, including spray deposition and inkjet printing, offer a promising protocol for future roll-to-roll production of MSC arrays, which can be rapidly processed onto both plastic and paper substrates at low temperature and over large areas. As a key component for printing techniques, the selected ink should be stable, low-cost and easily

printable on appropriate substrates; it should display excellent electrical properties, without the need for aggressive post-treatments. Graphene is well suited for use in printable supercapacitors because of its large theoretical surface area (2630 $m^2 g^{-1}$), excellent electrical conductivity, high intrinsic areal capacitance (21 μF cm^{-2} for a single layer), theoretical gravimetric capacitance (550 F g^{-1}), and mechanical robustness.

In this work, we demonstrate novel and directly printable in-plane MSCs on paper and ultra-thin polyethylene terephthalate (PET) substrates. Graphene ink with a concentration of 0.8 mg mL^{-1} was obtained by electrochemically exfoliating graphite under mild conditions. Such a graphene dispersion was stable in volatile 2-propanol (IPA) for at least 4 weeks. A hybrid ink composed of electrochemically exfoliated graphene (EG) and an electrochemically active poly(3,4-ethylenedioxythiophene):poly(styrenesulfonate) (PEDOT:PSS) formulation (Clevios PH1000) was subsequently prepared. By spray coating the EG/PH1000 hybrid ink through a shadow mask with the designed MSC device geometry, the direct printing of MSCs was realized. The fabricated MSC on a paper substrate offered a significant areal capacitance as high as 5.4 mF cm^{-2}, which is among the best reported performances of graphene based MSCs, and exhibited an excellent rate capability with a capacitance retention of 75% when operated from 10 to 1000 mV s^{-1}. We further demonstrated that light-emitting diodes (LED) could be readily illuminated by MSC arrays that were printed on a paper substrate. Moreover, using a PET (2.5-μm-thick) substrate for the formation of the printed hybrid film resulted in an ultra-thin MSC that exhibited "ultraflexiblity," thus making it suitable for the next-generation flexible micro-electrochemical energy storage devices.

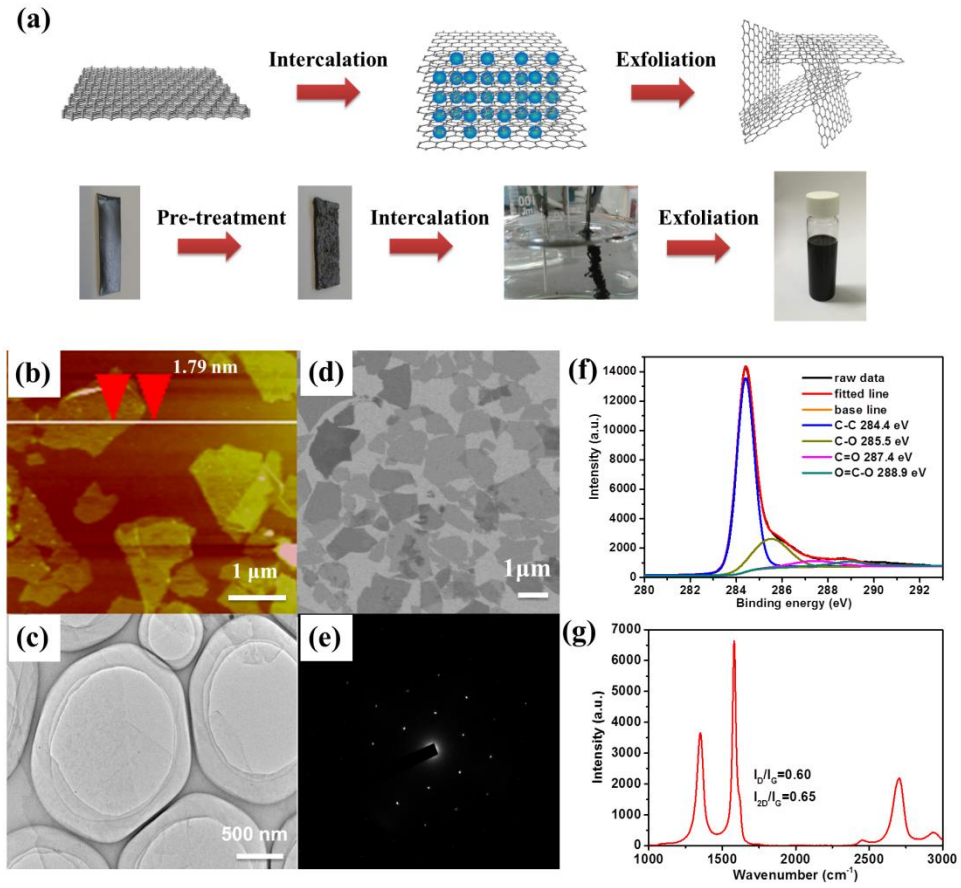

Figure 1. (a) Schematic illustration of the electrochemical exfoliation of graphene and photographs of the graphite foil volume change during exfoliation. (b) An AFM image of the EG sheets on SiO_2. (c) A TEM image of the EG sheets. (d) An SEM image of the EG sheets on SiO_2. (e) An SAED pattern of bilayer graphene. (f) High-resolution XPS of the C 1s spectrum for EG. (g) The Raman spectrum of a selected area of EG with the ratios of I_D/I_G and I_{2D}/I_G peaks indicated.

EG was produced with a two electrode system (**Figure 1**a) using platinum as the counter electrode and a pre-treated graphite foil as the working electrode (Supporting Information). Initially, high voltage pulses (+10 V) were applied to expand the graphite, as shown in Figure 1a. Afterward, 30 minutes of low voltage (+3 V) was applied for direct exfoliation. After washing of the exfoliated product, the collected EG powder was dispersed in IPA by

sonication for 30-40 min. Thus, EG ink with a high concentration of 0.8 mg mL^{-1} was readily obtained. The ink remained stable for 4 weeks without visible agglomeration. Atomic force microscopy (AFM) revealed the flat graphene morphology of the nanosheets (Figure 1b). The typical cross-section of a single graphene sheet shows an average thickness of 1.82 nm (statistically from 100 nanosheets by AFM measurement, [6] as shown in Figure S1), suggesting that the EG sheets are dominated by double layers[7]. The morphology of the EG sheets was further investigated by scanning electron microscopy (SEM) and transmission electron microscopy (TEM). Note that the lateral sizes of over 95% of the EG sheets were smaller than 2 μm (Figure 1c and d), which is ideal for most printing techniques because larger graphene sheets might block the nozzle.[8] The selected area electron diffraction (SAED) exhibited a typical 6-fold symmetric pattern with stronger diffraction from the (1-210) plane than from the (0-110) plane, indicating the high crystallinity of a bilayer graphene sheet (Figure 1e).[9] As presented in Figure S2 and Figure 1f, X-ray photoelectron spectroscopy (XPS) revealed a low oxygen-atom content (13%) in EG. The dominant oxygen species were attributed to the C−OH group at 285.5 eV, which is due to oxidation of the graphite electrode during the low-voltage exfoliation process, and also explains the good dispersibility of EG in IPA. Raman spectroscopy of the EG sheets on SiO_2/Si substrates (Figure 1g) revealed that the intensity of the G peak was almost two times that of the D peak. The derived I_D/I_G value (0.60) is much smaller than that of chemically or thermally reduced graphene oxide (~1.1−1.5), indicating a lower degree of defects and thus better electronic conductivity for EG.

The low boiling point of IPA and the high stability of EG ink are beneficial for the direct spray coating or ink-jet printing of graphene for MSC electrode patterning. **Figure 2**a depicts the general procedure for the mask-assisted spray deposition method for the direct printing of MSC devices and “arrays” (several devices connected in a series manner) on paper or PET

substrates. Firstly, EG ink was spray-coated onto paper substrates covered by the shadow mask (both finger and channel widths were 1000 μm, and the length was 2 cm).[10] Subsequently, a gel electrolyte of poly(vinyl alcohol) (PVA)/H_2SO_4 was drop-casted onto the finger electrodes and allowed to solidify overnight (inset of Figure 2c). After that, an all solid state EG-based MSC with in-plane geometry was obtained. One advantage of producing the MSC device on paper is that the porous structure of paper can lead to a large capillary force that acts on the ink. The strong capillary force enables a large contact surface area between the graphene sheets and the paper substrate after the ink is absorbed and the solvent evaporates. By adjusting the amount of EG ink and the number of spray coating cycles, the thickness of the patterned micro-electrodes was easily controlled. As shown in Figure 2a, the corresponding R_s of the EG based MSC patterns on SiO_2 and paper substrates reached as low as 15Ω sq^{-1}, which is comparable to the carbon nanotube paper obtained from a rod-coating method (with the same film thickness of approximately 1.5 μm).[11] Moreover, the R_s of the MSC electrode film perfectly maintained its original value after being bent to a radius of 5 mm 500 times (Figure S3), demonstrating a great potential for flexible MSC devices.[10]

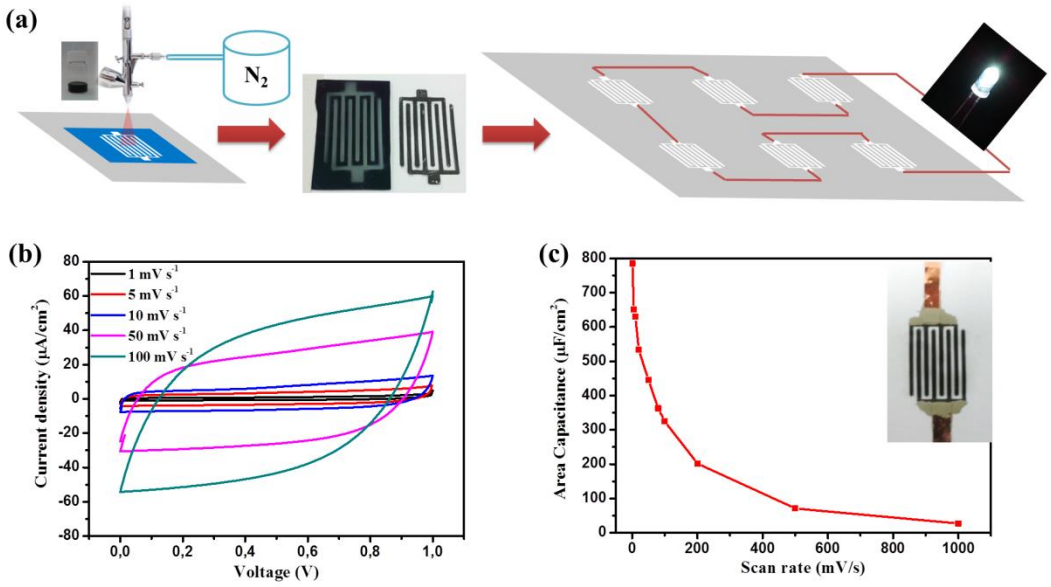

Figure 2. (a) Schematic illustration of the mask-assisted spray deposition method for the direct printing of single and arrayed MSC devices; pictures of EG-based MSC patterns on SiO_2 and paper substrates. (b) Cyclic voltammetry curves of a pristine EG ink (total amount 3 mL) MSC on a paper substrate at scan rates of 1 mV s^{-1} to 100 mV s^{-1}. (c) The evolution of areal capacitance versus scan rate, the inset shows a digital image of the as fabricated MSC device on normal printing paper.

To examine the electrochemical properties, we carried out cyclic voltammetry (CV) of the MSCs based on spray-coating 3 mL of EG ink (a film thickness of approximately 0.5 μm), as shown in Figure 2b and c. The device delivered an areal capacitance of 800 μF cm^{-2} at a scanning rate of 1 mV s^{-1}, whereas only 40% of this capacitance remained after scanning at 100 mV s^{-1}. The performance of such an EG-based MSC is mainly attributed to the capacitive nature of the electric double-layer in EG. To enhance the capacitance of the printed MSC, a hybrid ink containing EG and the electrochemically active PH1000 was fabricated. In a typical experimental procedure, 5 mL of the EG dispersion in IPA (1 mg mL^{-1}) was mixed with 0.5 mL of the PH1000 aqueous solution (1–1.3 wt%). This was followed by a mild sonication and gentle stirring, thus, forming a homogenous EG/PH1000 hybrid ink. The morphology study suggested that the polymer chains of PH1000 strongly interacted with the graphene surface via a non-covalent functionalization, which was responsible for the high stability of the hybrid ink.[10] The pseudocapacitive MSC device that was based on the EG/PH1000 film was fabricated by spray-coating 3 mL of the hybrid ink, and other procedures were kept the same as those for the pure EG-based MSCs.

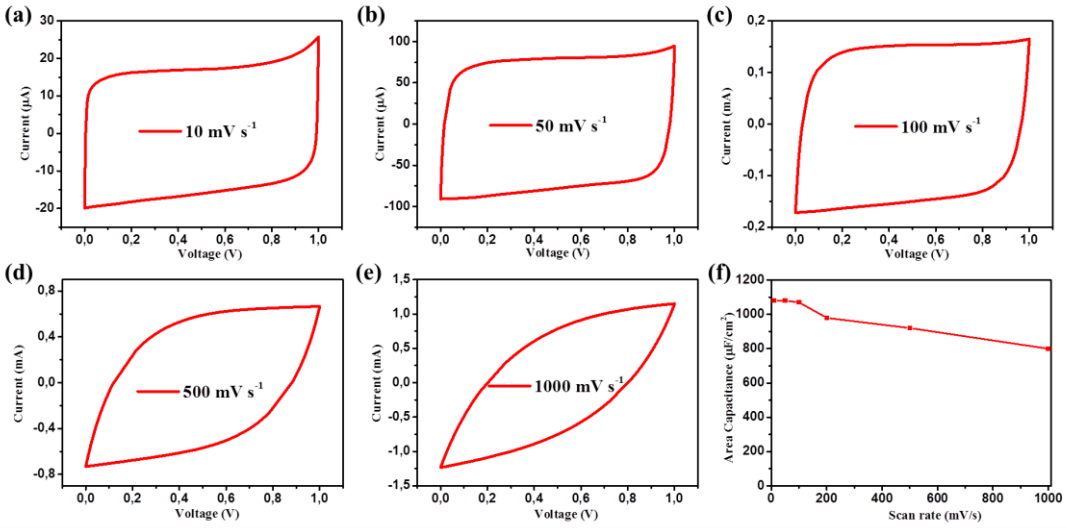

Figure 3.(a-e) Cyclic voltammetry curves of an EG/PH1000 hybrid ink (total amount 3 mL) MSC on a paper substrate with scan rates ranging from 10 to 1000 mV s^{-1}, and (f) the evolution of areal capacitance versus scan rate.

As shown in **Figure 3** a-e and Figure S4, CV experiments were performed at scan rates ranging from 5 to 5000 mVs^{-1}. Compared with pure EG-based MSCs, the devices based on the EG/PH1000 hybrid ink exhibited an exceptionally enhanced electrochemical performance with a nearly rectangular CV shape, even at a scan rate of 1000 mV s^{-1}, which is indicative of the pronounced capacitive behavior inherent to the EG/PH1000 hybrid. An areal capacitance of 1080 μF cm^{-2} at scan rate of 10 mV s^{-1} was delivered, and there was no obvious capacitance change when the scan rate increased to 100 mV s^{-1}. Moreover, the device exhibited capacitance retention of 75% when operated at 1000 mV s^{-1}, which indicated that a capability for fast charging and discharging. Such a high rate capacitance outperformed most of the reported graphene based MSCs.[3, 12] The device also exhibited excellent cycling stability with ~90% capacitance retention after 5000 charge/discharge cycles. (Figure S4d, measured at scan rate of 100 mV s^{-1}).

We further optimized the areal and volumetric capacitances of the device with different film thicknesses. When spray coating 10 mL of the EG/PH1000 hybrid ink, the thickness of the MSC electrode pattern reached up to 2 μm. Remarkably, a maximum areal capacitance of 5.4 mF cm^{-2} was achieved at 1 mV s^{-1} (**Figure 4**a), which is also superior to most of the reported values for graphene or porous carbon based MSCs, e.g., reduced graphene oxide (RGO) MSCs from the direct laser writing of GO films using a standard LightScribe DVD burner (2.32 mF cm^{-2}, thickness ~8 μm)[3], RGO microelectrodes by laser reduction and patterning of GO films (0.51 mF cm^{-2}, thickness ~20 μm),[5a] onion like carbon (1.7 mF cm^{-2}, thickness ~7 μm) [5b], and a methane plasma reduced RGO film (80.7 μF cm^{-2}, thickness ~15 nm)[13].

To further demonstrate the possible practical application of directly printable MSCs based on EG/PH1000, MSC arrays were fabricated by connecting four separately printed MSC devices in series (Figure 4b). To our delight, the charged MSC arrays could readily power an LED, demonstrating the great potential of MSCs as a portable and flexible micro-power supply. More interestingly, to meet the industrial requirements for scale-up production of MSC arrays, an ink-jet printing technique was also developed in this work. As shown in Figure 4c, the stable pristine EG ink was loaded into the cartridge of a commercial inkjet printer. By designing the MSC electrode geometry on the computer, we could easily print MSC arrays, which contained 10 individual MSC devices on standard A4 paper, with a commercially available printer; the whole process took only several minutes.

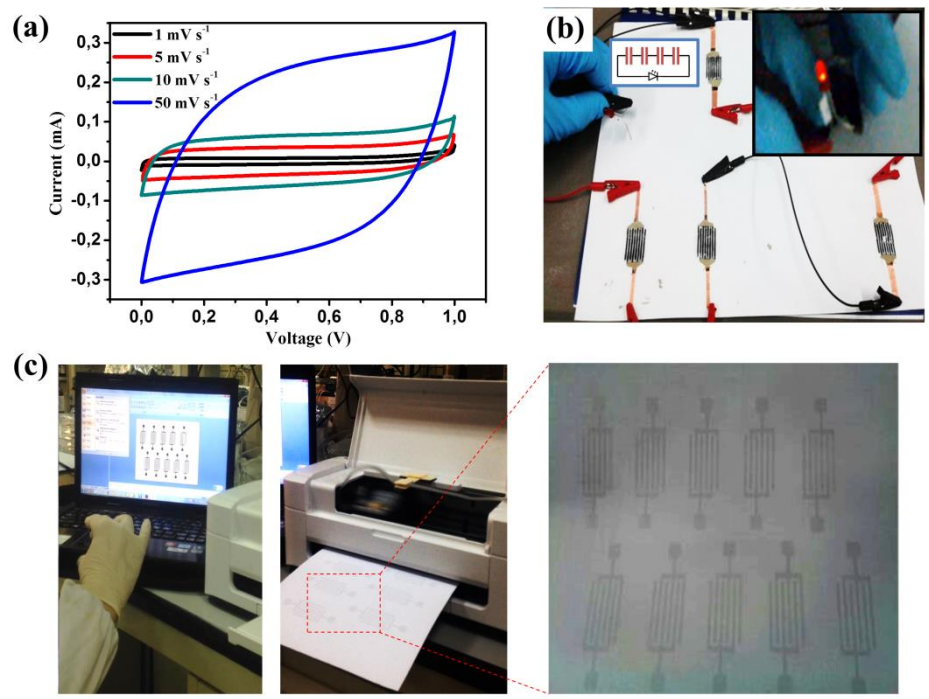

Figure 4. (a) Cyclic voltammetry curves of an EG/PH1000 hybrid ink (total amount 10 mL) MSC on a paper substrate at scan rates of 1 mV s^{-1} to 50 mV s^{-1}. (b) A charged MSC array containing 4 single devices can power an LED. (c) Inkjet printing of custom designed MSC arrays from a "home computer and printer" using pristine EG ink.

Ultra-thin MSCs based on EG/PH1000 hybrid films were also manufactured to demonstrate the MSCs as potential wearable micro-energy storage units. To this end, ultra-thin PET foils with a thickness of 2.5 μm were employed as the substrate. For the convenience of device fabrication, the ultra-thin PET foils were attached to PDMS-coated rigid glass slides. By adhering the ultra-thin PET foils to the supports, all subsequent processing steps including spray-coating of the EG/PH1000 hybrid ink and assembling the device were exactly the same as for processing on paper (Figure 2a). Afterward, the as-fabricated ultra-thin MSC device was carefully peeled off of the supporting PDMS without causing any damage to the device. By spray coating 5 mL of the EG/PH1000 hybrid ink, the thickness of the obtained hybrid film was approximately 1 μm. The MSC device delivered a maximum areal capacitance of 2

mF cm^{-2} at 5 mV s^{-1} (**Figure 5**a), which is higher than those of reported graphene-based MSCs;[5a, 5b, 13] however, this value is lower than the device fabricated on the paper substrate because of the limited thickness. As shown in Figure 5b, the total thickness of the fabricated MSC device including the thickness of the substrate and solid-state electrolyte is less than 5 μm, which is much thinner than a human hair, showing great potential for "ultra-flexible" device architectures. Interestingly, the ultra-thin MSC device can be attached to a human finger or other body parts (Figure 5b), which demonstrates tremendous flexibility and compatibility with artificial intelligent devices, such as wearable electronics that undergo bending and stretching. To evaluate the mechanical stability of such an ultra-thin MSC device for flexible energy storage, we further examined the areal capacitance retention of an as-fabricated device after 1000 cycles of a bending test (Figure 5c, bending radius of 5 mm). The resulting device measured at a scan rate of 100 mV s^{-1} exhibited stable performance with only a slight capacitance loss of 1.5%. This mechanical stability even outperformed a device fabricated on regular PET substrates (Figure 5d, after 1000 cycles of bending with a radius of 7 mm), which showed a capacitance loss of more than 2% at scan rate of 100 mV s^{-1}. Remarkably, even with random twisting and folding (similar conditions to wearing the device on a human finger), the device presented only a slight capacitance loss of 1% compared with the flat state, demonstrating the "ultra-flexibility" and highly stability of the ultra-thin MSC (inset in Figure 5c).

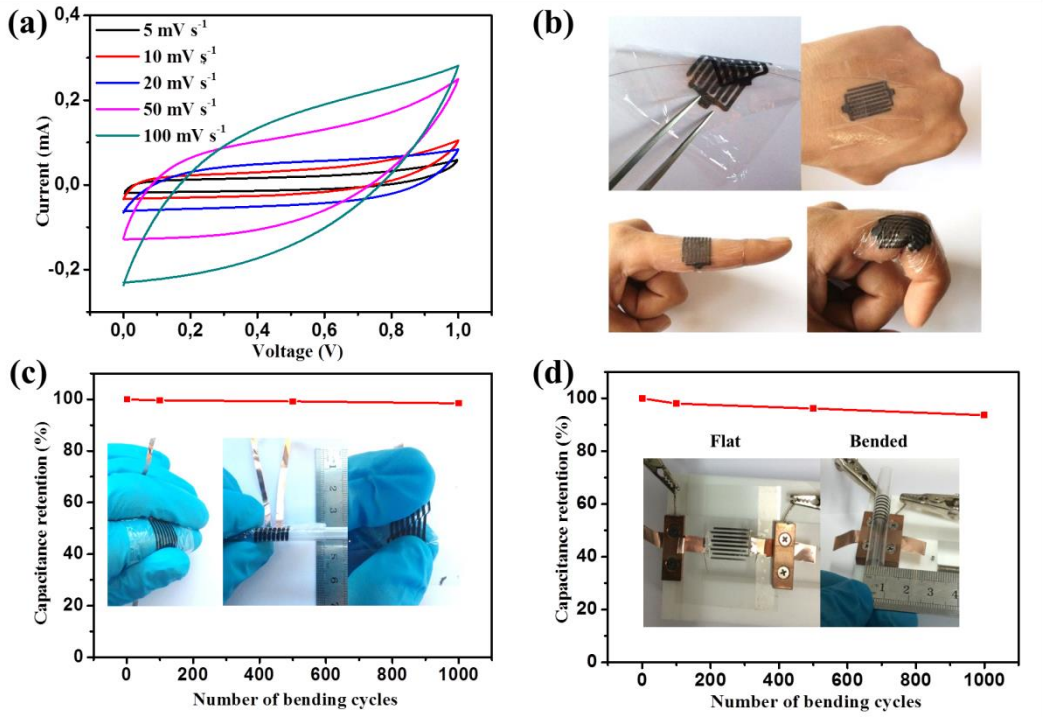

Figure 5. (a) Cyclic voltammetry curves of an EG/PH1000 hybrid ink (total amount 10 mL) MSC on an ultra-thin PET substrate at scan rates of 1 to 100 mV s^{-1}. (b) Ultra-thin and flexibility demonstrations of the fabricated MSC device indicating that the device is thinner than a human hair, wearable on the human hand, and capable of conforming to bent fingers. The MSC capacitance retention after 1000 cycles of the bending test using (c) ultra-thin and (d) regular PET substrates. The insets show flat, bent and deformable states of the MSC.

In conclusion, we demonstrated novel directly printable in-plane MSCs on paper substrates using an electrochemically exfoliated graphene ink and a hybrid ink with an electrochemically active conducting polymer. The fabricated MSCs on paper substrates offered a significant areal capacitance as high as 5.4 mF cm^{-2}, which is superior to that of state-of-the-art graphene-based MSCs. Furthermore, we developed an "ultra-flexible" MSC device by employing ultra-thin PET substrates, which exhibited excellent flexibility. Our

work may pave the way for the future development of scalable high performance portable and wearable power supplies.

Experimental Section

Experimental Details including Materials, EG Production, printing of EG/PH1000 hybrid inks, and MSC device fabrication and characterization are listed in supporting information.

Acknowledgements
This work was financially supported by the ERC Grant on NANOGRAPH and 2DMATER, and MoQuas, EC under Graphene Flagship (No. CNECT-ICT-604391), INSOLCELL and MaxNet Energy. We also thank the Center for Advancing Electronics Dresden (cfaed) for financial support.

Supporting Information

Ultraflexible in-plane Micro-Supercapacitors by Direct Printing of Solution-Processable Electrochemically Exfoliated Graphene

Experimental Section

Materials:

Graphite foil was purchased from Alfa Aesar. Clevios PH1000 (1.3 wt %) was purchased from Heraeus Clevios GmbH. Airbrush (Infinity CRplus) was purchased from Harder & Steenbeck GmbH. Ultrathin PET foils were supported by Pütz GmbH + Co. Folien KG.

EG Production:

EG was produced as previously reported. Briefly, graphite foil, platinum wires, and 0.1 M H2SO4 solutions were used as working electrodes, counter electrodes, and electrolytes, respectively. Initially, high voltage pulses (+10 V) were applied to expand the graphite, as shown in Figure 1a. Afterward, 30 minutes of low voltage (+3 V) was applied for direct exfoliation. After washing of the exfoliated product, the collected EG powder was dispersed in IPA by sonication for 30-40 min. Thus, EG ink with a high concentration of 0.8 mg mL^{-1} was readily obtained.

Printing of EG/PH1000 hybrid inks for MSC device fabrication:

A custom-made shadow mask was employed to define the required MSC pattern, with 4 digital fingers on each side. The diameter of the airbrush nozzle was 0.15 mm, and the spray coating pressure was fixed at 3 bar nitrogen gas. The distance between the substrate and the

airbrush nozzle was 10 cm. To achieve a homogeneous film, each spray process was conducted in a gentle manner. After each spray, a pause of 20 s should be taken for the film to be dried. The hybrid film will be heated 90 ºC in the oven overnight to remove residual solvent before use. Rs was measured by a standard four-point probe system with a Keithley 2700 Multimeter (probe spacing: 0.635 mm, Rs= 4.5324 V/I). We utilized cyclic voltammetry (CV) to test the MSC device, with potential window 0-1 V, and the capacitance values were calculated from the CV data according to the following equation:

$$C_{device} = \frac{1}{\nu(V_f - V_i)} \int_{V_i}^{V_f} I(V)dV$$

Where ν is the scan rate, V_f and V_i is are the integration potential limits of the CV curve. I (V) is the voltammetric discharge current. Specific area capacitance was calculated according to:

$$C_{area} = C_{device}/A$$

where A is the total area of the device.

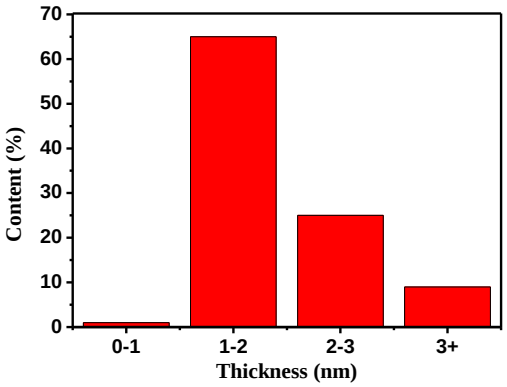

Figure S1. Graphene sheet thickness distribution.

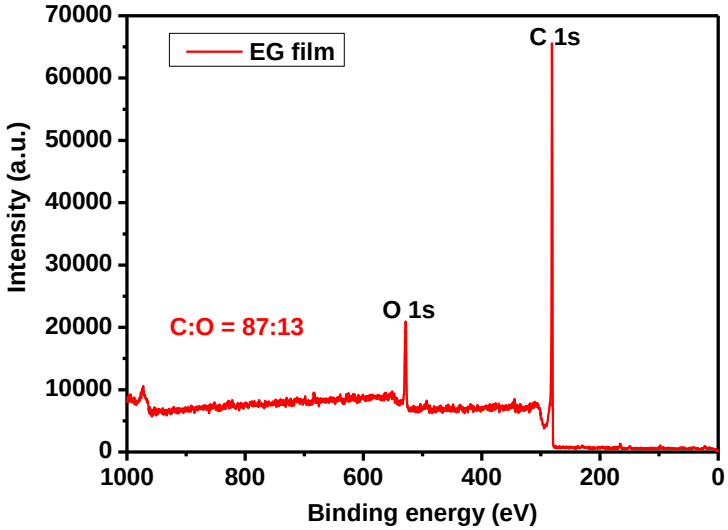

Figure S2. XPS spectrum of an EG film recorded over a range of 0-1000 eV.

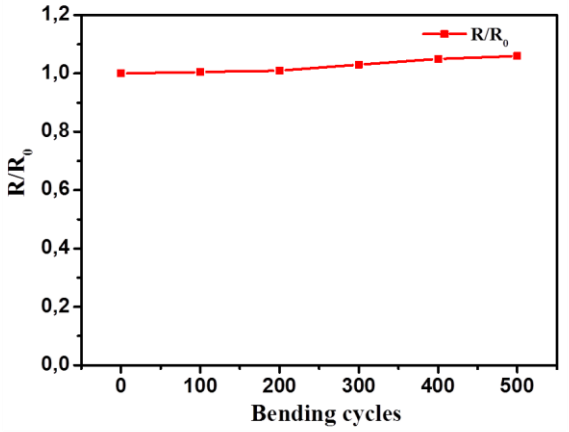

Figure S3. Change in R/R_0 with 500 bending cycles.

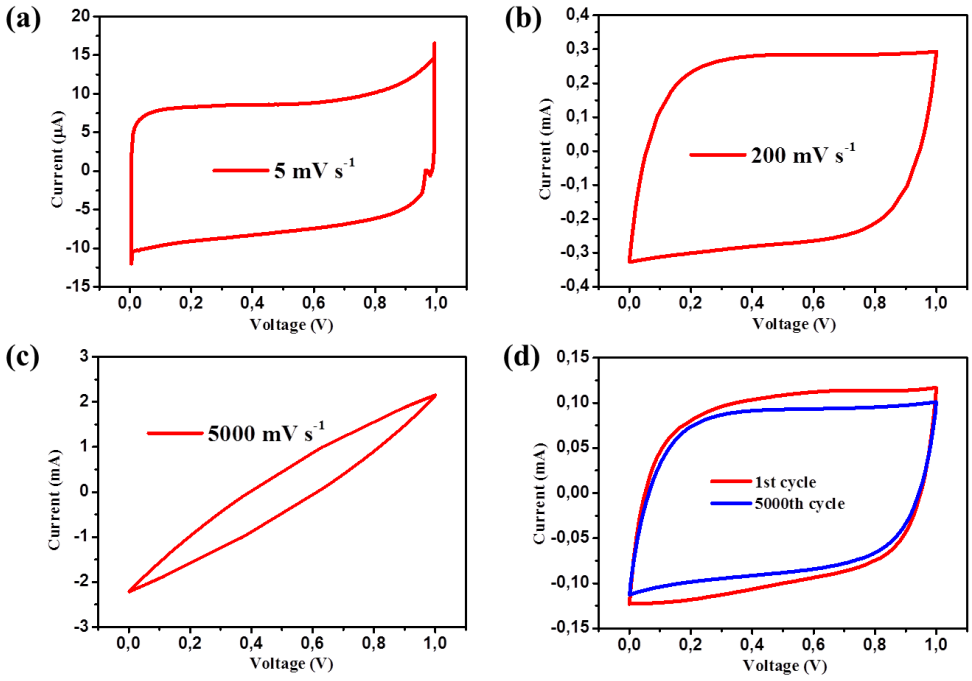

Figure S4. CV curves of an EG/PH1000 hybrid ink (total amount 3 mL) MSC on a paper substrate based at (a-c) scan rates of 5, 200 and 5000 mV s^{-1}, and (d) 1st and 5000th cycle measured at a scan rate of 100 mV s^{-1}.

References

[1] a) M. Beidaghi, Y. Gogotsi, *Energy and Environmental Science* **2014**, *7*, 867; b) Z.-S. Wu, X. Feng, H.-M. Cheng, *Natl. Sci. Rev.* **2014**, *1*, 277.

[2] a) J. W. Long, B. Dunn, D. R. Rolison, H. S. White, *Chem. Rev.* **2004**, *104*, 4463; b) M. Armand, J. M. Tarascon, *Nature* **2008**, *451*, 652; c) J. Chmiola, C. Largeot, P.-L. Taberna, P. Simon, Y. Gogotsi, *Science* **2010**, *328*, 480.

[3] M. F. El-Kady, R. B. Kaner, *Nat Commun* **2013**, *4*, 1475.

[4] Z. S. Wu, K. Parvez, X. Feng, K. Müllen, *Nat Commun* **2013**, *4*, 2487.

[5] a) W. Gao, N. Singh, L. Song, Z. Liu, A. L. M. Reddy, L. Ci, R. Vajtai, Q. Zhang, B. Wei, P. M. Ajayan, *Nat Nano* **2011**, *6*, 496; b) D. Pech, M. Brunet, H. Durou, P. Huang, V. Mochalin, Y. Gogotsi, P.-L. Taberna, P. Simon, *Nat Nano* **2010**, *5*, 651; c) M. F. El-Kady, V. Strong, S. Dubin, R. B. Kaner, *Science* **2012**, *335*, 1326; d) C. Shen, X. Wang, W. Zhang, F. Kang, *Scientific Reports* **2013**, *3*, 2294.

[6] a) Z. Y. Xia, S. Pezzini, E. Treossi, G. Giambastiani, F. Corticelli, V. Morandi, A. Zanelli, V. Bellani, V. Palermo, *Adv. Funct. Mater.* **2013**, *23*, 4684; b) M. J. McAllister, J.-L. Li, D. H. Adamson, H. C. Schniepp, A. A. Abdala, J. Liu, M. Herrera-Alonso, D. L. Milius, R. Car, R. K. Prud'homme, I. A. Aksay, *Chem. Mater.* **2007**, *19*, 4396; c) Z. Y. Xia, G. Giambastiani, C. Christodoulou, M. V. Nardi, N. Koch, E. Treossi, V. Bellani, S. Pezzini, F. Corticelli, V. Morandi, A. Zanelli, V. Palermo, *ChemPlusChem* **2014**, *79*, 439; d) H. C. Schniepp, J.-L. Li, M. J. McAllister, H. Sai, M. Herrera-Alonso, D. H. Adamson, R. K. Prud'homme, R. Car, D. A. Saville, I. A. Aksay, *The Journal of Physical Chemistry B* **2006**, *110*, 8535.

[7] K. Parvez, R. Li, S. R. Puniredd, Y. Hernandez, F. Hinkel, S. Wang, X. Feng, K. Müllen, *ACS Nano* **2013**, *7*, 3598.

[8] F. Torrisi, T. Hasan, W. P. Wu, Z. P. Sun, A. Lombardo, T. S. Kulmala, G. W. Hsieh, S. J. Jung, F. Bonaccorso, P. J. Paul, D. P. Chu, A. C. Ferrari, *Acs Nano* **2012**, *6*, 2992.

[9] a) J. Wang, K. K. Manga, Q. Bao, K. P. Loh, *J. Am. Chem. Soc.* **2011**, *133*, 8888; b) Z. Sun, Z. Yan, J. Yao, E. Beitler, Y. Zhu, J. M. Tour, *Nature* **2010**, *468*, 549.

[10] Z. Liu, K. Parvez, R. Li, R. Dong, X. Feng, K. Müllen, *Adv. Mater.* **2015**, *27*, 669.

[11] L. Hu, J. W. Choi, Y. Yang, S. Jeong, F. La Mantia, L.-F. Cui, Y. Cui, *Proceedings of the National Academy of Sciences of the United States of America* **2009**, *106*, 21490.

[12] a) Z.-S. Wu, K. Parvez, S. Li, S. Yang, Z. Liu, S. Liu, X. Feng, K. Müllen, *Adv. Mater.* **2015**, *27*, 4054; b) Z.-S. Wu, K. Parvez, A. Winter, H. Vieker, X. Liu, S. Han, A. Turchanin, X. Feng, K. Müllen, *Adv. Mater.* **2014**, *26*, 4552; c) Z. Niu, L. Zhang, L. Liu, B. Zhu, H. Dong, X. Chen, *Adv. Mater.* **2013**, *25*, 4035; d) W. Si, C. Yan, Y. Chen, S. Oswald, L. Han, O. G. Schmidt, *Energy & Environmental Science* **2013**, *6*, 3218; e) W. Liu, C. Lu, X. Wang, R. Y. Tay, B. K. Tay, *ACS Nano* **2015**, *9*, 1528.

[13] Z. S. Wu, K. Parvez, X. Feng, K. Müllen, *Nat. Commun.* **2013**, *4*, 2487.

Chapter 4. High Power In-Plane Micro-Supercapacitors Based on Mesoporous Polyaniline Patterned Graphene

Key words: high power, micro-supercapacitors, electrochemically exfoliated graphene, mesoporous polyaniline, energy storage

ToC Figure

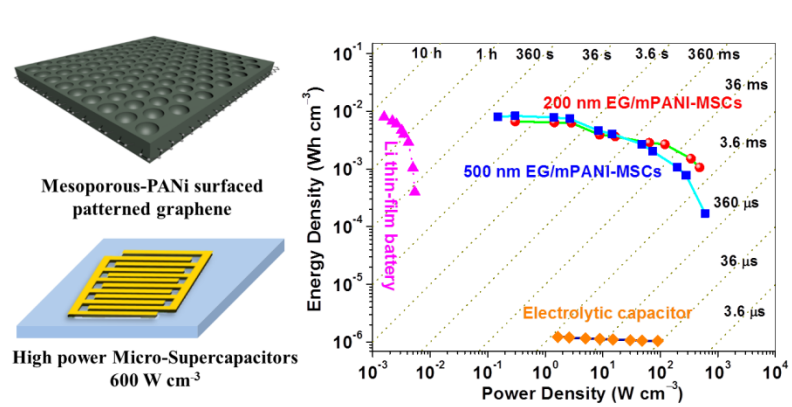

Micro-supercapacitors (MSCs) based on mesoporous polyaniline patterned graphene is demonstrated. The synergic effect from both electron-double-layer-capacitive graphene and pseudocapacitive mesoporous-PANi leads to excellent MSC device performances, in regards to excellent volumetric capacitance and rate capabilities, which further resulted in high power density of 600 W cm^{-3}, suggesting opportunities for future portable and wearable power supplies in diverse applications.

Published in:

Small

Reprinted with permission from (*Small* **2017**, 13, *1603388*.) Copyright: "John Wiley and Sons" publishing group.

Powerful micro-scale energy storage systems are the key components for a future generation of miniaturized, portable and wearable electronic devices, as well as implantable self-powered biosensors.[1] In-plane MSCs are newly emerging candidates to replace micro-batteries as on-chip micro-power energy sources, being able to provide long cycle life, fast charge/discharge rate, as well as capable of providing power densities several orders of magnitude higher than those of conventional supercapacitors and batteries.[2] Great efforts have been made in recent years to realize MSCs with high power densities, for instance, by employing nanostructured electrochemically active materials, such as carbide derived carbon,[2c] onion-like carbon,[2b] and certain pseudo-capacitive materials like conducting polymers,[3] such as polyaniline based on a mesoporous structure.[4] However, designing efficient MSCs with high-power capabilities for on-chip energy storage still remains a challenge, [1, 5] mainly due to the substantially low rate capability of the micrometre (or sub-micrometre) thick film electrodes; generally, the high capacitance is obtained at very low scan rate (~10 mV s^{-1}), while at high scan rate (~100 V s^{-1}, if affordable) the capacitance retention is quite low.[1, 6]

Graphene is very attractive for high power MSCs considering its excellent electrical conductivity, high surface-to-volume ratio, and outstanding intrinsic double-layer capacitance.[7] However, the performances of current MSCs based on pristine graphene films are still limited, being only capable of electrical double layer capacitance (EDLC) and lacking fast Faradaic pseudo-capacitive behaviour. Moreover, the restacking of graphene sheets through the strong π-π interactions can severely decrease the accessible surface area, and thus hinder the ion diffusion at high operating speed (i.e. 1000 V s^{-1}), compromising the rate capability of the MSCs. The conventional activation protocol, which generates abundant ultra-small micropores and ultrahigh specific surface area in graphene, also results in limited capacitance, because of the difficulty for the electrolyte ions to efficiently access the

micropore surfaces.[8] In this work, we report MSCs based on mesoporous polyaniline (mPANi) patterned graphene, by combining pseudo-capacitive mPANi and electron-double-layer-capacitive graphene, to tackle the current rate capability challenge of MSCs. We produced graphene sheets by electrochemical exfoliation of graphite, which is a promising wet-chemical method with advantages including high quality of graphene and solution processability, as well as up-scalability and eco-friendliness, in contrast to liquid-phase exfoliation in organic solvents. Compared with conventional reduced graphene oxide, EG can be produced via a much simpler and faster process while displaying better electronic properties.[9] The fabricated MSCs offered a significant volumetric capacitance as high as 75 F cm^{-3} at 10 mV s^{-1}, and exhibited an excellent rate capability with capacitance retention of 16% when operated from 10 to 10^5 mV s^{-1}. These micro-devices even allowed for operations at ultrahigh rate up to 1000 V s^{-1}, which is three orders of magnitude higher than conventional supercapacitors. The in-plane structured flat MSCs also delivered a high power density of 600 W cm^{-3}, which is about 6 times higher than that of high-power aluminum electrolytic capacitors, and outperformed the state-of-the-art high power MSCs. Moreover, the achieved energy densities of 6.67 mWh cm^{-3} are comparable to the commercially available lithium-thin film (LTF) batteries.

The synthetic process for EG/mPANi is shown in **Figure 1**. First, graphene was prepared by electrochemical exfoliation of graphite foil as previously reported.[9] Subsequently, the electrochemically exfoliated graphene (EG) was non-covalently functionalized with 1-pyrenesulfonic acid sodium salt (PSA) via π-π interactions between the pyrene moiety of PSA and graphene. The surface of EG was thus negatively charged with the sulfonyl group of PSA, rendering its improved aqueous dispersion. Next, amphiphilic block copolymer polystyrene-*b*-poly(ethylene oxide) (PS_{146}-*b*-PEO_{117}) monomicelles (self-assembled in THF/H_2O mixed solvent, in spherical shape with a diameter of 20 nm) were

assembled and anchored on PSA-functionalized-EG surface, followed by addition and polymerization of aniline along PS_{146}-*b*-PEO_{117} micelles to form mesoporous PANi on both sides of the EG. At last, the PS_{146}-*b*-PEO_{117} templates were removed by repeated washing with THF, and the obtained EG/mPANi sheets could be stably dispersed in 2-propanol (IPA) at a concentration of 1 mg mL^{-1}.

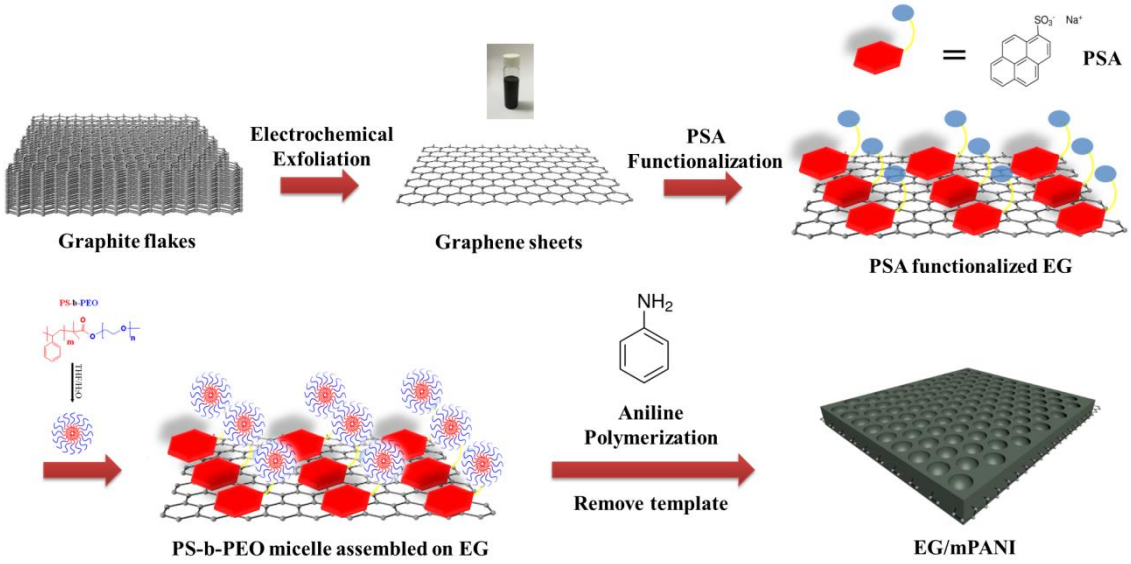

Figure 1. Schematic illustration of the synthetic process of EG/mPANi sheets.

The structural and morphological characterizations of the EG/mPANi sheets are shown in **Figure 2**. Scanning electron microscopy (SEM) suggests a uniformly arranged coating of mPANi on EG surface with the pore size of 25 nm (Figure 2a), which is in accordance with the transmission electron microscopy (TEM) results (Figure 2b and S1a). The selected area electron diffraction (SAED) pattern (inset of Figure 2b) showed a typical diffraction pattern of graphene and confirmed the presence of EG within EG/mPANi sheet, whereas PANi does not have any characteristic SAED patterns. Moreover, atomic force microscopy (AFM) reveals a 2D nanosheet morphology of EG/mPANi with an average thickness of ~51 nm (Figure 2c, Figure S1b and S2). Taking the average thickness of EG

sheets into consideration (Figure S3), this value is almost equal to twice the diameter of PS_{146}-*b*-PEO_{117} monomicelles, corroborating the confined growth mechanism of mPANi on both sides of EG surface. As shown in Figure 2d, X-ray photoelectron spectroscopy (XPS) is employed to probe the different chemical bond information of the EG/mPANi composites. The detected carbon element mainly originates from PANi, which is revealed from the C-C or C-H band at 284.1 eV, and C–N or C=N band at 285.2 eV of the C1s core-level spectrum. The N1s core-level spectrum (Figure S1c) shows three peaks which corresponds to different electronic states: the benzenoid amine with binding energy (BE) at 399.4 eV, the quinoid amine with BE at 398.6 eV, and the nitrogen cationic radical (N^+) with BE at 400.2 eV.[10] The presence of EG may also contribute to the strong C-C band at 284.1 eV, which is overlapping with the PANi signal. Since XPS detection range is limited to several nanometres from the sample surface, we used FT-IR and Raman spectroscopy to better analyse the composition of EG/mPANi composites.

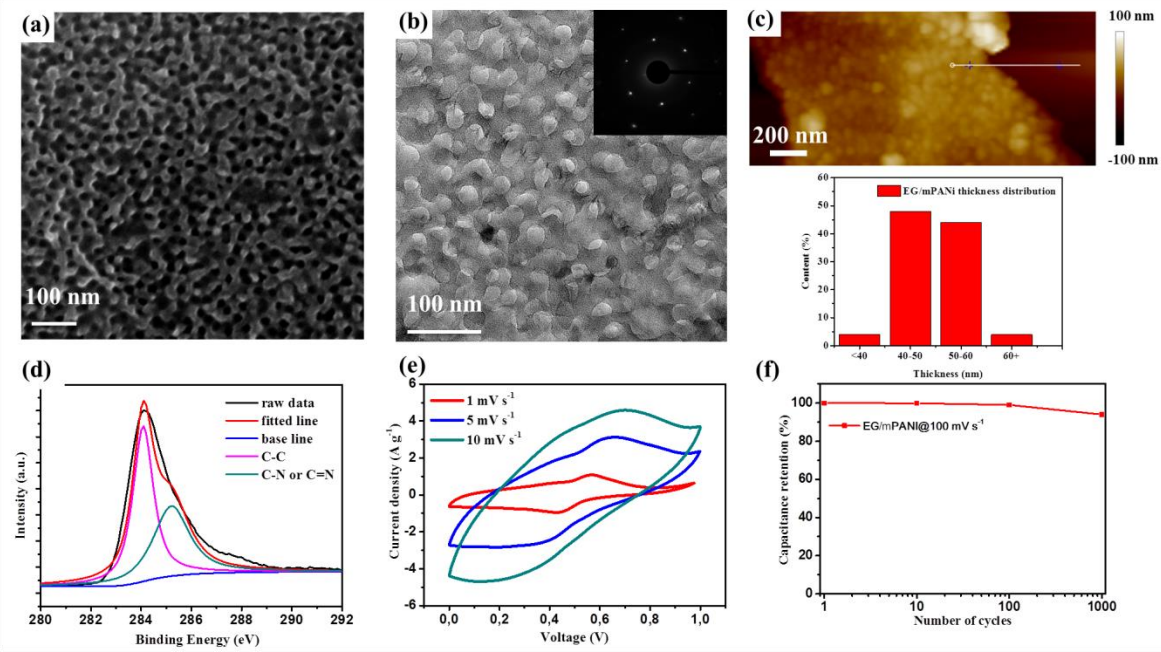

Figure 2. (a) SEM image of EG/mPANi sheet on SiO_2 substrate. (b) TEM image of EG/mPANi sheet, inset shows the corresponding SAED pattern of the EG/mPANi sheet. (c)

AFM image of the EG/mPANi sheet on SiO_2 substrates, and thickness distribution. (d) High-resolution XPS of the C 1s spectrum for EG/mPANi. (e) CV curves of EG/mPANi based supercapacitor electrode material with scan rates ranging from 1 to 10 mV s^{-1}. (f) Electrochemical stability test of EG/mPANi based supercapacitor electrode, the evolution of capacitance retention versus number of scanning cycles.

FT-IR spectra of the EG/mPANi sheets (Figure S4) shows the presence of C-OH (at 1376 cm^{-1} and ~3250 cm^{-1}) and C-C (at 1606 cm^{-1}), corresponding to the characteristic peaks of EG.[11] Moreover, the observation of characteristic stretching vibration bands of the quinonoid ring and benzenoid rings at 1568 cm^{-1} and 1496 cm^{-1}, as well as the characteristic bands for C-N stretching of secondary aromatic amines at 1299 cm^{-1}, C-H and C=N of the quinonoid ring at 1150 cm^{-1} and 1130 cm^{-1}, demonstrates the formation of PANI.[12] These observations suggest the successful combination of EG and PANi. Raman spectra of the EG/mPANi sheets (Figure S5) exhibits bands at 1168 cm^{-1}, 1240 cm^{-1}, 1488 cm^{-1}, 1586 cm^{-1}, and 1621 cm^{-1}, which can be assigned to the presence of PANi.[13] On the other hand, bands at 1351 cm^{-1}, 1586 cm^{-1}, and 2704 cm^{-1} correspond to the typical D, G, and 2D peak, respectively of EG.[14]

The Brunauer-Emmett-Teller (BET) surface area and pore size distribution of EG/mPANi sheets are calculated to be 60 m^2 g^{-1} and 5-30 nm (Figure S6), respectively. Because of the unique mesoporous structure, EG/mPANi sheets were expected to serve as promising materials for high-performance supercapacitor electrode. A three-electrode system was employed to evaluate the performance of EG/mPANi, where platinum foil and saturated Ag/AgCl were used as counter electrode and reference electrode, respectively. Figure 2e presents the cyclic voltammetry (CV) curves of the working electrode based on 8 mg of

EG/mPANi nanosheets at various scan rates. Typical pseudocapacitive behaviour of PANi with strong redox peaks was observed from the CV curves in the range of –0.2 to 0.8 V at low scan rates of 1 mV s^{-1}, showing a gravimetric capacitance of 438 F g^{-1}, which is comparable to most of the state-of-the-art graphene-PANi composite electrodes, i.e. 3D network, hollow spheres, or composite paper based on rGO/PANi.[15] The cycling stability tests suggest that the EG/mPANi electrode could maintain 94% of its original capacitance after 1000 cycles at 100 mV s^{-1} (Figure 2f). This result indicates that the mesoporous structure of PANi on EG surface can afford large volumetric expansion effect during rapid charging/discharging process.

In order to further highlight its electrochemical performance as supercapacitor electrode material, we fabricated on-chip in-plane structured MSCs based on thin films of the EG/mPANi. The fabrication process of MSCs is schematically illustrated in **Figure 3**a. Briefly, the thin electrode film was prepared by filtration of an EG/mPANi dispersion in IPA, followed by transfer of the obtained filter cake onto SiO_2/Si substrate with a pressure assisted dry transfer method. In order to improve the stability of the film, the EG/mPANi layer was sandwiched between two very-thin layers of EG (10 nm thick for each layer) during filtration. Subsequently, well-established lithography techniques were applied to produce interdigital microelectrode patterns (Figure S1d shows the detailed device geometry): A homemade shadow mask was used for the deposition of gold current collectors, followed by oxidative etching of MSC channels in oxygen plasma. Finally, the electrolyte based on 1 M H_2SO_4 solution was drop-cast onto the interdigital microelectrodes, yielding the in-plane structured MSC.

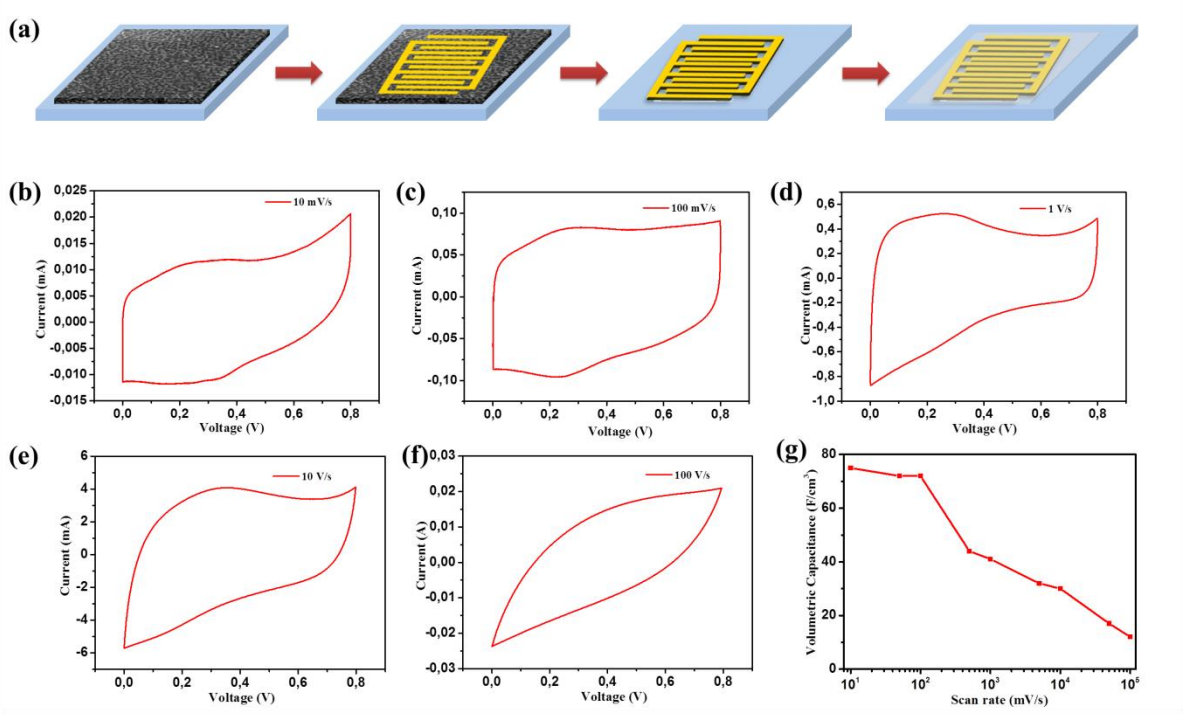

Figure 3. (a) Schematic illustration of fabrication process of the MSC devices; (b-f) CV curves of MSC based on 200 nm thick EG/mPANi with scan rates ranging from 10 to 10^5 mV s^{-1}, and (g) the evolution of volumetric capacitance versus scan rate.

The electrochemical behaviour of on-chip planar MSCs based on 200 nm thick EG/mPANi film was studied by CV. As shown in Figure 3b-f and Figure S7, all the CV curves delivered significant redox responses and quasi-rectangular shapes between the voltage potential of 0 and 0.8 V at different scan rates ranging from 10 to 10^5 mV s^{-1}, suggesting both pronounced pseudocapacitive characteristics from mPANi and large double-layer capacitance from EG. These results agreed very well with our design of combining double-layer capacitances and pseudocapacitive for MSCs. Remarkably, a maximum areal capacitance of 1.5 mF cm^{-2} and a volumetric capacitance of 75 F cm^{-3} were achieved at a scan rate of 10 mV s^{-1}, which are superior to most of the reported values for other MSCs based on graphene, porous carbon and graphene/PANi composite (as listed in Table S1), with

areal capacitance from 80.7 μF cm^{-2} to 3.31 mF cm^{-2}, and volumetric capacitance from 1.3 F cm^{-3} to 17.9 F cm^{-3}. [2a] [2b] [16] [17] [18]

Moreover, as shown in Figure 3g, the MSCs exhibited an excellent rate capability with capacitance retention of 16% when the operating speed increased by four orders of magnitude, from 10 to 10^5 mV s^{-1}, which is comparable to onion-like carbon and outperformed most of the other reported cases. The corresponding galvanostatic charge-discharge (GCD) curves at different current densities of the MSC are shown in Figure S8. At 0.1 A cm^{-3}, a volumetric capacitance of 73 F cm^{-3} was achieved, which corresponds well with the results from CV measurement at 10 mV s^{-1}. Upon increasing the current density by 100 times (at 10 A cm^{-3}), the MSC can still deliver a volumetric capacitance of 31 F cm^{-3} (capacitance retention of 42%). These results demonstrated the high capacitance and rate capability of EG/mPANi-based MSCs. We attribute this synergistic effect of the EG/mPANi composite material to the following advantages: (1) The EG in the polymer matrix essentially provides rigid support for the stability of the PANi during charging/discharging; (2) The mesoporous morphology of PANi is readily accessible to ions, which improved the overall capacitance of the composite to a greater extent; (3) The presence of PANi avoids the restacking of EG flakes, thus maintaining the accessible surface area, which guarantee the ion diffusion at high operating speed; (4) The π electron cloud stacking between graphene and aromatic/quinoid structure in PANi may facilitate the electron transfer, thus enhancing the electrochemical properties of the composite materials.[19] The excellent rate capability of the MSC resulted in a very high power density of 480 W cm^{-3}. However, the device was not capable of running at higher scan rates, presumably due to the limited thickness of the EG/mPANi thin film. In this regard, we further optimized the device performance with different EG/mPANi film thicknesses. The thickness of the MSC electrode patterns could reach up to 500 nm, and the corresponding CV and GCD curves at different scan rates are

presented in Figure S9 and S10. An improved areal capacitance of 3 mF cm^{-2} is achieved at 10 mV s^{-1}, which can be explained by the increase of the total accessible electrochemical surface area in the interdigital electrodes. Notably, such MSCs allow for operations at ultrahigh rate up to 10^6 mV s^{-1}, which are three orders of magnitude larger than that of conventional supercapacitors.

The electrochemical impedance spectroscopy (EIS) of MSCs based on both 200 nm and 500 nm thick EG/mPANi films are shown in Figure S11. The 200 nm thick MSC showed a near-vertical line intersection with the real axis at low frequency (inset in Figure S11a), indicating the fast ion diffusion in such in-plane structured micro-devices. The dependence of the phase angle on the frequency of the MSCs is presented in Figure S11b. The characteristic frequency at the phase angle of -45º was 100 Hz for 500 nm thick MSC device. Therefore, the corresponding time constant, which is the minimum time needed to discharge all the energy from the device with an efficiency of more than 50%, was only 10 ms. These results strongly suggests that the EG/mPANi-based MSCs possess enormous potential for the instantaneous delivery of high power.

The detailed Ragone plot is shown in **Figure 4**a to demonstrate the overall performance of the EG/mPANi-based MSCs. The data from a commercially available high-energy lithium thin-film battery (4 V/500 μAh), and high-power aluminium electrolytic capacitor (3 V/300 μF) are included for comparison. The 200-nm-thick EG/mPANi-film-based MSCs provided volumetric energy densities of 1.06-6.67 mWh cm^{-3}, which are one order of magnitude higher than that of typical activated-carbon-based supercapacitors (less than 1 mWh cm^{-3}), and within the same range to that of lithium thin-film batteries (1–10 mWh cm^{-3}). Moreover, at ultrahigh scan rate of 10^6 mV s^{-1}, 500-nm-thick EG/mPANi-film-based MSCs furnished a high power density of 600 W cm^{-3} (even at a high energy density of

0.17 mWh cm^{-3}). This significant power density is 50 times higher than that of conventional supercapacitors and 6 times higher than that of high-power aluminum electrolytic capacitors (10–10^3 W cm^{-3}) as well as superior to most of the reported graphene-based MSCs.[2a, 2b, 16-17, 20] To demonstrate practical applications of the EG/mPANi-based MSCs, four separate MSC devices were connected in series as shown in Figure 4b. To our delight, a red colour light-emitting diode (LED) could be readily powered up by the charged MSCs, highlighting the great potential of EG/mPANi as efficient electrode material for MSCs as future portable micro-power supplies.

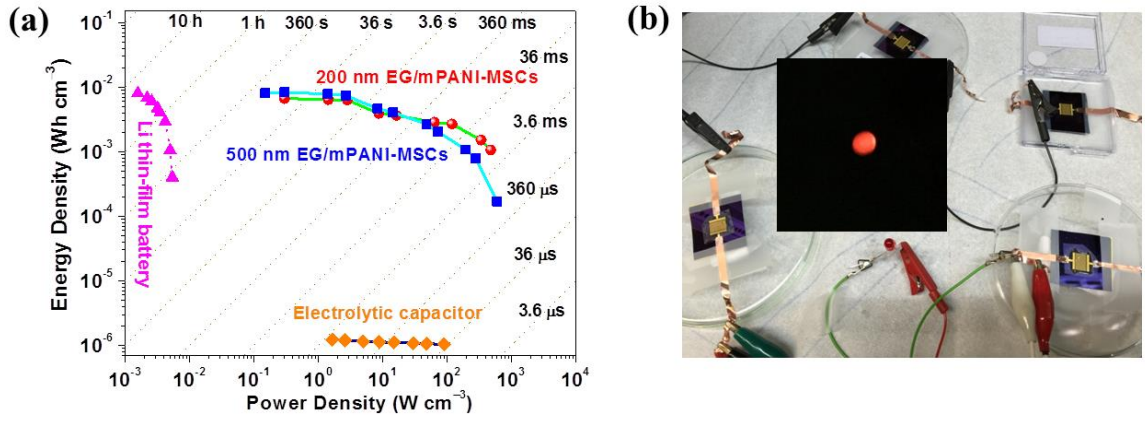

Figure 4. (a) Ragone plots of MSCs based on EG/mPANi films with different thickness, LTF battery (LTFB, 4 V/500 µAh) and electrolytic capacitor (3 V/300 µF). (b) Optical image of an LED powered by connecting four charged MSCs in a series way, inset shows the digital pictures of LED lighten up by MSCs.

In conclusion, we demonstrated in-plane structured planar MSCs based on mesoporous polyaniline patterned graphene. The synergistic effect from electron-double-layer-capacitive graphene and pseudocapacitive mesoporous-PANi leads to excellent MSC device performances with outstanding volumetric capacitance and rate capabilities, which

further resulted in high power densities of up to 600 W cm^{-3}. This value is about 6 times higher than the one obtained with state-of-the-art high power aluminum electrolytic capacitors, and also surpassed most of the reported graphene-based high power supercapacitors/MSCs results. Energy densities of 6.67 mWh cm^{-3} delivered by such MSCs are also comparable to current commercially available LTF batteries. The concept of combining both pseudo-capacitive mesoporous polymer and electron-double-layer-capacitive graphene thus offers promising opportunities for future portable and wearable power supplies in diverse applications.

Supporting Information
Supporting Information is available from the Wiley Online Library or from the author.

Acknowledgements
This work was financially supported by the ERC Grant on NANOGRAPH and 2DMATER, EC under Graphene Flagship (No. CNECT-ICT-604391), BMBF under INSOLCELL and MaxNet Energy. [redacted] gratefully acknowledges funding from the Alexander von Humboldt Foundation. [redacted]. also acknowledges the scholarship from Center for Advancing Electronics Dresden (cfaed).

References

[1] M. Beidaghi, Y. Gogotsi, *Energy Environ. Sci.* **2014**, *7*, 867.

[2] a) W. Gao, N. Singh, L. Song, Z. Liu, A. L. M. Reddy, L. Ci, R. Vajtai, Q. Zhang, B. Wei, P. M. Ajayan, *Nat. Nanotechnol.* **2011**, *6*, 496; b) D. Pech, M. Brunet, H. Durou, P. Huang, V. Mochalin, Y. Gogotsi, P.-L. Taberna, P. Simon, *Nat. Nanotechnol.* **2010**, *5*, 651; c) J. Chmiola, C. Largeot, P.-L. Taberna, P. Simon, Y. Gogotsi, *Science* **2010**, *328*, 480.

[3] a) Z. Li, G. Ma, R. Ge, F. Qin, X. Dong, W. Meng, T. Liu, J. Tong, F. Jiang, Y. Zhou, K. Li, X. Min, K. Huo, Y. Zhou, *Angew. Chem. Int. Ed.* **2016**, *55*, 979; b) F. H. Meng, Y. Ding, *Adv. Mater.* **2011**, *23*, 4098; c) L. Nyholm, G. Nystrom, A. Mihranyan, M. Stromme, *Adv. Mater.* **2011**, *23*, 3751; d) C. Z. Meng, C. H. Liu, L. Z. Chen, C. H. Hu, S. S. Fan, *Nano Lett.* **2010**, *10*, 4025; e) T. Liu, L. Finn, M. Yu, H. Wang, T. Zhai, X. Lu, Y. Tong, Y. Li, *Nano Lett.* **2014**, *14*, 2522.

[4] a) Q. Wang, J. Yan, Z. Fan, T. Wei, M. Zhang, X. Jing, *J. Power Sources* **2014**, *247*, 197; b) J. Zhang, J. Wang, J. Yang, Y. Wang, M. B. Chan-Park, *ACS Sustainable Chemistry & Engineering* **2014**, *2*, 2291; c) L. Pan, G. Yu, D. Zhai, H. R. Lee, W. Zhao, N. Liu, H. Wang, B. C.-K. Tee, Y. Shi, Y. Cui, Z. Bao, *Proceedings of the National Academy of Sciences* **2012**, *109*, 9287; d) Y. Meng, K. Wang, Y. Zhang, Z. Wei, *Adv. Mater.* **2013**, *25*, 6985; e) L. Z. Fan, Y. S. Hu, J. Maier, P. Adelhelm, B. Smarsly, M. Antonietti, *Adv. Funct. Mater.* **2007**, *17*, 3083; f) Y. Wang, X. Yang, A. G. Pandolfo, J. Ding, D. Li, *Advanced Energy Materials* **2016**, *6*, 1600185.

[5] P. Huang, C. Lethien, S. Pinaud, K. Brousse, R. Laloo, V. Turq, M. Respaud, A. Demortière, B. Daffos, P. L. Taberna, B. Chaudret, Y. Gogotsi, P. Simon, *Science* **2016**, *351*, 691.

[6] Z.-S. Wu, K. Parvez, S. Li, S. Yang, Z. Liu, S. Liu, X. Feng, K. Müllen, *Adv. Mater.* **2015**, *27*, 4054.

[7] J. Xia, F. Chen, J. Li, N. Tao, *Nat. Nanotechnol.* **2009**, *4*, 505.

[8] a) P. Simon, Y. Gogotsi, *Nat Mater* **2008**, *7*, 845; b) Y. Zhai, Y. Dou, D. Zhao, P. F. Fulvio, R. T. Mayes, S. Dai, *Adv. Mater.* **2011**, *23*, 4828.

[9] K. Parvez, Z.-S. Wu, R. Li, X. Liu, R. Graf, X. Feng, K. Müllen, *J. Am. Chem. Soc.* **2014**, *136*, 6083.

[10] K. Zhang, L. L. Zhang, X. S. Zhao, J. Wu, *Chem. Mater.* **2010**, *22*, 1392.

[11] C. Y. Su, A. Y. Lu, Y. P. Xu, F. R. Chen, A. N. Khlobystov, L. J. Li, *ACS Nano* **2011**, *5*, 2332.

[12] S. Liu, J. Zhang, R. Dong, P. Gordiichuk, T. Zhang, X. Zhuang, Y. Mai, F. Liu, A. Herrmann, X. Feng, *Angew. Chem. Int. Ed.* **2016**, *55*, 12516.

[13] J. Zhang, C. Liu, G. Shi, *J. Appl. Polym. Sci.* **2005**, *96*, 732.

[14] K. Parvez, R. Li, S. R. Puniredd, Y. Hernandez, F. Hinkel, S. Wang, X. Feng, K. Müllen, *ACS Nano* **2013**, *7*, 3598.

[15] a) M. Wang, X. Duan, Y. Xu, X. Duan, *ACS Nano* **2016**, *10*, 7231; b) Y. Shao, M. F. El-Kady, L. J. Wang, Q. Zhang, Y. Li, H. Wang, M. F. Mousavi, R. B. Kaner, *Chem. Soc. Rev.* **2015**, *44*, 3639; c) Y. Shi, L. Peng, Y. Ding, Y. Zhao, G. Yu, *Chem. Soc. Rev.* **2015**, *44*, 6684.

[16] M. F. El-Kady, R. B. Kaner, *Nat Commun* **2013**, *4*, 1475.

[17] Z. S. Wu, K. Parvez, X. Feng, K. Müllen, *Nat Commun* **2013**, *4*, 2487.

[18] B. Song, L. Li, Z. Lin, Z.-K. Wu, K.-s. Moon, C.-P. Wong, *Nano Energy* **2015**, *16*, 470.

[19] a) J. Xu, K. Wang, S.-Z. Zu, B.-H. Han, Z. Wei, *ACS Nano* **2010**, *4*, 5019; b) M. Baibarac, I. Baltog, C. Godon, S. Lefrant, O. Chauvet, *Carbon* **2004**, *42*, 3143.

[20] a) M. F. El-Kady, V. Strong, S. Dubin, R. B. Kaner, *Science* **2012**, *335*, 1326; b) M. Beidaghi, C. Wang, *Adv. Funct. Mater.* **2012**, *22*, 4501.

Supporting Information

High Power In-Plane Micro-Supercapacitors Based on Mesoporous Polyaniline Patterned Graphene

Materials:

Graphite foil was purchased from Alfa Aesar. 1-Pyrenesulfonic acid sodium salt (PSA), aniline and all solvents were purchased from Sigma-Aldrich.

Non-covalent functionalization of EG by PSA:

After electrochemical exfoliation, 100 mg of the EG powder was dispersed in 500 mL of dimethylformamide (DMF) by mild sonication for 20 min. Then, 500 mg of PSA was slowly added to the dispersion. The dispersion was vigorously stirred for 1 hour, followed by centrifugation for 20 min at 12,000 rpm, and then the supernatant was discarded. This procedure was repeated once more before the final product was dispersed in deionized (DI) water by mild sonication for 20 min. Finally, aqueous dispersion EG with a maximum concentration of 1 mg mL^{-1} was obtained.

Synthesis of EG/mPANi:

First, 50 mg of PS_{146}-*b*-PEO_{117} was dissolved in 1 mL of tetrahydrofuran (THF), followed by dropwise addition of 1 mL of DI water into the solution. Subsequently, the mixture was slowly added into 7 mL of DI water. After stirring for 30 min, aqueous dispersion of PSA-EG (6 mL, 1 mg mL^{-1}) was added dropwise over another 30 min while stirring. Then, 35 μL of

aniline was added to the solution and stirred for 30 min, followed by injecting 1 mL of HCl aq. (1 mol L^{-1}) into the solution and stirring for another 30 min. Subsequently, 90 mg of ammonium persulfate was added to initiate the polymerization of aniline into mPANi on EG surface. The reaction mixture was stirred at room temperature for about 1 hour, and then left without stirring at the same temperature overnight. Finally, the EG/mPANi nanosheets were obtained after repeated washing with THF and DI water to remove the BCPs and excess ions.

Device characterization

The cyclic voltammetry (CV), galvanostatic charge-discharge (GCD) and electrochemical impedance spectroscopy (EIS) measurements was all performed by a CHI 760D electrochemical workstation. For the MSCs device evaluation, CV curve was recorded with a potential range from 0 to 0.8 V, or from -0.2 to 0.8 V. GCD curve was recorded with a potential range from 0 to 0.8 V. EIS was recorded in the frequency range of 10^{-2}-10^{5} Hz, with 5 mV ac amplitude.

For the three-electrode system to evaluate the performance of EG/mPANi, CV curve was recorded with a potential range from 0 to 1 V. Working electrode: 8 mg EG/mPANi powder was mixed with 1 mg carbon black, and 1 mg poly(tetrafluoroethylene) binder dispersed in ethanol. After sufficient grinding, the mixture was pressed onto a platinum mesh (1×1 cm) as current collector. Platinum foil (2×2 cm^2) and saturated Ag/AgCl (saturated KCl) were used as counter electrode and reference electrode, respectively. 1M H_2SO_4 was used as electrolyte.

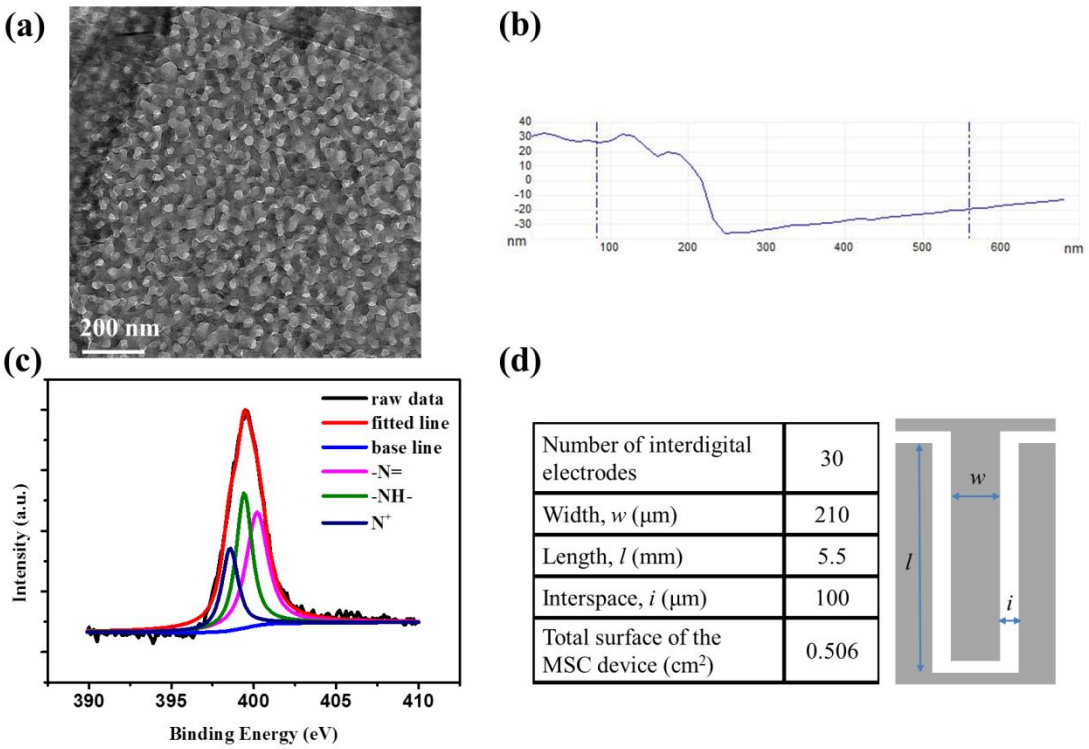

Number of interdigital electrodes	30
Width, *w* (μm)	210
Length, *l* (mm)	5.5
Interspace, *i* (μm)	100
Total surface of the MSC device (cm^2)	0.506

Figure S1. (a) TEM images of EG/mPANi sheets. (b) Height measurement of EG/mPANi sheets by AFM. (c) High-resolution XPS of the N 1s spectrum for EG/mPANi. (d) Detailed device geometry of MSCs.

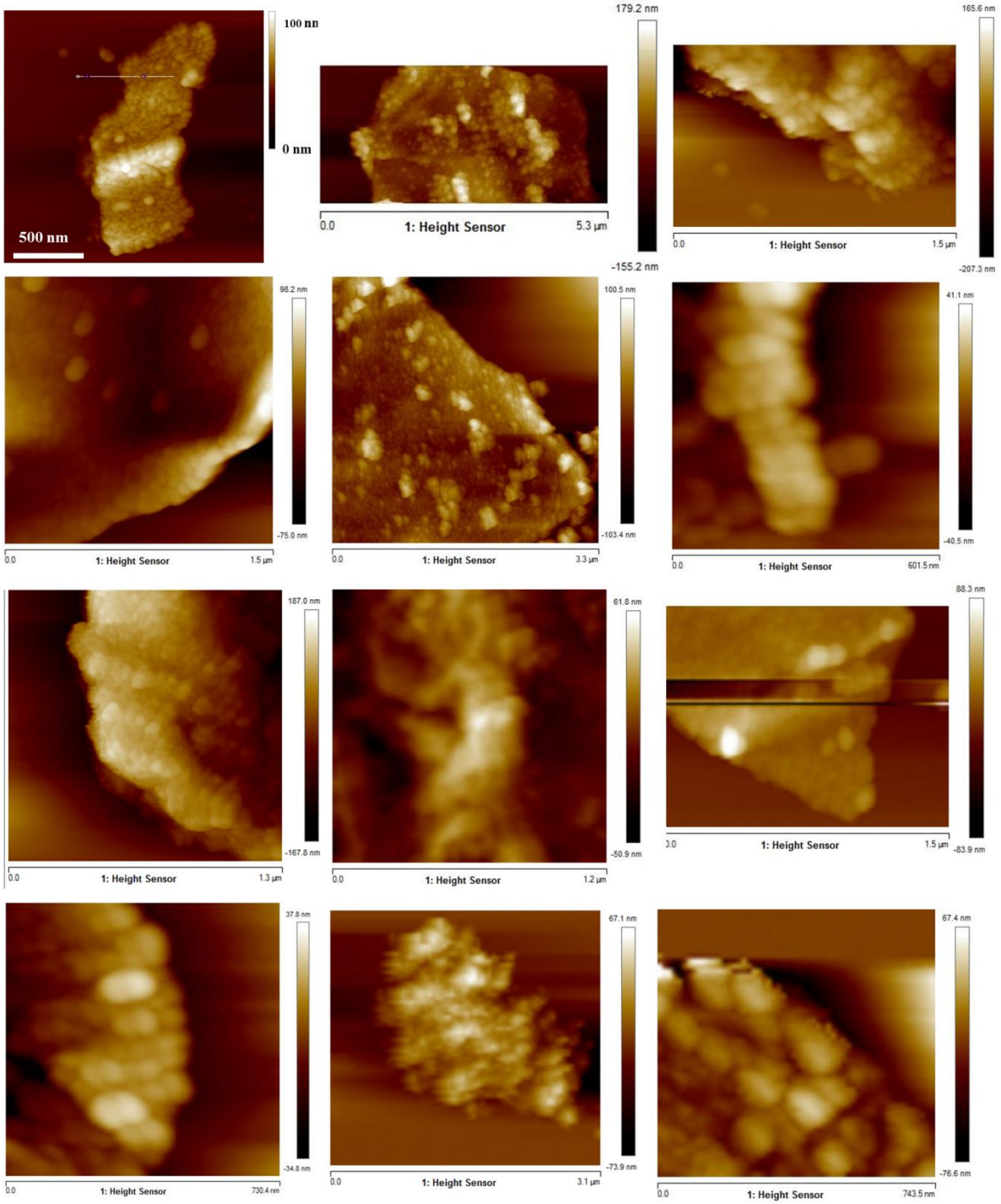
100 nn
0 nm
500 nm
179.2 nm
0.0
1: Height Sensor
5.3 µm
165.6 nm
0.0
1: Height Sensor
1.5 µm
-207.3 nm
-155.2 nm
98.2 nm
-75.0 nm
0.0
1: Height Sensor
1.5 µm
100.5 nm
-103.4 nm
0.0
1: Height Sensor
3.3 µm
41.1 nm
-40.5 nm
0.0
1: Height Sensor
601.5 nm
187.0 nm
-167.8 nm
0.0
1: Height Sensor
1.3 µm
61.8 nm
-50.9 nm
0.0
1: Height Sensor
1.2 µm
88.3 nm
-83.9 nm
0.0
1: Height Sensor
1.5 µm
37.8 nm
-34.8 nm
0.0
1: Height Sensor
730.4 nm
67.1 nm
-73.9 nm
0.0
1: Height Sensor
3.1 µm
67.4 nm
-76.6 nm
0.0
1: Height Sensor
743.5 nm

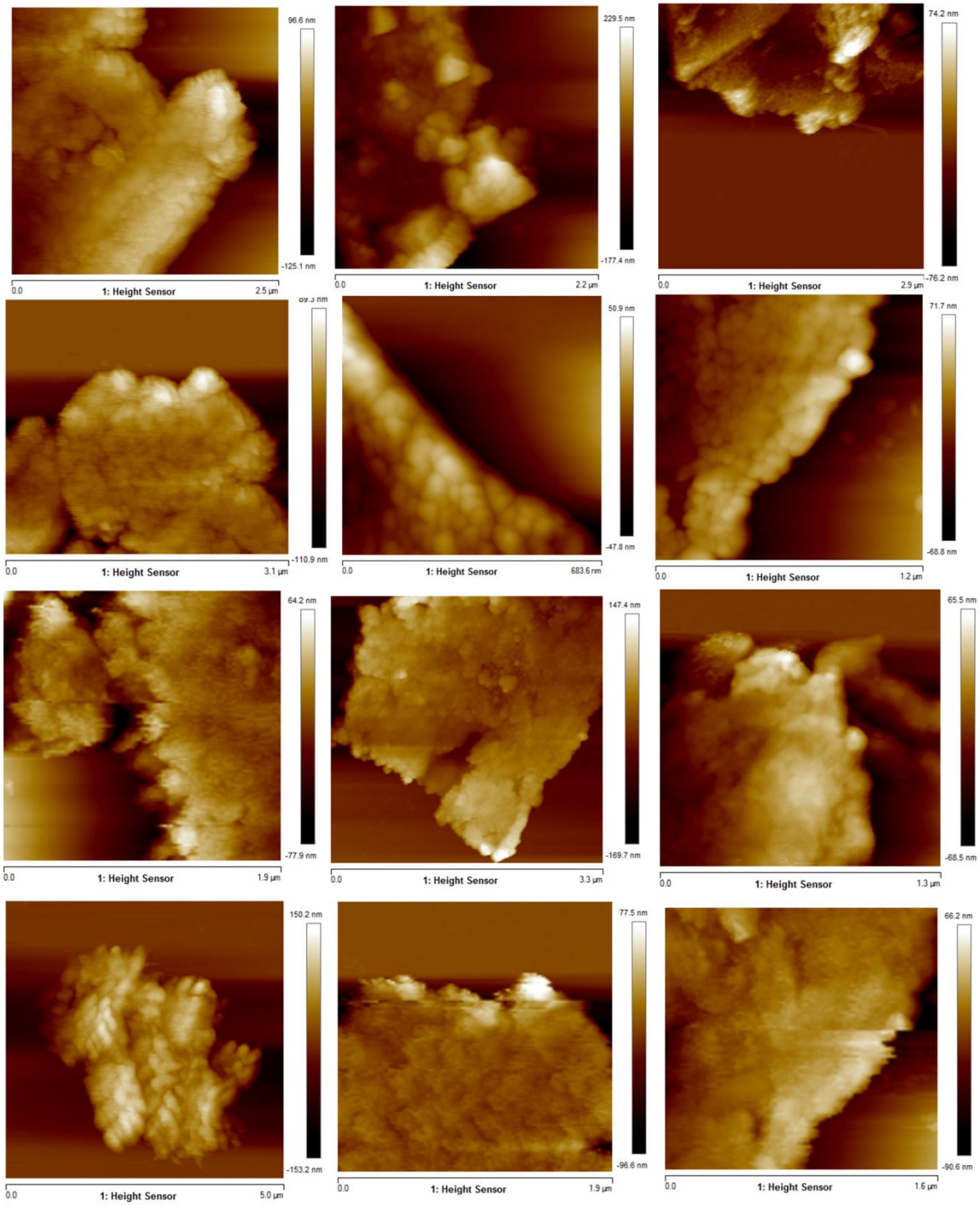

Figure S2. AFM images of 24 pieces of EG/mPANi sheets for thickness distribution analysis, from which an average thickness of ~51 nm was obtained.

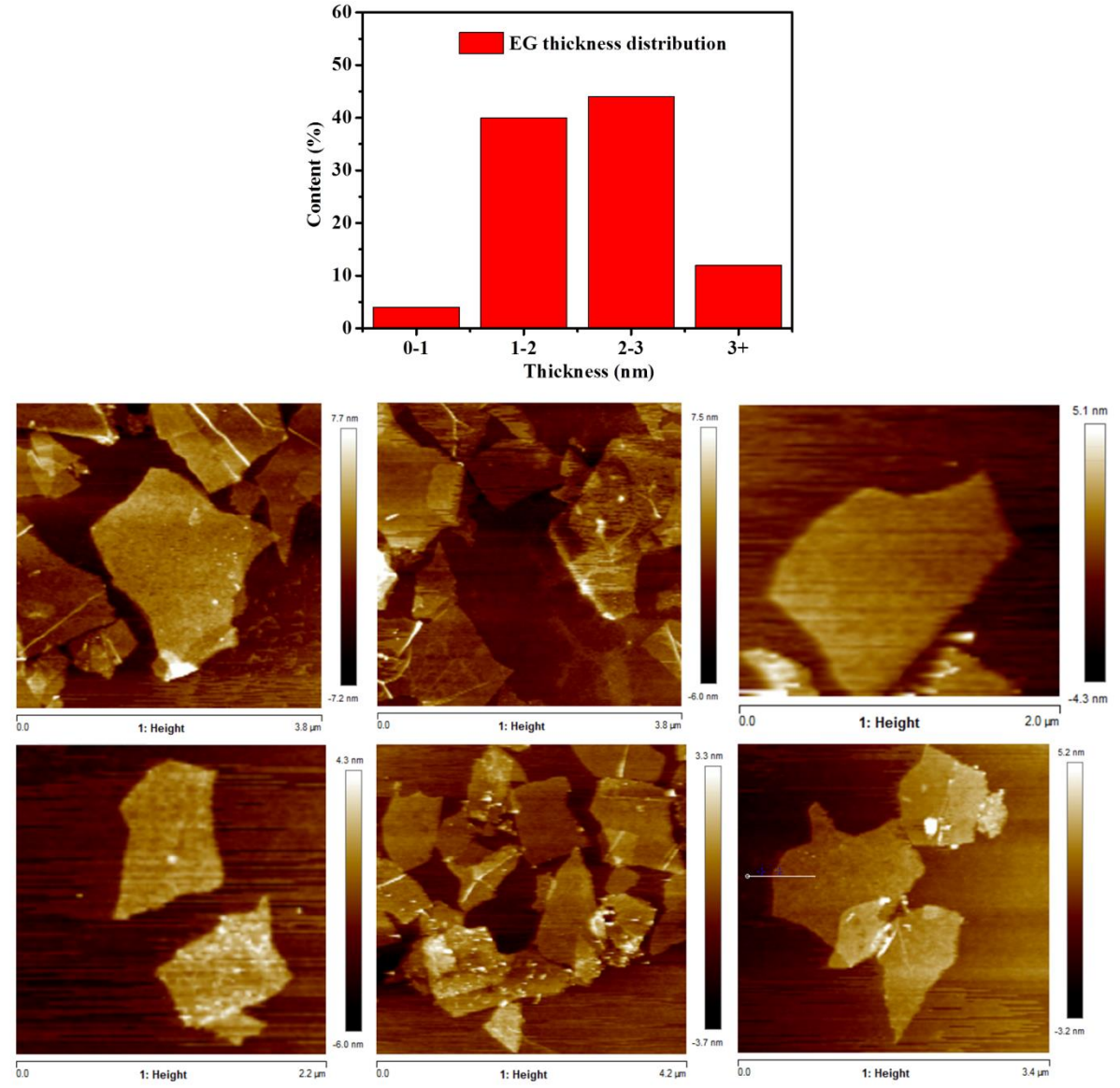

Figure S3. AFM images of 25 pieces of EG sheets for thickness distribution analysis, from which an average thickness of 1.8 nm was obtained.

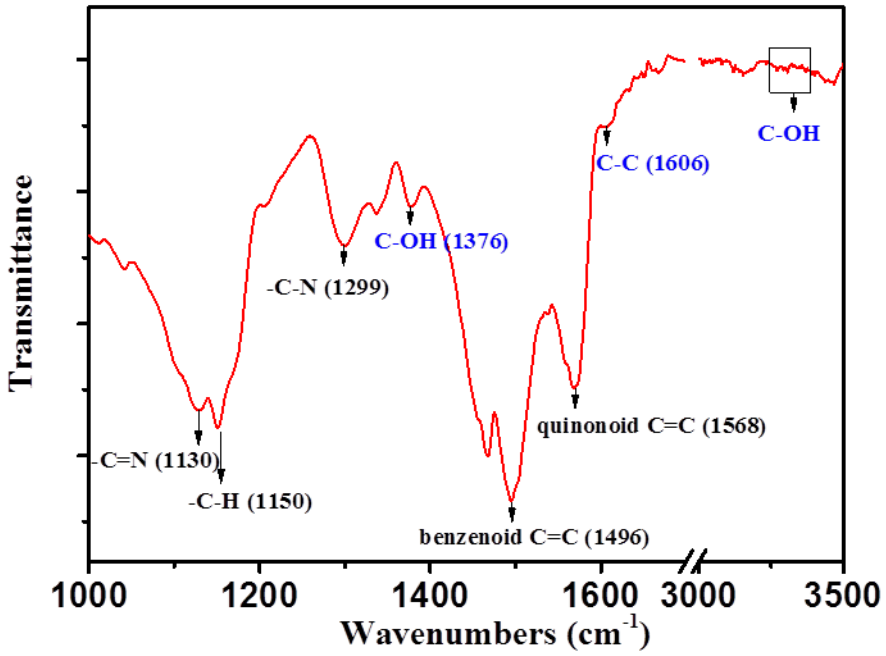

Figure S4. FT-IR spectrum of the EG/mPANi sheets.

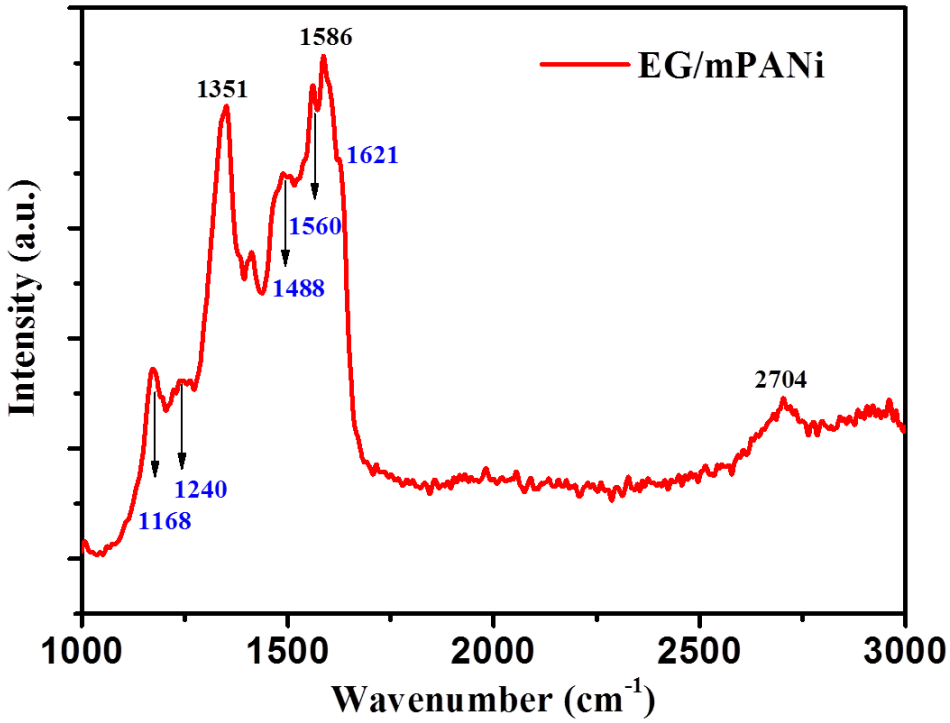

Figure S5. Raman spectrum of the EG/mPANi sheets, recorded under 532 nm laser at 20 mW.

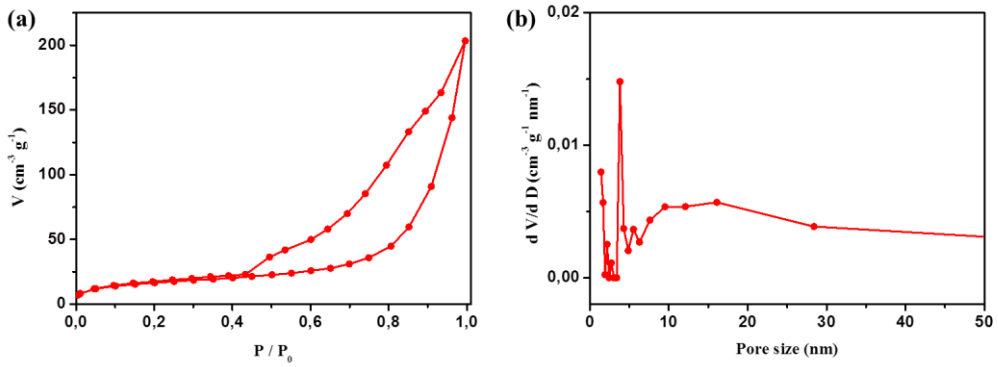

Figure S6. (a) The nitrogen adsorption-desorption isotherms of EG/mPANi sheets. (b) The pore-size distribution curves calculated from the adsorption branches.

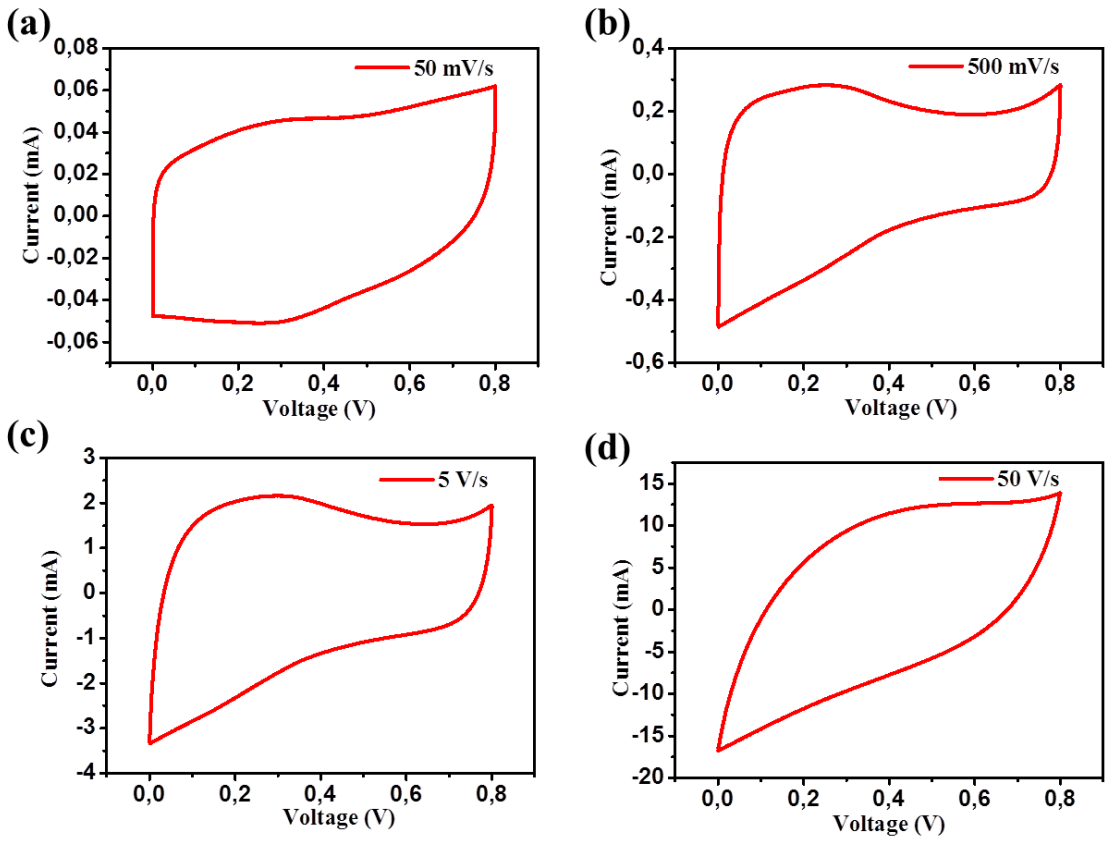

Figure S7. Cyclic voltammetry curves of MSC based on 200 nm thick EG/mPANi film with other scan rates ranging from 50 to 5×10^4 mV s^{-1}.

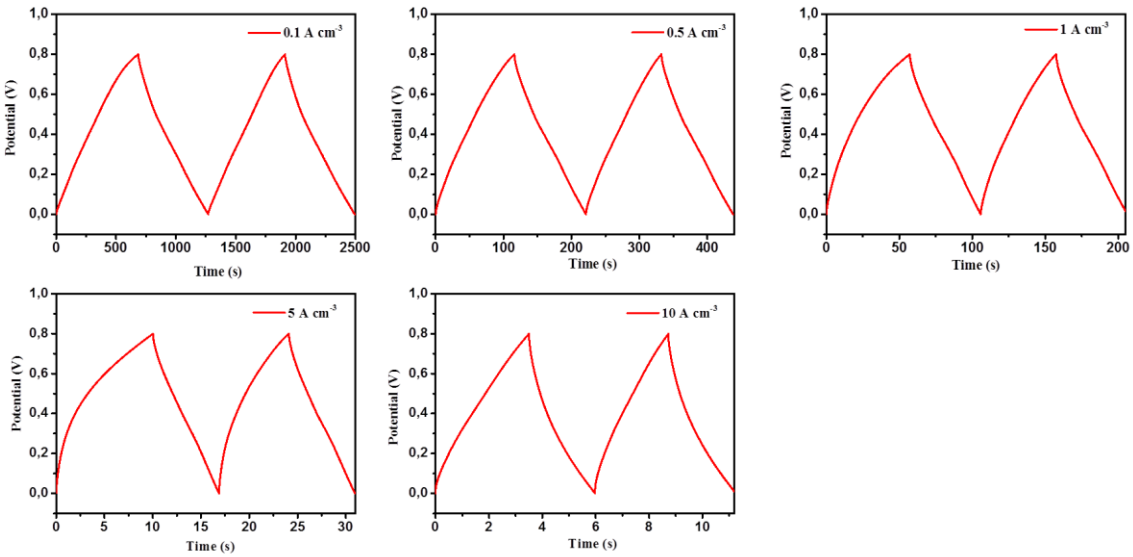

Figure S8. GCD curves of MSC based on 200 nm thick EG/mPANi film at different current densities ranging from 0.1 to 10 A cm^{-3}.

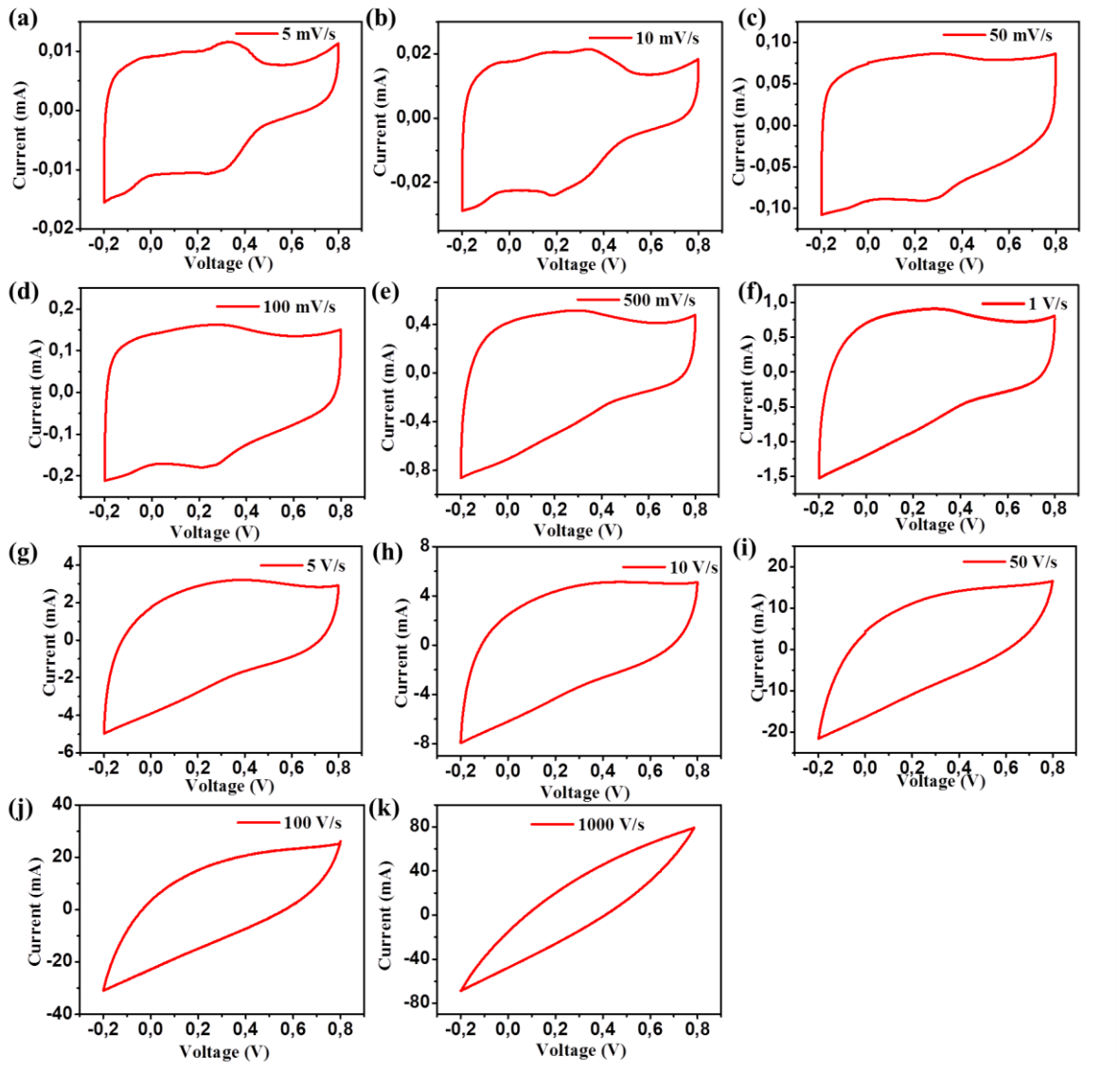

Figure S9. Cyclic voltammetry curves of MSC based on 500 nm thick EG/mPANi film with scan rates ranging from 5 to 10^6 mV s^{-1}.

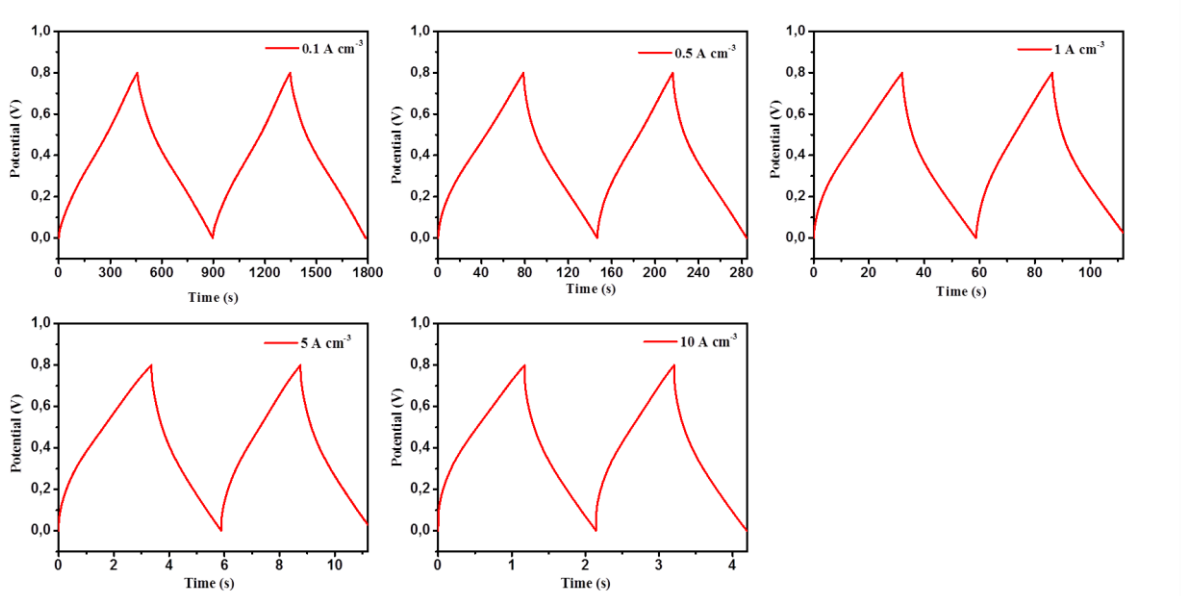

Figure S10. GCD curves of MSC based on 500 nm thick EG/mPANi film at different current densities ranging from 0.1 to 10 A cm^{-3}.

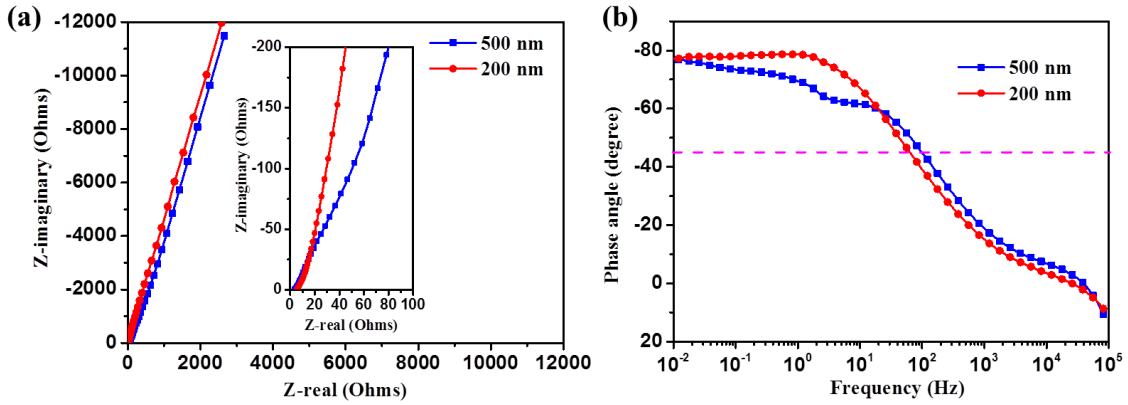

Figure S11. EIS of MSCs based on both 200 nm and 500 nm thick EG/mPANi films. (a) Complex plane plot of the impedance of the MSCs. Inset is a magnified plot of the high-frequency region. (b) Impedance phase angle as a function of frequency for the MSCs.

Table S1. State-of-the-art MSCs performance.

	C_{area}	C_{vol}	Energy Density	Power Density	Material
1	1.7 mF cm^{-2}	1.3 F cm^{-3}	1.6 mWh/cm^3	250 W/cm^3	onion like carbon
2	0.51 mF cm^{-2}	3.1 F cm^{-3}	0.43 mWh/cm^3	1.7 W/cm^3	RGO by laser reduction
3	2.32 mF cm^{-2}	3.05 F cm^{-3}	2 mWh/cm^3	200 W/cm^3	Laser writing of GO film
4	80.7 μF cm^{-2}	17.9 F cm^{-3}	2.5 mWh/cm^3	495 W/cm^3	methane plasma reduced RGO film
5	3.31 mF cm^{-2}	16.6 F cm^{-3}	1.51 mWh/cm^3		RGO/PANi composite film
6	1.5 mF cm^{-2}	75 F cm^{-3}	6.67 mWh/cm^3	600 W/cm^3	200 nm thick EG/mPANi film, this work

Chapter 5. Photoswitchable Micro-Supercapacitors Based on a Diarylethene-Graphene Composite film

Key words: photo-switchable, micro-supercapacitors, diarylethene, CVD graphene

ToC figure

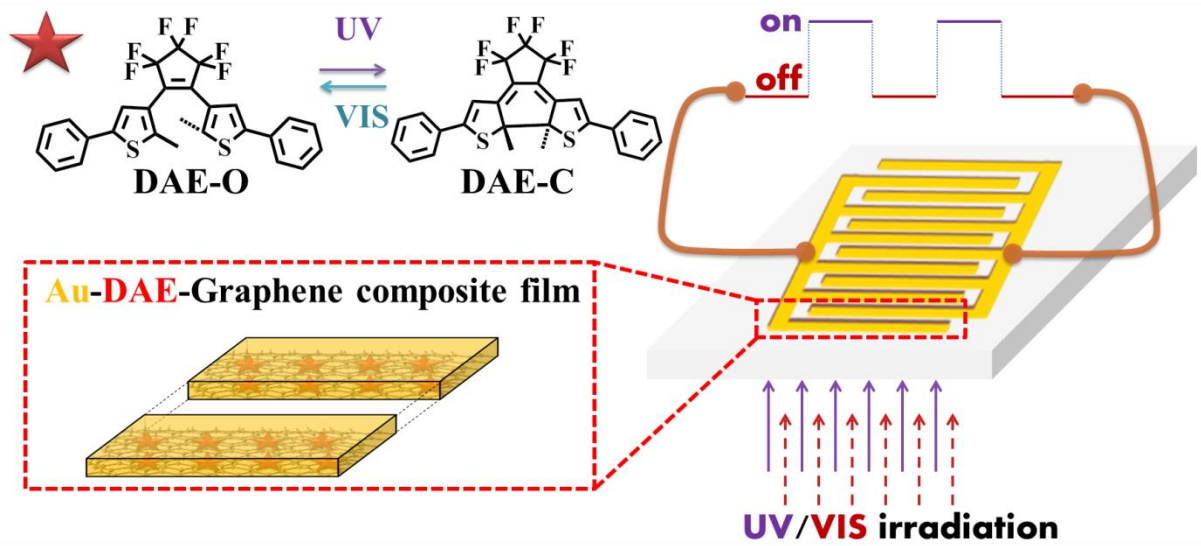

Abstract

Stimuli-responsive micro-supercapacitors (MSCs) controlled by external stimuli can enable a wide range of applications for future on-chip energy storage. Here, we report on a photoswitchable MSC based on a diarylethene-graphene composite film. The micro-device delivers an outstanding and reversible capacitance modulation of up to 20%, demonstrating a prototype photoswitchable MSC. Terahertz spectroscopy indicates that the photoswitching of the capacitance is enabled by the reversible tuning of interfacial charge injection into

diarylethene molecular orbitals, as a consequence of charge transfer at the diarylethene-graphene interface upon light modulation.

Published in:

***Journal of the American Chemical Society*, DOI: 10.1021/jacs.7b04491**

Stimuli-responsive devices that can instantly react to an external stimulus, such as mechanical force, pH, light, and magnetic field, have recently been attracting increasing attention for various applications, including smart logic circuits, diagnostics, and electronic-skins.[1] Photoresponsive systems are currently under particularly intense investigations, since light is arguably one of the most advantageous stimuli owing to its ubiquitous presence and technological maturity, as well as high spatial and temporal resolution, which allows for genuine remote control.[2] Diarylethene derivatives (DAEs) are promising photoswitchable molecules, which can be efficiently interconverted between two thermodynamically stable photoisomers by UV or white light with distinctively different electronic properties upon irradiation.[1e, 3]

Micro-supercapacitors (MSCs), which are capable of delivering high power densities, fast charge-discharge rates, and long cycle lives, have recently been emerging as promising candidates for on-chip micro-power energy sources.[4] Efficient graphene-based MSCs have demonstrated not only high energy and power densities, but also operation at ultrahigh scan rates up to 10^3 V s^{-1}.[4e, 5] Such high operating speed corresponds to extremely short device charging-discharging cycles of 2 ms (potential window of 1 V), which is sufficiently fast for some sensing-detecting applications.[6] Moreover, the unique 2D structure of graphene

provides a compatible platform for controlled molecular doping,[7] which allows for efficient modulation of the capacitive behavior. Based on this concept, it is possible to bestow the switching characters of stimuli-responsive molecules on MSCs, which would open up considerable perspectives for various off-grid applications of MSCs with novel responsive properties, beyond their typical sole purpose of energy storage.

While, to the best of our knowledge, there is thus far only one reported example of stimuli-responsive MSC showing a reversible electrochromic effect,[1d] photoresponsive MSCs have never been developed, which would nevertheless be valuable as non-contact tunable devices. In this work, we report for the first time photoswitchable MSC based on a thin-layer of DAE deposited on top of graphene electrodes. We demonstrate that the efficient photoisomerization behavior of DAE molecules is combined with a significant and reversible control of electro-double layer capacitance in the graphene-DAE composite. Remarkably, the as-fabricated all-solid-state MSC with in-plane geometry can be operated at ultrahigh rates up to 10^4 V s^{-1}, which is four orders of magnitude higher than that of conventional supercapacitors, and one order of magnitude higher than other graphene-based MSCs. The areal capacitance of these MSC devices increases linearly with UV light irradiation up to saturation, and can then be switched back to the original state upon white light irradiation, showing an outstanding and reversible capacitance modulation up to 20%. Employing THz spectroscopy, we further reveal that the reversible modulation of the capacitance is accompanied by a reversible shift of charge equilibrium at the DAE/graphene interface upon photoisomerization. We propose that alongside the charge equilibrium process, a static dipole is generated across the DAE-graphene interface, which reduces the charge injection barrier in the capacitor and thus enhances the capacitance of the system.

Figure 1 demonstrates the fabrication process and concept of our photoresponsive MSC. In short, two layers of graphene sheets prepared on copper foils by a low pressure chemical vapor deposition (CVD) process (see Supporting Information (SI) for details) were transferred onto a sapphire substrate, and photochromic DAE, 1,2-bis(2,4-dimethyl-5-phenyl-3-thienyl)-3,3,4,4,5,5-hexafluoro-1-cyclopentene (Figure 1) was spin-coated on top, thus forming the DAE-graphene composite film. In order to fabricate the interdigitated microelectrode pattern of MSC, an Au current collector (30 nm thick) was deposited through a shadow mask, followed by oxygen plasma etching of the channels. Finally, a thin layer of polymer gel electrolyte poly(vinyl alcohol) (PVA)/H_2SO_4 was drop-cast onto the interdigitated microelectrodes, thus yielding the all-solid-state MSC based on in-plane geometry. The open-ring isomer DAE-O and the ring-closed isomer DAE-C can be interconverted upon ultraviolet (UV) and visible (VIS) light irradiation; both forms are thermodynamically stable at ambient conditions.[3d] We have performed density functional theory (DFT) calculations of the two photoisomers, which showed that the position of the highest occupied molecular orbital (HOMO) level shifts from –6.25 to –5.46 eV, and the optical gap is significantly decreased from 4.44 to 2.63 eV upon photoisomerization from DAE-O to DAE-C (see SI for details).

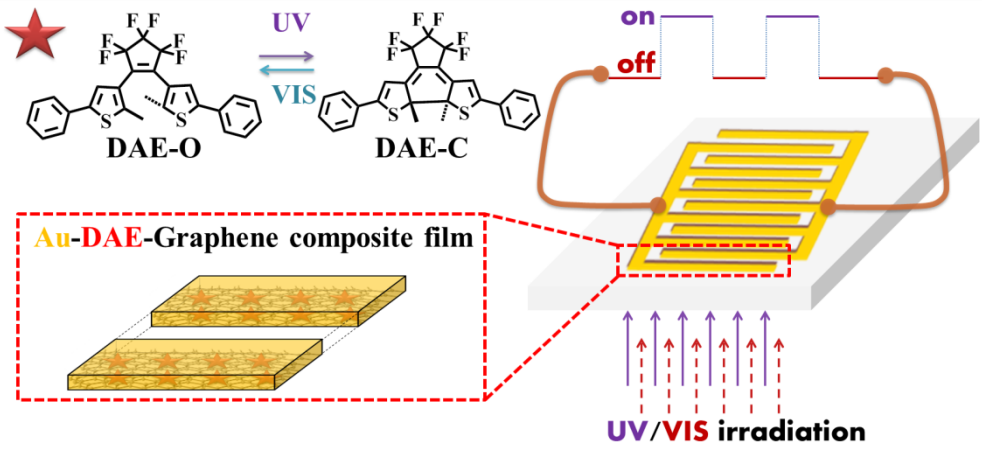

Figure 1. Schematic illustration of photoresponsive MSC device with DAEs on the top of graphene electrodes.

To examine the electrochemical properties, we carried out cyclic voltammetry (CV) of the MSC based on DAE-graphene composite film. Remarkably, the as-fabricated MSC can be operated at ultrahigh rates up to 10^4 V s^{-1} (Figure 2a), corresponding to an extremely short charging-discharging cycle of only 0.2 ms. This is most probably enabled by the facilitated ion transport due to the in-plane device geometry and the superior electron-double-layer capacitance of graphene. This operating speed is four orders of magnitude higher than that of conventional sandwich-structured supercapacitors,[4e] and also sufficiently high to realize "real-time monitoring" of the device capacitance change upon external light stimulation.

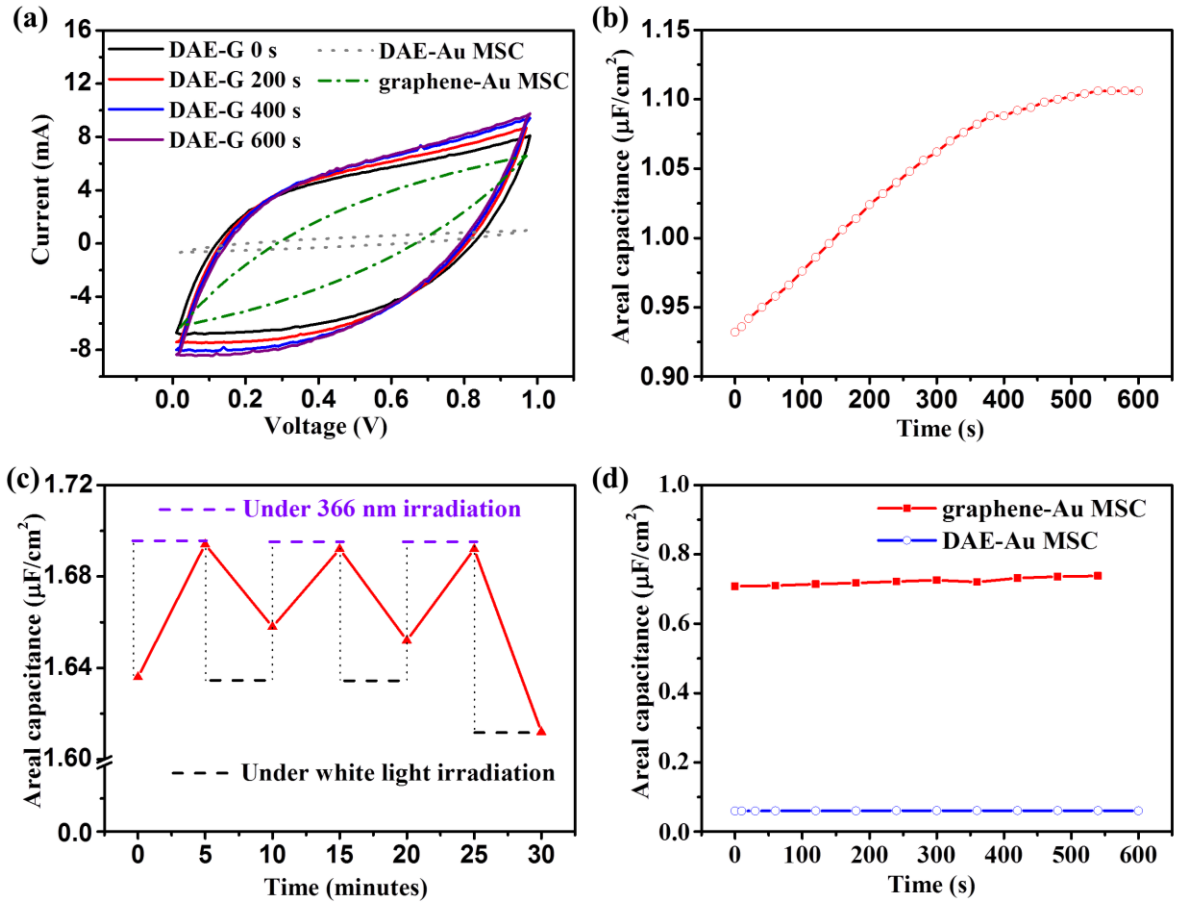

Figure 2. (a) CV curves of DAE-graphene (G) MSC device after different UV irradiation times as well as reference MSC devices with DAE-Au or graphene-Au geometry. (b)

Capacitance change of DAE-graphene MSC after different UV irradiation times. (c) On-off switching behavior of DAE-graphene MSC by alternating UV (366 nm, 5 min) and white light (5 min) irradiation. (d) Capacitance change of graphene-Au MSC and DAE-Au MSC, after different UV irradiation times. The negligible increase for graphene-Au MSC device may be attributed to photochemical process at graphene surfaces.[8]

We have subsequently examined the photoswitching capability of the DAE-graphene-based MSC, first by exposing the device to UV light at 366 nm during the operation to turn it "on" (see Supporting Information (SI) for details). From Figure 2b, we can see that the capacitance of the MSC (with 50 nm thick DAE layer) increases almost linearly with UV irradiation time, and gradually saturates after 400 s. Remarkably, the total capacitance of the MSC increased to 120% of its original value under UV irradiation. We have next tested the reversible photoisomerization of DAE by alternating UV and white light irradiation, and observed the "switching" of the capacitance between "high" and "low" states (MSC with 10 nm thick DAE layer, Figure 2c and Figure S3). Although the light modulation requires much longer time than the charging/discharging time, such on-off switching behavior of the output signal in the MSC over extended time periods can fulfil the very basic requirements for on-chip logic circuits.

To unveil the origin of photoswitchable capacitance at DAE-graphene-Au interfaces, we have conducted control measurements in MSC devices based on DAE-Au geometry without the graphene layer, and graphene-Au geometry without the DAE layer. While the reversible photoisomerization process of DAE molecules still takes place, as apparent from the color change during UV/white light treatment, the corresponding capacitance modulation is negligible in the absence of the interface between graphene and DAE as shown in Figure

2d and Figure S3. This lack of phototunable capacitance in both DAE-Au and graphene-Au system strongly suggests that the charge transfer-equilibrium at graphene-DAE interfaces is an essential ingredient for the photomodulation of the capacitance.

To investigate charge transfer across the DAE-graphene interface during light treatment, DAE-graphene was investigated on fused silica (SiO_2) using terahertz (THz) spectroscopy, as sketched in Figure 3a. THz spectroscopy can quantify photoconductivity in a contact-free fashion, and as such has been shown to provide valuable insight into the carrier transport mechanism in graphene.[8-9] As control measurements, we first investigated THz transmission through either DAE-SiO_2 or graphene-SiO_2 samples by monitoring the peak intensity changes of THz pulse upon light treatments. As shown in Figure S4, no THz signal modulation was observed for both cases, under all the tested light irradiation conditions. In contrast, for the DAE-graphene-SiO_2 system, irradiation triggers a reversible, substantial ~4% change of the transmitted THz field, observed after 15 minutes of UV-white light, as shown in Figures 3b and 3c. The saturation time of the THz signal change by the light treatment is about 5-10 minutes in good agreement with that of the MSC device measurements. As the DAE molecular layer is rather insulating (even for DAE-C with a relatively small energy gap of ~2.4 eV), the change of transmitted (~4 meV) THz field must be attributed to the modulation of charge carrier density in graphene, which originates from charge transfer accompanying the photoisomerization process. This assignment is corroborated by more detailed measurements of transport characteristics in the structure before-after UV light irradiation by time domain THz spectroscopy. As shown in Figure 3c, after UV light treatment, we observed a higher transmitted THz electrical field E. As the initial graphene is known to be p-doped,[8] increased THz transmittance indicates that the Fermi level is shifted upwards in graphene due to molecular doping effect from DAE molecules as a consequence

of electron transfer. More quantitatively, we can obtain the frequency-resolved conductivity $\sigma(\omega)$ of the samples as shown in Figure 3d from: [10]

$$\frac{E_{Gr+sub}}{E_{sub}} = \frac{1 + n_{sub}}{1 + n_{sub} + Z_0 * \sigma(\omega) * d_{sub}} ,$$

in which, Z_0 is the impedance of free space; nsub and dsub are the refractive index and thickness of the SiO_2 substrate, respectively. The measured frequency dependent conductivity is shown in Figure 3d, and can be adequately described with a simple [redacted] model, as expected for graphene.[8, 10a] The [redacted] model provides the key transport properties: carrier scattering time τ and Fermi level relative to the Dirac point. The [redacted] model reveals that the charge scattering time in graphene increased from 70 fs to 100 fs by UV light treatments, while the Fermi energy changes from –80 meV to –40 meV. This result is, again, in line with an upshift of the Fermi level due to the ET process from the DAE layer to graphene.

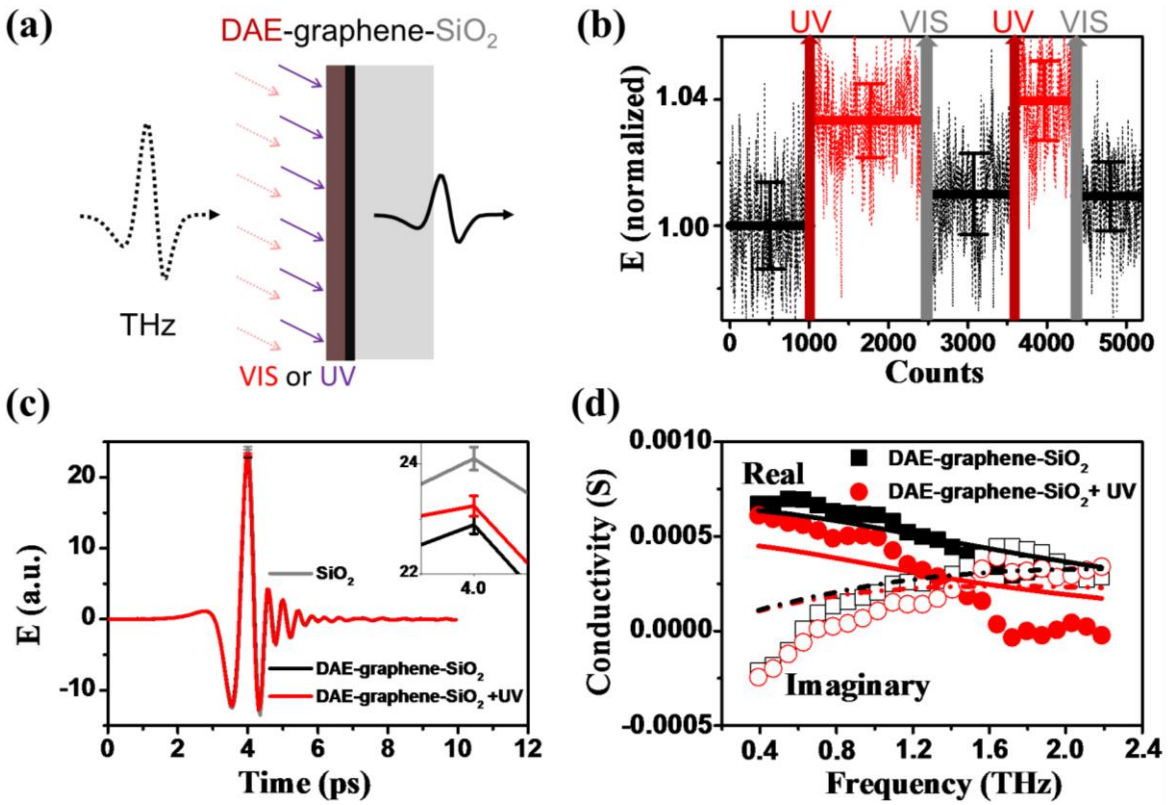

Figure 3. THz conductivity characterization of DAE on graphene supported by silica (DAE-graphene-SiO2) irradiated by UV and VIS light. (a) Schematic of the measurements; (b) Relative change of THz electrical field (E) modulated by UV and VIS light. The original data are shown in dotted lines, and their averages over a static period are plotted as solid horizontal lines (with errors indicating the standard deviation). The data are normalized to 1 for the initial THz peak intensity in absence of light modulation. (c) Static THz transmission through the bare SiO2 substrate (as reference, grey), DAE-graphene-SiO2 before (black) and after UV treatment (red); (d) Frequency-dependent optical conductivity (the solid data for real, and the open ones for imaginary conductivity) before (black) and after (red) UV irradiation treatment, and the corresponding [redacted] model calculations (described in the SI, solid and dash-dotted lines).

Now we turn our focus on discussing the potential effect on the system capacitance of charge transfer across the DAE-graphene interface following UV/white light stimulus. The UV-induced transfer of electrons into the graphene will decrease the chemical potential closer to the Dirac point. As a result, the quantum capacitance, and thus the overall capacitance in graphene is expected to decrease due to the associated reduction of density of states at the Fermi surfaces.[11] Remarkably, we observe an increase in capacitance, indicating that additional capacitance channels, such as additional chemical capacitance from DAE molecules, dominate the overall capacitance. Based on these features, we here propose the following scenario: accompanying the interfacial charge transfer at DAE-graphene surfaces, a static, interfacial dipole pointing from the DAE layer to graphene is created. Owing to the low dielectric environment and associated weak charge screening in molecular system, the dipoles can strongly modify interfacial energetics between substrate and molecules. Indeed,

dipole-assisted tuning of interfacial energetics has long been known and reported in the organic molecule-metal interfaces,[12] and its impact on controlling energy levels in material systems with low density of states (such as semiconducting quantum dots) has also been widely demonstrated.[13] Specifically, with an interfacial dipole moment pointing from graphene to the DAE molecular layer in our case, an associated downward-shift of the lowest unoccupied molecular orbital (LUMO) levels in DAE is expected. This leads to a reduced charge injection barrier for electrons into LUMO orbitals of DAE molecules from the graphene electrode, and increase the capacitance accordingly.

In conclusion, we have demonstrated in-plane structured MSC with photoswitchable behavior. The device can be operated at ultrahigh rates of 10^4 V s^{-1}, with an outstanding areal capacitance modulation of up to 20%. THz spectroscopy indicates that the reversible shift of charge equilibrium at the diarylethene-graphene interface enabled a photoswitching of the MSC capacitance. The achievement of such stimuli-responsive MSC devices opens up exciting opportunities for future portable and wearable power supplies in diverse applications with non-contact modulation of the properties. The resulting UV-sensitive MSC behavior could also be considered as a new way of photodetection and is promising for visible-blind UV-detection such as fire and missile plume detection and optical communications.

Supporting Information

Experimental Details including Materials, CVD graphene production, and MSC device fabrication and characterization are listed in supporting information. Supporting Information is available free of charge on the ACS Publications website or from the author.

Notes

The authors declare no competing financial interests.

ACKNOWLEDGMENT

This work was financially supported by the ERC Grant on NANOGRAPH and 2DMATER, EC under Graphene Flagship and Marie-Curie ITN project "iSwitch" (GA No. 642196), MoQuaS (Molecular Quantum Spintronics FP7-ICT-2013-10 610449), the DFG (SPP 1459 Graphene), the Max Planck Society, and MaxNet Energy. We gratefully acknowledge the support of the Graduate School of Excellence Materials Science in Mainz (MAINZ) GSC 266 and the Center for INnovative and Emerging MAterials (CINEMA).

Reference

[1] a) M. A. C. Stuart, W. T. S. Huck, J. Genzer, M. Muller, C. Ober, M. Stamm, G. B. Sukhorukov, I. Szleifer, V. V. Tsukruk, M. Urban, F. Winnik, S. Zauscher, I. Luzinov, S. Minko, *Nat. Mater.* **2010**, *9*, 101; b) J. Hu, S. Liu, *Macromolecules* **2010**, *43*, 8315; c) R. Yerushalmi, A. Scherz, M. E. van der Boom, H.-B. Kraatz, *J. Mater. Chem.* **2005**, *15*, 4480; d) P. Zhang, F. Zhu, F. Wang, J. Wang, R. Dong, X. Zhuang, O. G. Schmidt, X. Feng, *Adv. Mater.* **2017**, *29*, 1604491; e) E. Orgiu, N. Crivillers, M. Herder, L. Grubert, M. Pätzel, J. Frisch, E. Pavlica, D. T. Duong, G. Bratina, A. Salleo, N. Koch, S. Hecht, P. Samorì, *Nat. Chem.* **2012**, *4*, 675; f) P. Naumov, S. Chizhik, M. K. Panda, N. K. Nath, E. Boldyreva, *Chem. Rev.* **2015**, *115*, 12440; g) X. Hu, E. McIntosh, M. G. Simon, C. Staii, S. W. Thomas, *Adv. Mater.* **2015**, *28*, 715.

[2] a) M. Massicotte, P. Schmidt, F. Vialla, K. G. Schädler, A. Reserbat-Plantey, K. Watanabe, T. Taniguchi, K. J. Tielrooij, F. H. L. Koppens, *Nat Nano* **2016**, *11*, 42; b) M.-M. Russew, S. Hecht, *Adv. Mater.* **2010**, *22*, 3348; c) L. Zhang, X. Zhong, E. Pavlica, S. Li, A.

Klekachev, G. Bratina, T. W. Ebbesen, E. Orgiu, P. Samorì, *Nat Nano* **2016**, *11*, 900; d) Y. Tai, G. Lubineau, Z. Yang, *Adv. Mater.* **2016**, *28*, 4665; e) S. Nau, C. Wolf, S. Sax, E. J. W. List-Kratochvil, *Adv. Mater.* **2015**, *27*, 1048; f) Y. Hu, G. Wu, T. Lan, J. Zhao, Y. Liu, W. Chen, *Adv. Mater.* **2015**, *27*, 7867; g) H. Dong, H. Zhu, Q. Meng, X. Gong, W. Hu, *Chem. Soc. Rev.* **2012**, *41*, 1754.

[3] a) M. Irie, T. Fukaminato, T. Sasaki, N. Tamai, T. Kawai, *Nature* **2002**, *420*, 759; b) T. Leydecker, M. Herder, E. Pavlica, G. Bratina, S. Hecht, E. Orgiu, P. Samorì, *Nat Nano* **2016**, *11*, 769; c) X. Zhang, L. Hou, P. Samori, *Nat. Commun.* **2016**, *7*, 11118; d) S. Fredrich, R. Göstl, M. Herder, L. Grubert, S. Hecht, *Angew. Chem., Int. Ed.* **2016**, *55*, 1208; e) D. Kim, H. Jeong, W.-T. Hwang, Y. Jang, D. Sysoiev, E. Scheer, T. Huhn, M. Min, H. Lee, T. Lee, *Adv. Funct. Mater.* **2015**, *25*, 5918.

[4] a) B. Mendoza-Sánchez, Y. Gogotsi, *Adv. Mater.* **2016**, *28*, 6104; b) Z.-S. Wu, X. Feng, H.-M. Cheng, *Natl. Sci. Rev.* **2014**, *1*, 277; c) M. F. El-Kady, Y. Shao, R. B. Kaner, *Nat. Rev. Mater.* **2016**, 16033; d) P. Huang, C. Lethien, S. Pinaud, K. Brousse, R. Laloo, V. Turq, M. Respaud, A. Demortière, B. Daffos, P. L. Taberna, B. Chaudret, Y. Gogotsi, P. Simon, *Science* **2016**, *351*, 691; e) Z. S. Wu, K. Parvez, X. Feng, K. Müllen, *Nat. Commun.* **2013**, *4*, 2487; f) D. Pech, M. Brunet, H. Durou, P. Huang, V. Mochalin, Y. Gogotsi, P.-L. Taberna, P. Simon, *Nat Nano* **2010**, *5*, 651; g) Z. Liu, Z.-S. Wu, S. Yang, R. Dong, X. Feng, K. Müllen, *Adv. Mater.* **2016**, *28*, 2217; h) Z. Niu, L. Zhang, L. Liu, B. Zhu, H. Dong, X. Chen, *Adv. Mater.* **2013**, *25*, 4035; i) M. F. El-Kady, R. B. Kaner, *Nat. Commun.* **2013**, *4*, 1475.

[5] Z.-S. Wu, Y.-Z. Tan, S. Zheng, S. Wang, K. Parvez, J. Qin, X. Shi, C. Sun, X. Bao, X. Feng, K. Müllen, *J. Am. Chem. Soc.* **2017**, *139*, 4506.

[6] a) X. Zhou, L. Gan, W. Tian, Q. Zhang, S. Jin, H. Li, Y. Bando, D. Golberg, T. Zhai, *Adv. Mater.* **2015**, *27*, 8035; b) F. Liu, H. Shimotani, H. Shang, T. Kanagasekaran, V. Zólyomi, N. Drummond, V. I. Fal'ko, K. Tanigaki, *ACS Nano* **2014**, *8*, 752.

[7] P. Wei, N. Liu, H. R. Lee, E. Adijanto, L. J. Ci, B. D. Naab, J. Q. Zhong, J. Park, W. Chen, Y. Cui, Z. A. Bao, *Nano Lett.* **2013**, *13*, 1890.

[8] H. I. Wang, M.-L. Braatz, N. Richter, K.-J. Tielrooij, Z. Mics, H. Lu, N.-E. Weber, K. Müllen, D. Turchinovich, M. Kläui, M. Bonn, *J. Phys. Chem. C* **2017**, *121*, 4083.

[9] R. Ulbricht, E. Hendry, J. Shan, T. F. Heinz, M. Bonn, *Rev. Mod. Phys.* **2011**, *83*, 543.

[10] a) G. Jnawali, Y. Rao, H. Yan, T. F. Heinz, *Nano Lett.* **2013**, *13*, 524; b) M. Tinkham, *Phys. Rev.* **1956**, *104*, 845.

[11] J. Xia, F. Chen, J. Li, N. Tao, *Nat Nano* **2009**, *4*, 505.

[12] a) A. Vilan, A. Shanzer, D. Cahen, *Nature* **2000**, *404*, 166; b) D. Cahen, A. Kahn, *Adv. Mater.* **2003**, *15*, 271; c) D. Cahen, A. Kahn, E. Umbach, *Mater. Today* **2005**, *8*, 32; d) Y. L. Huang, W. Chen, F. Bussolotti, T. C. Niu, A. T. S. Wee, N. Ueno, S. Kera, *Physical Review B* **2013**, *87*, 085205.

[13] P. R. Brown, D. Kim, R. R. Lunt, N. Zhao, M. G. Bawendi, J. C. Grossman, V. Bulović, *ACS Nano* **2014**, *8*, 5863.

Supporting Information

Photoswitchable Micro-Supercapacitor Based on a Diarylethene-Graphene Composite Film

Materials

Cu foils were purchased from Alfa Aesar. PMMA solution was from Micro Resist Technology GmbH (950 PMMA C2). Cu etchant and other solvents were from Sigma-Aldrich. DAE molecule, 1,2-bis(2,4-dimethyl-5-phenyl-3-thienyl)-3,3,4,4,5,5-hexafluoro-1-cyclopentene, was purchased from TCI Europe Fine Chemicals (CAS Registry Number: 172612-67-8).

CVD graphene production

Chemical vapor deposition (CVD) graphene films were grown on 25-μm thick Cu foils (size: 3×3 cm^2) in a custom-made hot wall furnace.

Growth process: (1) Clean Cu foils were loaded into the quartz tube, followed by pumping down the sealed tube below a pressure of 5×10^{-3} mTorr. (2) The hydrogen gas (99.999%) was opened and flowed at 100 sccm (pressure inside the quartz tube was maintained at 1 mTorr). (3) Programed heating of the tube from room temperature to 1020 ºC was set within 40 min, followed by annealing at 1020 ºC for another 40 min. (4) After annealing of the Cu foil surface, methane gas flow (>99.9%) at 25 sccm was opened as carbon source for 20 min, and then switched off. (5) Cooled down to the room temperature with hydrogen gas flow on.

Photoswitchable MSC device fabrication

First, we transferred two layers of CVD graphene onto a pre-cleaned sapphire substrate. A typical film transfer approach was:[1] (1) poly(methyl methacrylate) (PMMA) was spin-coated on top of graphene/Cu foil as supporting layer, followed by heating at 140 ºC for 5 min to solidify the polymer layer; (2) the PMMA/graphene/Cu foil was put onto the liquid surface of Cu etchant solution, and the Cu foil underneath graphene was etched; (3) the floating PMMA/graphene film was rinsed for 3 times with deionized water, and then transferred onto the pre-cleaned sapphire substrate (size: 3 × 3 cm^2); (4) the PMMA/graphene/sapphire substrate was soaked into acetic acid for 24 h to remove the PMMA layer; (5) rinsed with methanol and water, and dried with N_2 flow.

Next, we deposited a thin layer of DAE molecules on the top of graphene by spin-coating a solution in chloroform (concentration: 10 mg mL^{-1}; 1500 rpm for 60 s) to form the photoactive-layer of the device.

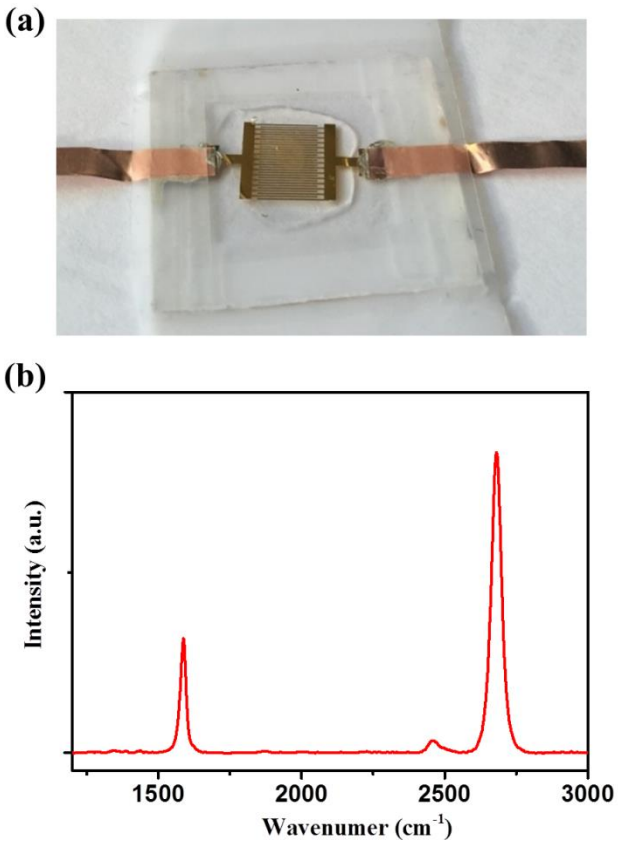

Figure S1. (a) The digital picture of as-fabricated photoresponsive MSC device. (b) Raman spectrum at 532 nm of transferred CVD graphene on sapphire substrate, showing very low defect intensities.

Subsequently, well-established lithography techniques were applied to produce interdigital microelectrode patterns using a homemade shadow mask for the deposition of gold current

collectors, followed by oxidative etching of micro-supercapacitor (MSC) channels in oxygen plasma.[2]

Finally, a gel electrolyte of poly(vinyl alcohol) (PVA)/H_2SO_4 was drop-casted onto the finger electrodes and allowed to solidify overnight to obtain an all solid state MSC with in-plane geometry. The digital picture of as fabricated photo-responsive MSC device is shown in Figure S1a.

Sample characterizations

As shown in Figure S1b, Raman spectrum of transferred CVD graphene was recorded by a SENTERRA dispersive Raman microscope (Bruker Corporation); with 532 nm laser (power was 10 mW).

Cyclic voltammetry (CV) was utilized to test the MSC device, with potential window of 0–1 V. The operating rate of the MSC was set at 10^4 V s^{-1} to realize "real-time monitoring". UV lamp (366 nm, light intensity: 6 W m^{-2}) was used as the light source for the MSC. The transparent side of MSC was placed 2 cm above the UV lamp during CV measurements at various UV irradiation times. The CV curve was recorded every 30 s. White light was provided by an LED with light intensity of ~50 W m^{-2}. The measurement was operated in a dark room.

The areal capacitance values were calculated from the CV curves according to the following equation:

$$C_{areal} = C_{device}/A$$

and

$$C_{device} = \frac{1}{\nu(V_f - V_i)} \int_{V_i}^{V_f} I(V)dV$$

where A is the total area of the device, ν is the scan rate, V_f and V_i are the integration potential limits of the CV curve, I (V) is the discharge current.[3]

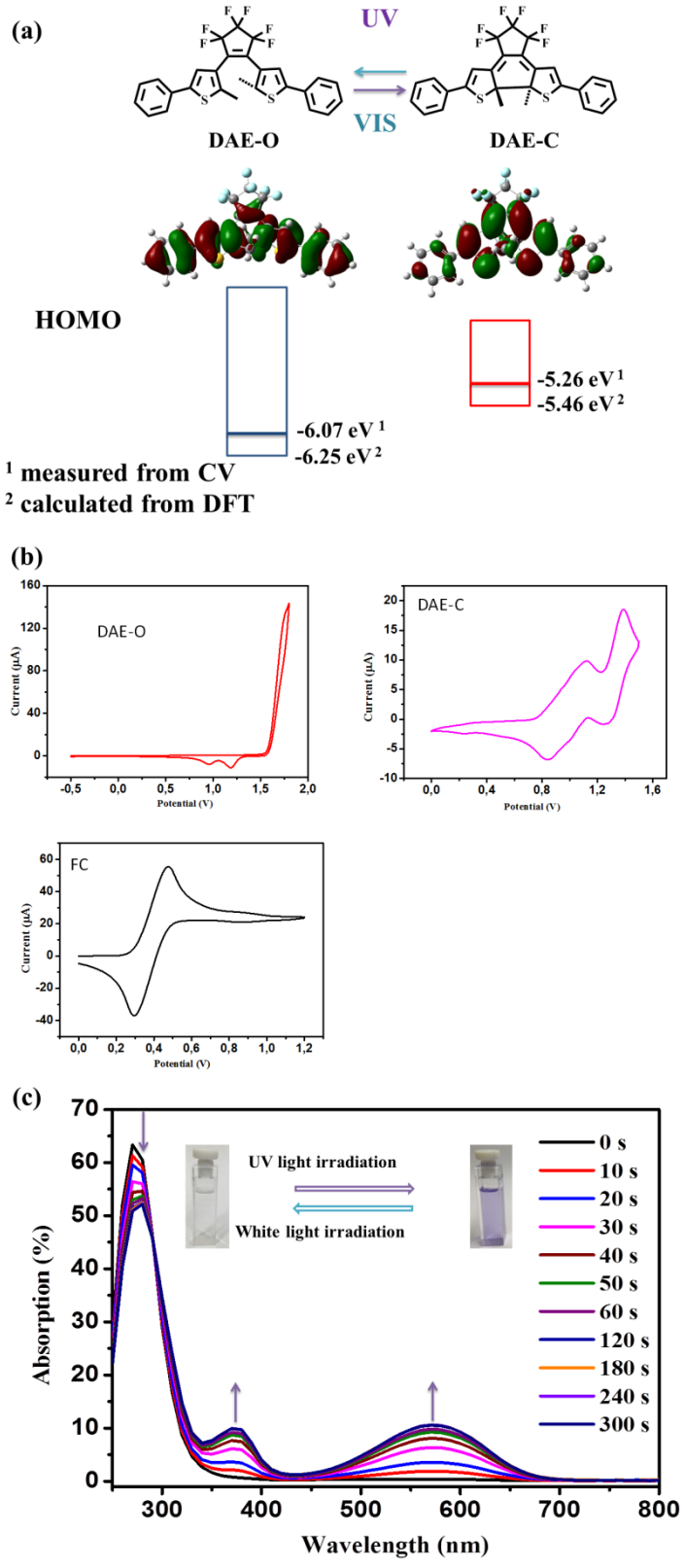

Figure S2. (a) Structural change of DAE upon the photoisomerization; DFT-simulated HOMOs of the two photoisomers; and the HOMO levels based on the CV measurements and

DFT calculations. (b) CV curves of DAE-O, DAE-C, and ferrocene (FC). (c) UV-vis absorption spectra of DAE solution in chloroform after different UV irradiation times.

DFT calculation

We have studied the photoisomerization of DAE with the density functional theory (DFT) calculation.[4] As shown in Figure S2a, the highest occupied molecular orbital (HOMO) level was predicted to decrease significantly by about 0.8 eV (from –6.25 to –5.46 eV) upon the photoisomerization from DAE-O to DAE-C. To verify the modification of HOMO level during UV treatment, CV measurements (Figure S2b) have also been carried out. In line with the DFT results, the HOMO level was shifted from –6.07 to –5.26 eV, corresponding to a decrease of 0.8 eV, upon the UV treatment. As shown in Figure S2c, we also monitored the changes in the UV-Vis absorption spectrum of DAE in dilute chloroform solution upon UV irradiation. As we can see, irradiation from 0 to 300 s resulted in a gradual photoconversion from DAE-O to DAE-C with the absorption peak shift from 380 nm and 580 nm. Inset of Figure 1c features the significant color change of the DAE solution before/after UV light treatments.

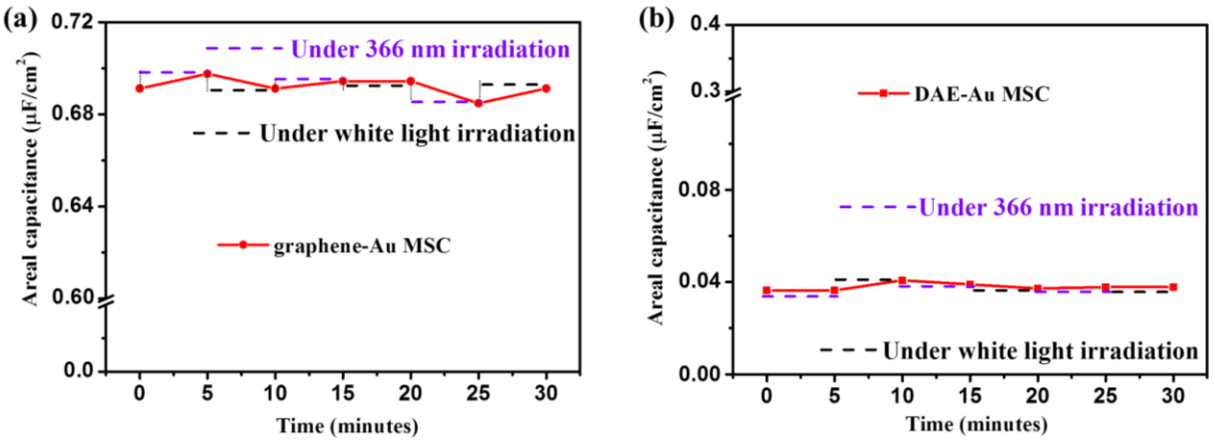

Figure S3. Capacitance change of (a) graphene-Au MSC and (b) DAE-Au MSC with alternating UV and white light irradiations.

THz measurements on DAE-SiO_2 and graphene-SiO_2 samples under light modulation conditions

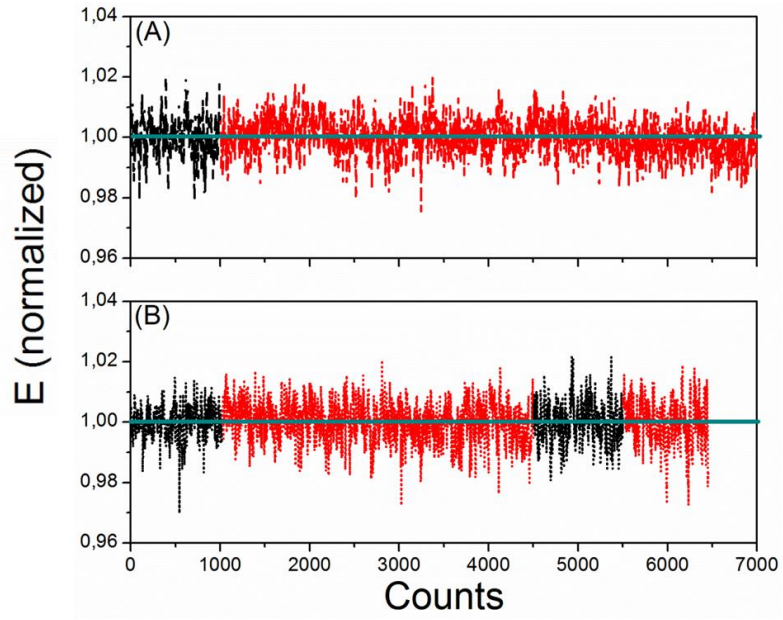

Figure S4. Relative change of THz electrical field (E) modulated by UV and Vis light. The data are normalized to 1 for the initial THz peak intensity in absence of light modulation, or after white light treatment (the black dotted lines); the red dotted lines for THz transmission after 15 minutes of UV light irradiation.

Reference

[1] M. Her, R. Beams, L. Novotny, *Phys. Lett. A* **2013**, *377*, 1455.

[2] Z. Liu, S. Liu, R. Dong, S. Yang, H. Lu, A. Narita, X. Feng, K. Müllen, *Small* **2017**, *13*, 1603388.

[3] Z. S. Wu, K. Parvez, X. Feng, K. Müllen, *Nat. Commun.* **2013**, *4*, 2487.

[4] *Gaussian 09, Revision D.01, M. J. Frisch, G. W. Trucks, H. B. Schlegel, G. E. Scuseria, M. A. Robb, J. R. Cheeseman, G. Scalmani, V. Barone, B. Mennucci, G. A. Petersson, H. Nakatsuji, M. Caricato, X. Li, H. P. Hratchian, A. F. Izmaylov, J. Bloino, G. Zheng, J. L. Sonnenberg, M. Hada, M. Ehara, K. Toyota, R. Fukuda, J. Hasegawa, M. Ishida, T.*

Nakajima, Y. Honda, O. Kitao, H. Nakai, T. Vreven, J. A. Montgomery, Jr., J. E. Peralta, F. Ogliaro, M. Bearpark, J. J. Heyd, E. Brothers, K. N. Kudin, V. N. Staroverov, T. Keith, R. Kobayashi, J. Normand, K. Raghavachari, A. Rendell, J. C. Burant, S. S. Iyengar, J. Tomasi, M. Cossi, N. Rega, J. M. Millam, M. Klene, J. E. Knox, J. B. Cross, V. Bakken, C. Adamo, J. Jaramillo, R. Gomperts, R. E. Stratmann, O. Yazyev, A. J. Austin, R. Cammi, C. Pomelli, J. W. Ochterski, R. L. Martin, K. Morokuma, V. G. Zakrzewski, G. A. Voth, P. Salvador, J. J. Dannenberg, S. Dapprich, A. D. Daniels, O. Farkas, J. B. Foresman, J. V. Ortiz, J. Cioslowski, and D. J. Fox, Gaussian, Inc., Wallingford CT **2013**.

Chapter 6. Summary and Outlook

Up to now, the market for on-chip micro scale energy storage is still mainly dominated by micro-batteries, whereas significant drawbacks such as low power density, limited cycle life and safety issues need to be overcome. The discovery of graphene provided a promising choice for flexible and transparent electronic systems. Due to its unique electrical, mechanical and optical properties, graphene can be widely employed in energy storage devices, with enhanced performance compared with other carbon materials. For the above reasons, in this thesis, micro-supercapacitors (MSCs) based on graphene or graphene composite materials were fabricated to address their unique properties such as facile printable device, high power density, and multi-functional application.

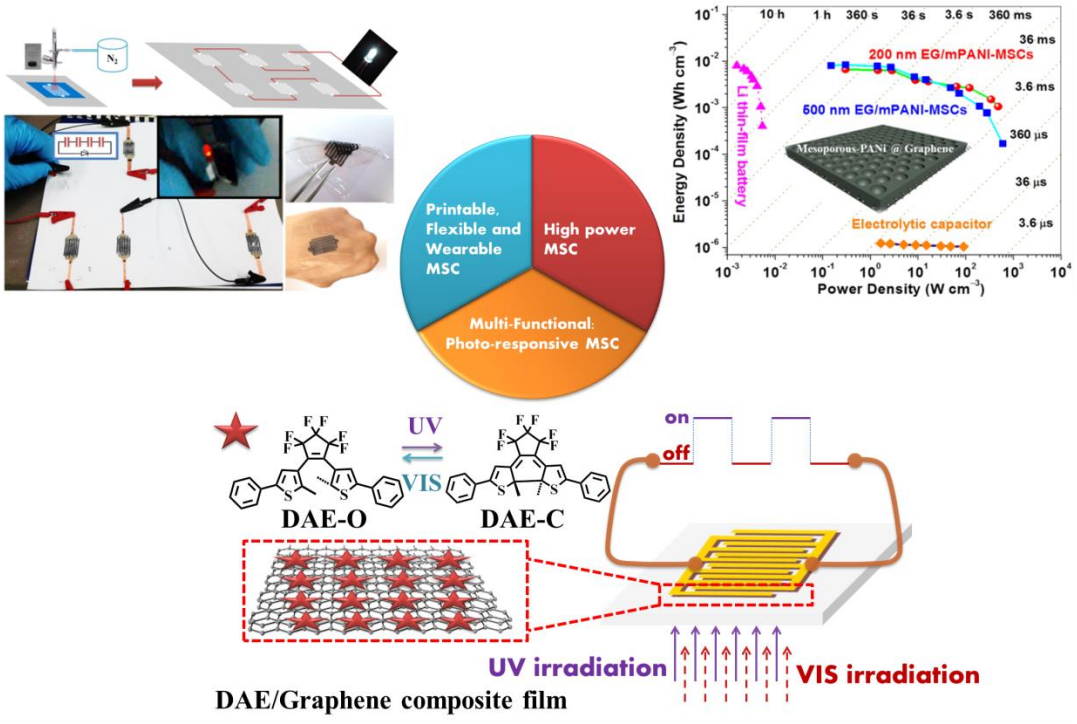

Figure 6-1. Overview of this thesis: the demonstrated unique properties of MSCs, such as (1) Printable, flexible and wearable; (2) High power; (3) Photo-responsive.

In the 2nd chapter, solution fabrication of large area and highly conductive graphene films was developed, by facile spray coating of graphene-conductive polymer hybrid ink. The obtained graphene films exhibited excellent mechanical properties, which enabled their application as bottom electrodes for ultrathin organic photodetector devices. Remarkably, the device performance was comparable to that of state-of-the-art Si based inorganic photodetectors. Further optimized electrochemically exfoliated graphene employed for the hybrid ink may pave the way to the future development of transparent conductive electrodes for optoelectronics, and other emerging flexible devices, such as electronic skins and wearable supercapacitors. This chapter is the basis of Chapter 3.

In the 3rd chapter, direct printing of in-plane MSCs on flexible substrates was demonstrated, employing both an electrochemically exfoliated graphene ink and a hybrid ink with an electrochemically active conducting polymer. The as fabricated MSCs on paper substrates delivered a significant areal capacitance. By employing ultra-thin PET substrates, "ultra-flexible" MSC devices were also achieved with excellent flexibility. These results may be interesting for the future development of high performance portable and wearable power supplies.

In the 4th chapter, in-plane structured planar MSCs based on mesoporous polyaniline patterned graphene were introduced. The strong synergistic effect from electron-double-layer-capacitive graphene and pseudocapacitive mesoporous-PANi leads to excellent MSC device performances. The fabricated micro devices delivered both significant volumetric capacitance and rate capabilities, which further lead to high power densities of 600 W cm^{-3}. This performance outperformed most of those reported graphene-based high power supercapacitors/MSCs results. Such MSCs also delivered energy densities of 6.67 mWh cm^{-3}, comparable to current commercially available LTF batteries. The concept of incorporating

pseudo-capacitive mesoporous polymer onto electron-double-layer-capacitive graphene surface thus offers promising opportunities for future portable and wearable supercapacitors in diverse applications.

In the 5th chapter, in-plane structured planar MSCs with photo-switchable behavior were demonstrated, the fabricated devices can be operated at ultrahigh rates. The areal capacitance of these MSC devices display a linear increase upon UV light irradiation till saturated state, and can then be switched back to the original state upon white light irradiation, showing an outstanding and reversible capacitance modulation up to 20%. THz spectroscopy suggests that the optically switchable capacitance during UV/Vis light treatments was enabled by the optically shifted charge equilibrium at the diarylethene/graphene interface. The achievement of such smart MSC device opens up exciting opportunities for future portable and wearable power supplies in diverse applications with non-contact modulation of the properties. The resulting UV/Vis sensitive MSC behavior makes it attractive for visible-blind UV detection applications such as fire and missile plume detection and optical communications. Future photo-switchable semiconductors with tuneable absorption and improved electronic properties would open up the way to more sophisticated photo-sensitive designs.

Above all, the focus of this thesis has been centred on the MSC applications of high quality graphene from electrochemical exfoliation method (or chemical vapour deposition in Chapter 5). The achieved results in this thesis have already shown several unique advantages of future MSCs, which would contribute to a meaningful feedback in regards of graphene preparation method, suitable processing of graphene, and the desired properties of graphene for high performance MSC device fabrication.

Current challenges faced by graphene based MSCs: (i) How to further improve the electrochemical exfoliation method for graphene production. Stable dispersions of graphene in suitable liquid media (for most cases, low boiling point solvents are preferable for subsequent processing steps) should be achieved. The high electrical conductivity of the obtained graphene film requires a low oxidation degree during electrochemical exfoliation process. Moreover, reducing the costs for the whole process is the key factor if such future graphene based MSCs can be commercially available.

(ii) Fabrication of composite materials which combine the advantages of EDL capacitive graphene and pseudo-capacitive materials is an effective way to enhance the overall MSC performance. Thus, developing a deeper understanding of the energy storage mechanisms of MSCs, especially for the interfacial reactions between the electrode material and electrolyte is of utmost importance.

(iii) Incorporating porous structures inside the MSC electrodes to form hierarchical interconnected porous microstructures and avoid the formation of dead volume or the collapse of the porous microstructures; and control the interfacial interactions between graphene sheets and pseudo-capacitive materials to achieve a well-designed electrode material with high electrochemical performance (in regards of both volumetric capacitance and rate capability).

(iv) How to pattern graphene based MSCs at low costs without complex photolithography techniques and oxidative channel-etching methods. For example, facile 3D-printing of graphene inks for on-chip MSCs, can effectively increase the amount of active materials loaded per area while fast ion diffusion is unaffected, leading to a significant improvement of the total output energy and power.

Further optimization of MSC device architectures is also a challenging issue. So far, it is still necessary to optimize the main geometric parameters of planar interdigital MSCs, including the interspace, width, length and number of finger electrodes. An appropriate geometric adjustment of these parameters for increasing the active area by increasing the number of finger electrodes or reducing the interspace between adjacent finger electrodes can efficiently decrease the device resistance and thus increase the energy and power densities.

(v) The trend for the development of flexible and wearable MSCs is to integrate or embed them into electronic devices to create multi-functional or self-powered hybrid systems. Some efforts have been paid to combine flexible supercapacitors with different electronics, such as solar cells, Li-ion batteries, electrochromic devices, and nanogenerators. However, integration of these devices into practical applications is still a challenge.

Although many challenges remain, recent research results still indicate that graphene based materials will play an important and perhaps irreplaceable role in on-chip MSCs due to their intriguing features, we believe that flexible and wearable graphene-based MSCs will emerge as a widely used technology in the near future. Graphene research is also expected to continue to expand rapidly during the next decade with the promise of making a real impact on our lives.

Acknowledgements

Four years of PhD study is like a long-term chemical reaction, after so many steps, I am about to collect my product now.

They say time flies when having fun. When I look back through the path I was struggling on, the feeling was like being on a roller coaster. I had my ups and downs, laughter and tears, which all made this very moment worthwhile. I will be always grateful to all the people who kindly helped me during my PhD study.

First and foremost, I would like to express my sincere gratitude to my supervisor, Prof. Dr. [redacted], for his constant encouragement and guidance. Prof. [redacted] has a deep understanding in organic chemistry and insightful perspectives regarding electronics and energy storage devices, which guided me through my PhD study and also will be influential for my future careers. I feel so lucky for this amazing opportunity to work with him.

I would like to cordially thank my project leader, Prof. Dr. [redacted], for numerous exciting scientific discussions and enlightening suggestions for my topics, kind and proper corrections for my reports, manuscripts and thesis. His knowledge and experiences about graphene are always valuable for the progress of my work. He always encourages me to be creative and innovative in scientific research, and to be positive and optimistic in life. In both cases, he is a valuable mentor to me.

I would like to extend my thanks to Dr. [redacted], for his kind supports for my research projects and always being there for both scientific discussions and detailed lab works. Dr. Narita also contributed a lot of helpful suggestions and revisions about this thesis.

My sincere gratitude also goes to Dr. [redacted], who involved actively in most of my ideas discussions, his insightful comments and encouragement walked me through the difficult times.

Furthermore, I really appreciate the kind efforts from all AK [redacted] members and our cooperation partners:

Dr. [redacted] contributed great efforts with SEM, TEM and EDX measurements;

Dr. [redacted], Dr. [redacted] and [redacted] helped me a lot regarding the electrochemical exfoliation of graphite;

Dr. [redacted] contributed to the surface polymerization of aniline on graphene;

Dr. [redacted] and Dr. [redacted] offered great help about the fabrication of micro-supercapacitors;

Dr. [redacted], Dr. [redacted] and [redacted] offered helpful discussions and kind assistant about CVD graphene;

Dr. [redacted] and Prof. [redacted] kindly offered great help regarding THz spectroscopy measurement and discussions;

Dr. [redacted] helped me with some XPS measurements;

Mr. [redacted] kindly trained me about the AFM measurement;

Dr. [redacted], Dr. [redacted], Dr. [redacted], Dr. [redacted], Dr. [redacted], Dr. [redacted], [redacted], [redacted], and Dr. [redacted] offered plenty discussions of organic synthesis problems;

Ms. [redacted] always created a safe and comfortable working atmosphere in our lab, and always willing to help me in my daily life. I will remember her words, “People help people”, and try to spread the kindness whenever I can.

Dr. [redacted], Dr. [redacted], Dr. [redacted], Dr. [redacted], [redacted], [redacted], Dr. [redacted], [redacted], [redacted], Dr. [redacted], [redacted], [redacted], [redacted], [redacted], Dr. [redacted], [redacted], [redacted], Dr. [redacted], Dr. [redacted], Dr. [redacted], Dr. [redacted], Dr. [redacted], [redacted], their genuine friendship brought me a lot of joyful moments and helped me ease the pain of homesick.

I also appreciate Ms. [redacted] and Ms. [redacted] for all the generous support and kind help.

Finally, I would like to thank my parents, and my wife as well as her parents for their unconditional love, continuous and considerate support during my PhD study.

Many thanks also to everybody whom I might have unintentionally forgot to mention here.

List of Publications

1. **Z. Liu,** H. I. Wang, A. Narita, Q. Chen, Z. Mics, D. Turchinovich, M. Kläui, M. Bonn, K. Müllen, Photoswitchable Micro-supercapacitors Based on a Diarylethene-Graphene Composite Film, *J. Am. Chem. Soc.* **2017, DOI:** 10.1021/jacs.7b04491.

2. **Z. Liu,** S. Liu, S. Yang, R. Dong, X. Zhuang, X. Feng, K. Muellen, High Power In-Plane Micro-Supercapacitors Based on Mesoporous Polyaniline Patterned Graphene, *Small* **2017**, *13*, 1603388.

3. **Z. Liu,** Z.-S. Wu, S. Yang, R. Dong, X. Feng, K. Müllen, Ultraflexible In-Plane Micro-Supercapacitors by Direct Printing of Solution-Processable Electrochemically Exfoliated Graphene, *Adv. Mater.* **2016**, *28*, 2217.

4. **Z. Liu,** K. Parvez, R. Li, R. Dong, X. Feng, K. Muellen, Transparent Conductive Electrodes from Graphene/PEDOT:PSS Hybrid Inks for Ultrathin Organic Photodetectors, *Adv. Mater.* **2015**, *27*, 669.

5. Z.-S. Wu, **Z. Liu,** K. Parvez, X. Feng, K. Muellen, Ultrathin Printable Graphene Supercapacitors with AC Line-Filtering Performance, *Adv. Mater.* **2015**, *27*, 3669.

6. R. Li, **Z. Liu,** K. Parvez, X. Feng, K. Muellen, High-performance deformable photoswitches with p-doped graphene as the top window electrode, *Journal of Materials Chemistry C* **2015**, *3*, 37.

7. S. Liu, P. Gordiichuk, Z.-S. Wu, **Z. Liu,** W. Wei, M. Wagner, N. Mohamed-Noriega, D. Wu, Y. Mai, A. Herrmann, K. Mullen, X. Feng, Patterning two-dimensional free-standing surfaces with mesoporous conducting polymers, *Nat Commun* **2015**, *6*: 8817

8. S. Yang, S. Brüller, Z.-S. Wu, **Z. Liu,** K. Parvez, R. Dong, F. Richard, P. Samorì, X. Feng, K. Müllen, Organic Radical-Assisted Electrochemical Exfoliation for the Scalable Production of High-Quality Graphene, *J. Am. Chem. Soc.* **2015**, *137*, 13927.

9. Z.-S. Wu, K. Parvez, S. Li, S. Yang, **Z. Liu,** S. Liu, X. Feng, K. Muellen, Alternating Stacked Graphene-Conducting Polymer Compact Films with Ultrahigh Areal and

Volumetric Capacitances for High-Energy Micro-Supercapacitors, *Adv. Mater.* **2015**, *27*, 4054.

10. **Z. Liu,** X.-F. Wang, Z. Wang, H. Ojima, Z. Hong, W. Tian, J. Kido, Indoline-based donor molecule for efficient co-evaporated organic photovoltaics, Org. Electron. **2013**, *14*, 2210.

11. **Z. Liu,** H. Ojima, Z. Hong, J. Kido, W. Tian, X.-F. Wang, Solution-Processed Organic Photovoltaics Based on Indoline Dye Molecules Developed in Dye-Sensitized Solar Cells, Molecules, **2013**, *18*, 3107.

Curriculum Vitae

Personal Details

Name: Zhaoyang Liu

Gender: Male

Place of birth: Jilin, China

Nationality: Chinese

Marital status: Married

University Education

08.2012-06.2017 **PhD studies**, Max Planck Institute for Polymer Research, Mainz, Germany.
Research adviser: Prof. Dr. [redacted]

09.2009-06.2012 **M.Sc.** State Key Laboratory of Supramolecular Structure and Materials, Jilin University, Jilin, China.
Research adviser: Prof. Dr. [redacted]
Thesis title: Organic solar cells based on solution processed graphene.

09.2005-06.2009 **B.A.** College of Physics, Jilin University, Jilin, China.

Research experience

01.2012-06.2012 **Research assistant**, OPV department of Research Center for Organic Electronics, Yamagata University, Japan.
Research adviser: Prof. Dr. [redacted], Prof. Dr. [redacted]
Project title: "Indoline-based donor molecules for efficient organic photovoltaics"

Tutorial Jobs

2013-2014	Assistant tutor in supervising undergraduate students in organic chemistry experimental courses in Johannes Gutenberg University of Mainz.

School Education

09 2002 – 06 2005	Changchun Experimental High School, Jilin, China
09 1999 – 06 2002	NO.52 Middle School, Changchun, Jilin, China
09 1993 – 06 1999	Chun-Cheng Primary School, Changchun, Jilin, China

Awards and Fellowships

2016	Scholarship from Center for Advancing Electronics Dresden (cfaed), Technische Universität Dresden
2015	Prestigious Chinese Government Award for Outstanding Self-Financed Students Abroad
2012	"Elite Cup" Academic Competition Prize for Graduate Students, Jilin University